

STUDIES IN NUCLEATE BOILING

Thesis submitted for the Degree of
Doctor of Philosophy
at the University of Edinburgh

by

I.D.R. GRANT, A.R.C.S.T.

October 1963



ACKNOWLEDGMENTS

This study was carried out in the Sanderson Engineering Laboratories of the University of Edinburgh, and the author is indebted to Professor R.N. Arnold for providing the necessary research facilities.

Grateful thanks are due to Dr. T.D. Patten, under whose direction this work was undertaken. His guidance and discussion at each phase of the work are deeply appreciated.

The assistance of the Engineering Workshop staff during the construction of the experimental apparatus is also gratefully acknowledged.

SYNOPSIS

The thesis describes an experimental and theoretical study of the early stage of nucleate pool boiling of saturated and slightly subcooled water from a flat heating surface.

In the first chapters is described the experimental pressure vessel and test procedure used in carrying out experiments in the pressure range from atmospheric to 749 lbs./inch² abs. Also is described the methods by which cavities with mouth radii from 100 to 550×10^{-6} inches are produced on the heating surface, and these sizes measured. A micro-thermocouple (0.002 inch dia. wires) welded to the lower, insulated surface of the electrically heated test strip measures the strip temperature, and by calculating the temperature drop across the strip, the heating surface temperature is determined. A procedure involving a reversal of the heating strip current is used to calibrate the heating strip thermocouple for the small unavoidable voltage "pick up" from the strip. The heat flux is computed from the electrical power input to the strip.

An intermediate chapter deals with the derivations of theoretical equations to predict (i) the initiation of boiling, (ii) the rate of increase in bubble sites with increase in superheat temperature and (iii) the bubble frequency at each site. The first equation is derived by applying the Gibbs and Clausius-Clapeyron equations to a model of an ideal vapour-filled conical cavity; the second follows from the first equation and the measured cavity distribution; and the third is derived from

assumptions regarding conditions in the liquid layer adjacent to the heating surface (thermal layer), and the assumption that this layer is heated by transient conduction only. The theoretical predictions of initiation and the rate of increase in the number of bubble sites with superheat temperature, are in good agreement with the experimentally recorded values. The theoretical values for the increase in the number of bubble sites with increase in superheat temperature, and the bubble frequency at the first eight bubble sites, are combined to give the increase in the number of bubbles per unit area of heating surface per unit time for pressures of 14.3, 30 and 122 lbs./inch² abs. An equation has been derived, which takes account of both the free convection heat flux and the heat flux associated with bubble growth; this equation is shown to correlate experimental weak boiling curves at 14.3 and 30 lbs./inch² abs.

Two methods for measuring the thickness of the thermal layer at pressures of atmospheric and 30 lbs./inch² abs. are described in later chapters. The first or shadowgraph method, which is based on the refraction of light rays by density change corresponding to temperature change in the water, is also used to study the growth and behaviour of the thermal layer before and after the initiation of boiling. The second method employs a traversing thermocouple to measure the temperature distribution in the liquid, and to determine the layer thickness. Thicknesses of 0.036 and 0.034 inches have been measured by this method for pressures of 14.4 and 30 lbs./inch² abs. and subcoolings of 4.5 and 5.0°F respectively. The thicknesses of the layer measured

at atmospheric pressure by the two methods are in fair agreement. An equation by Chang [33] from an analysis of free convection heat transfer, predicts with some success the thickness of the thermal layer at atmospheric pressure. A discussion of the experimental boiling curves for a pressure range from 14.3 to 749 lbs./inch² abs. is also included.

It is claimed that much of this thesis is concerned with new information on the region of weak nucleate boiling.

TABLE OF CONTENTS

	<u>Page No.</u>
SYNOPSIS	i
TABLE OF CONTENTS	iv
LIST OF FIGURES	viii
CHAPTER 1. <u>Introduction</u>	1
CHAPTER 2. <u>Historical</u>	
2.1. Initiation of boiling	8
2.2. Correlation of nucleate boiling data	11
CHAPTER 3. <u>Experimental Apparatus</u>	
3.1. General description	15
3.2. Boiler shell design and fabrication	16
3.3. Boiler window design and fitting	16
3.4. Test heater design and choice of heat supply	17
3.5. Design of the heating strip d.c. electrodes, insulation and method of support	20
3.6. Manufacture of artificial cavities on the heating strip and their measurement	21
3.7. Welding technique for fixing a thermocouple to the heating strip	24
3.8. Heating surface, bulk liquid and boiler wall temperature measurement	27
3.8.1. Boiler wall thermocouple circuits	27
3.8.2. Heating strip thermocouple circuit	28
3.8.3. Bulk liquid thermocouple circuit	29
3.9. Heating strip d.c. supply and power measurement circuits	30

TABLE OF CONTENTS (contd.)

3.10.	Bulk liquid and boiler wall a.c. heater circuits	31
3.11.	Boiler pressure systems	32
3.11.1.	Pressure range from atmospheric to 1 lb./inch ² abs.	32
3.11.2.	Atmospheric pressure	33
3.11.3.	Pressure range from atmospheric to 1000 lbs./inch ² abs.	33
3.12.	Auxiliary equipment	34
CHAPTER 4.	<u>Experimental Procedure</u>	
4.1.	Calibration of a 0.0076 inch diameter chromel-alumel thermocouple at fixed points on the International Temperature Scale	36
4.1.1.	Ice point	36
4.1.2.	Steam point	37
4.1.3.	Freezing point of tin	38
4.1.4.	Freezing point of lead	39
4.2.	Specification for cleaning the heating surface, test liquid and boiling vessel	39
4.2.1.	Heating surface	40
4.2.2.	Test liquid	40
4.2.3.	Boiling vessel	40
4.3.	Degassing of the heating surface	41
4.3.1.	Degassing at atmospheric pressure	42
4.3.2.	Degassing at 1 lb./inch ² abs.	43
4.4.	Calibration of the voltage "pick up" by the heating strip thermocouple	44
4.5.	Corrosion of the boiler walls	46

TABLE OF CONTENTS (contd.)

4.6.	Effect of pressure and bulk liquid subcooling on nucleate boiling	48
CHAPTER 5.	<u>Nucleate Boiling Theory</u>	
5.1.	Bubble initiation	53
5.2.	Bubble site density	58
5.3.	Bubble frequency	61
5.4.	Weak nucleate boiling heat flux	66
CHAPTER 6.	<u>Shadowgraph Measurement of the Thermal Layer Thickness</u>	
6.1.	Introduction	70
6.2.	Application of the shadowgraph method	71
6.3.	Experimental apparatus	72
6.4.	Experimental procedure	74
6.5.	Results and discussion	75
CHAPTER 7.	<u>Thermocouple Measurement of the Thermal Layer Thickness</u>	
7.1.	Introduction	80
7.2.	Experimental apparatus	81
	7.2.1. Thermocouple probe	81
	7.2.2. Probe mechanism	83
7.3.	Experimental procedure	84
7.4.	Results and discussion	86
	7.4.1. Conduction equation	90
	7.4.2. Chang's equation	91

TABLE OF CONTENTS (contd.)

CHAPTER 8.	<u>Results and Discussion</u>	
8.1.	Effect of liquid pressure and subcooling on heat flux	96
8.2.	Free convection heat transfer	106
8.3.	Nucleation properties of the heating surface	108
CHAPTER 9.	<u>Conclusions and Remarks</u>	115
APPENDICES		
	Accuracy of Results	119
	Nomenclature	121
	References	125
	Experimental data Tables 1 to 12	125
	References	137

LIST OF FIGURESFigure No.

- 1 Regimes of Boiling (Nukiyama [1] in 1934)
- 2 Half Sectional View of Boiler Shell
- 3 Photograph of Boiler and Other Parts of the Apparatus
- 4 Sectional View of Boiler Window
- 5 Heating Strip Assembly
- 6 Cavity Distribution
- 7 Photograph of Talysurf Records
- 8 Heating Strip Isothermal Contours
- 10 Welder for 0.002 inch dia. Thermocouple Wires
- 11 Stages in the Manufacture of the Heating Strip Thermocouple
- 12 Schematic Arrangement of Thermocouple Circuits
- 13 Photograph of Heating Strip Assembly
- 14 Sectional View of Thermocouple Pressure Seal
- 15 Schematic Arrangement of d.c. Power Supply and Measurement Circuits
- 16 Photograph of Bulk Liquid Heater
- 17 Schematic Arrangement of Bulk Liquid and Boiler Wall a.c. Heater Circuits
- 18 Boiler Pressure Systems
- 19 Photograph of Recording Equipment
- 20 Heating Strip Thermocouple e.m.f. Difference vs. Heating Strip Voltage
- 21 Ideal Vapour Filled Cavity
- 22 Initiation Superheat Temperature Difference for First Bubble Site vs. Liquid Pressure

LIST OF FIGURES (contd.)

- 23 Number of Bubble Sites vs. Superheat Temperature Difference
- 24 Model of Thermal Layer
- 25 Bubble Frequency vs. Superheat Temperature Difference
($p_L = 14.3$ lbs./inch² abs.)
- 26 Bubble Flux vs. Superheat Temperature Difference
- 27 Correlation of Weak Boiling Region
($p_L = 14.3$ lbs./inch² abs.)
- 28 Correlation of Weak Boiling Region
($p_L = 30$ lbs./inch² abs.)
- 29 Maximum Bubble Diameter vs. Heat Flux (Experimental Results of Staniszweski [21])
- 30 Cylindrical Heating Surface Shadowgraph (Jakob [30])
- 31 Shadowgraph Optical Bench
- 32 Shadowgraphs of Free Convection and Nucleate Boiling
($p_L = 14.2$ lbs./inch² abs.)
- 33 Thermal Layer Thickness vs. Heating Surface Temperature
($p_L = 14.2$ lbs./inch² abs.)
- 34 Thermal Layer Thickness vs. Heating Surface Temperature
($p_L = 30$ lbs./inch² abs.)
- 35 Sectional View of Thermocouple Probe
- 36 Relative Position of Heating Strip and Thermocouple Junction
- 37 Temperature Gradient above Heating Surface
($p_L = 14.7$ lbs./inch² abs.)
- 38 Free Convection and Boiling Flow Pattern
- 39 Temperature Gradient above Heating Surface
($p_L = 14.4$ lbs./inch² abs.)
- 40 Temperature Gradient above Heating Surface
($p_L = 30$ lbs./inch² abs.)

LIST OF FIGURES (contd.)

- 41 Figures 37 and 39 reproduced
- 42 Heat Flux vs. Heating Surface Temperature
($p_L = 14.3$ lbs./inch² abs.)
- 43 Heat Flux vs. Heating Surface Temperature
($p_L = 122$ lbs./inch² abs.)
- 44 Heat Flux vs. Heating Surface Temperature
($p_L = 201$ lbs./inch² abs.)
- 45 Heat Flux vs. Heating Surface Temperature
($p_L = 279$ lbs./inch² abs.)
- 46 Heat Flux vs. Heating Surface Temperature
($p_L = 401$ lbs./inch² abs.)
- 47 Heat Flux vs. Heating Surface Temperature
($p_L = 549$ lbs./inch² abs.)
- 48 Heat Flux vs. Heating Surface Temperature
($p_L = 749$ lbs./inch² abs.)
- 49 Heat Flux vs. Heating Surface Temperature (Effect of
Subcooling, $p_L = 122$ and 126 lbs./inch² abs.)
- 50 Heat Flux vs. Heating Surface Temperature (Effect of
Subcooling, $p_L = 201$ and 204 lbs./inch² abs.)
- 51 Bulk Liquid Subcooling vs. Superheat Temperature
Difference (Extrapolation to Zero Subcooling)
- 52 Effect of Pressure on "Established Boiling" Curves
- 53 Free Convection Heat Transfer ($p_L = 14.3$ lbs./inch² abs.)
- 54 " " " " ($p_L = 30$ lbs./inch² abs.)
- 55 " " " " ($p_L = 122$ lbs./inch² abs.)
- 56 Cavity Radius vs. Initiation Superheat Temperature
Difference ($p_L = 14.7$ lbs./inch² abs.)

CHAPTER 1

Introduction

The advent of highly-rated nuclear reactor systems has brought a renewed interest in boiling heat transfer and a subsequent demand for more exact knowledge on the mechanisms of boiling. Design engineers, who have to be able to predict heat transfer coefficients for a new system, derive their information in many cases from either previous experience, ad hoc experiments, or from costly pilot plant, rather than fundamental knowledge of the processes involved. Information on boiling heat transfer is not only required for the present-day Nuclear Power Station with its associated steam raising units and for design studies on boiling water reactors, but for every kind of evaporator in practical use.

This work is concerned with the initiation of nucleate pool boiling of saturated and slightly subcooled, i.e. temperature below saturation, water on a metal surface. Nucleate boiling is characterised by the formation of bubbles at discrete centres or sites on the surface. It is true that pool boiling is a special case of heat transfer and that forced convection boiling, in which liquid has an externally applied velocity, has a wider application in industry. On the other hand, pool boiling is better suited to the study of the growth and departure/collapse (depending on whether liquid is saturated or subcooled) of vapour bubbles on a heating surface.

The existence of several regimes of boiling was first

discussed by Nukiyama in 1934 (see McAdams [1]), and a typical pool boiling curve showing these regimes appears in Figure 1; the heat flux Q/A , is plotted against the temperature difference between the heating surface and liquid saturation temperature ($T_{sur} - T_{sat}$), to a logarithmic scale. In the range A - B, heat is transferred by free convection, and evaporation occurs only at the surface of the pool. At B, boiling is initiated, causing an increase in the heat transfer rate so that the curve bends upwards forming a "knee". Beyond the "knee", the curve becomes straight, corresponding to vigorous nucleate boiling. At C, the heat flux goes through a maximum, which is termed the "critical heat flux" and in some way is connected with the overcrowding of bubbles on the heating surface. In the range C - D, part of the surface is insulated by a vapour film and Q/A decreases as ($T_{sur} - T_{sat}$) increases. At point D, the heat flux goes through a minimum, the heating surface being completely covered with a film of vapour. In the film boiling region D - E, heat is transferred by conduction across the vapour film and by radiation from the heating surface. Beyond E, the curve continues until the temperature difference ($T_{sur} - T_{sat}$) corresponds to the melting point of the metal; a further increase in temperature causes "burn-out".

Westwater [2], reviewed several equations published after 1952, for the correlation of nucleate pool boiling of a saturated liquid, and it would seem that a safety factor of at least two should be included in the calculations. In many the factor should be much greater. Most of the equations contain a constant, whose value is either given, or has to be evaluated from experimental

results for a particular liquid-surface combination. The inclusion of this constant is to account for heating surfaces having different nucleation characteristics.

It is pertinent to ask, "what are the nucleation characteristics of a heating surface?" The answer is (i) the incidence of nucleation, (ii) the distribution of active sites and (iii) the bubble frequency at each site. A knowledge of these three factors would give the bubble flux distribution, i.e. the number of bubbles on the heating surface per unit area and unit time, which may then be multiplied by the energy associated with the growth of a bubble, to build up the shape of the nucleate boiling curve.

The nucleate boiling studies to be discussed here were therefore confined to evaluating both the nucleation characteristics of the experimental heating surface, and the energy associated with the growth of a bubble, and to using these values to predict the boiling curve. As a result, only the very beginning of the nucleate boiling regime B - C, in Figure 1, was investigated. The extent of the study is that region outlined in the left hand bottom corner of Figure 1.

The initiation of boiling in a superheated liquid resembles the onset of cavitation in a hydraulic system, where the reduction of liquid pressure is brought about by the rapid relative movement of the liquid and solid boundary surface, and may be related to the start of dropwise condensation on a colder surface. Each of these examples is a nucleation process, and information gained on this phenomena in the field of boiling may prove valuable in

understanding other nucleation processes.

It is widely accepted that a vapour bubble growing in a superheated liquid must have originated from a vapour bubble so small that it was in equilibrium with the surrounding liquid. The mechanical equilibrium of a vapour bubble in a liquid is given by Gibbs [3] equation $p_v - p_L = \frac{2\sigma}{r_c}$, where p_v is the vapour pressure within the bubble, p_L the liquid pressure outside the bubble, σ the surface tension of the vapour-liquid boundary and r_c the critical value of r for equilibrium. The kinetic theory of liquids has also been used to predict the size of the critical nucleus, by adopting a model which assumes the existence of holes in a liquid. Blake [4], in a review of the so called "hole" theory by several authors, has shown that the kinetic theory fails to predict the existence in pure liquids of a bubble nucleus of the size required to explain experimental results. An acceptable alternative explanation is the presence of bubble nuclei by the adsorption of gas in minute cracks or cavities on the metal boundary surface. This explanation is consistent with experimental evidence, which shows bubble formation to be favoured at solid surfaces.

The first step in the preparation of the experimental heating surface was to remove the existing grooves and cavities and introduce cavities with well defined boundaries (see Section 3. 6.). The cavity sizes were then measured by optical means and the distribution approximated by the normal law (see Figure 6). Surface cavities of this kind would seem to be very different from that of a surface found in industry, where, after a long

period of boiling, the surface is probably covered with a film of deposits or oxide. On the other hand, at a recent conference on Boiling Heat Transfer [5], it was pointed out that during nucleate boiling, deposits (silica) were laid down in rings around the bubble sites, thus preserving the cavity distribution. This means that the nucleation characteristics for a clean surface of known cavity distribution may still be the same, even when the surface is covered with a film or scale; although it is possible, however, that some modification may result from oxidation of the cavities themselves, thus reducing their size for criticality.

A model based on an ideal vapour filled surface cavity is postulated in Chapter 5, and an equation (Equation (5. 1. 14.)) derived to determine the superheat which is required to initiate a cavity of characteristic radius r_c' , where r_c' is the cavity mouth radius. This equation was derived using a combination of Gibbs [3] equilibrium equation, and the Clausius-Clapeyron relation, which converts the pressure difference term ($p_v - p_L$) in the equilibrium equation to the corresponding degree of superheat. Equation (5. 1. 14.) is based on the assumption that just prior to initiation the cavity vapour nucleus is in contact with a uniformly superheated liquid. If this is so, then the thickness of the heated liquid layer adjacent to the surface (thermal layer) must be very much greater than the radius of the vapour nucleus; a fact which was borne out in measurements of the thermal layer thickness. In Chapter 6 is described the method of measurement of the thermal layer by a shadowgraph technique,

which is based on the refraction of light rays passing through the liquid. Refraction is caused by the density change corresponding to the temperature change (for an incompressible fluid) in the thermal layer. The thickness of the layer was also measured, by measuring the temperature distribution in the liquid above the heating surface, using a traversing thermocouple, and this is described in Chapter 7.

In this study much effort has been directed towards obtaining reproducible experiments, and a correspondingly large part of the thesis is devoted to describing the experimental apparatus and procedure in detail. Of particular importance is the method by which the heating surface temperature was measured (see Section 3. 7.). Here, a micro-thermocouple (0.002 inch diameter wires) was discharge welded to the lower, insulated surface of the heating strip, in such a way that the thermocouple voltage "pick up" and heat losses from the vicinity of the junction were reduced to a minimum. A calibration procedure, which corrects for the thermocouple voltage "pick up", is described in Chapter 4. The temperature at the heating surface (upper surface of strip) was obtained by subtracting the temperature drop across the strip from the measured lower surface temperature. Chapter 4 also includes a description of the method for preventing corrosion of the boiler walls and the procedure for degassing the heating surface at a low pressure.

The experimental curves of heat flux versus heating surface temperature, for a pressure range from 14.3 to 749 lbs./inch² abs., are described in Chapter 8, and the effect of pressure and sub-

cooling on the different regions of these curves is discussed. The experimental curves at 14.3, 124 and 203 lbs./inch² abs., were extrapolated to zero subcooling and correlated for the effect of pressure by an equation of Forster and Greif [6], (Equation 8. 1. 1.). A discrepancy between free convection results and theory is also discussed in Chapter 8.

The thesis concludes with Chapter 9, which lists the main conclusions of this work and shows that some degree of success has been achieved in the correlation of nucleate boiling parameters.

This success was achieved by the derivation of equations to predict the initiation of boiling, the bubble flux, and the energy associated with the growth of a bubble.

CHAPTER 2

Historical

2.1. Initiation of boiling

Kenrick, Gilbert and Wismer [7] used two methods to investigate the extent to which a liquid can be superheated without boiling taking place.

- (a) Sudden heating of the liquid in open capillary tubes at atmospheric pressure.
- (b) Reducing the pressure on the liquid in closed tubes at a fixed temperature.

The results of many tests carried out in an exactly similar manner showed that the maximum value of superheat temperature varied in a random way from test to test. These variations were attributed to the initiation of boiling from nuclei attached to the walls of the tubes. The radius r_c , of the stable equilibrium vapour nucleus given by Gibbs [3] equation $\Delta p = \frac{2\sigma}{r_c}$, where Δp is the pressure difference across the nucleus boundary and σ the surface tension of the vapour-liquid boundary, was calculated for several different liquids and found to be of the same order of magnitude. Further importance was attached to the equilibrium radius, and it was shown that for the same liquid (ether), the change in maximum superheat temperature with external pressure was satisfied by a constant value of the radius.

Fisher [8] was probably the first to discuss in detail the incomplete penetration of liquid into a surface cavity and the possibility of these cavities being nuclei for bubble initiation.

Dean [9] carried out experiments which showed that surface geometry alone would not produce bubble nuclei, but that the surface should also be contaminated by adsorbed gases or be hydrophobic, or both.

Clark, Streng and Westwater [10] photographed active bubble sites through a microscope, during and after nucleate boiling of ether and pentane on zinc and aluminium surfaces at atmospheric pressure. The active sites were found to be circular pits on the metal surfaces, with diameters ranging from 300 to 3300 x 10⁻⁶ inches.

Claude and Foust [11] boiled ether, normal pentane and Freon 113 on a nickel surface at atmospheric pressure, and derived an equation for the equilibrium radius by applying Gibbs [3] equation to an idealised conical surface cavity. The experimental data at initiation, together with a cavity cone angle and metal-liquid contact angle, were substituted in the equation to give a value for the equilibrium radius. Representative values of cone angle and contact angle were obtained by measuring the cone angles of grooves on the heating surface, which were caused by treatment with emery papers and the contact angles of bubbles, which were about to leave the surface. The equilibrium radius was found to be of the same order of magnitude as the width of the surface grooves.

Westwater [12] classifies surface cavities into four groups depending on their geometry, and then determines for each group whether they will fill with liquid or trap gas. The first group, which are wide shallow pits, are said to fill with liquid; the

second, which are pits with rounded bottoms, can either fill with liquid or trap gas depending on their cone angle and metal-liquid contact angle; the third are narrow pointed pits and cannot be filled by a liquid having a metal-liquid contact angle significantly greater than zero; the fourth group are re-entrant cavities with narrow mouths and are described as excellent gas traps.

Hsu [13] proposes a model in which a vapour nucleus of radius r_c is at rest at the mouth of a heating surface cavity and is surrounded by the relatively cool liquid at bulk temperature. As the heating surface temperature is raised, a liquid layer of limited thickness is heated by transient conduction, until the superheat temperature in the layer at a distance $2 r_c$ from the surface equals the vapour nucleus temperature, and the nucleus starts to grow. The Clausius-Clapeyron and Gibbs [3] equation were combined to give the nucleus temperature. The period of heating is termed the "waiting time", and this ends when the nucleus starts to grow. This criterion for the end of the "waiting time" is one of the major features of the model, since a nucleus can only be effective if the "waiting time" is finite. This fact is therefore used to give the limiting sizes of effective cavities, i.e. maximum and minimum sizes of r_c . The equation for r_c can also be used to give the superheat temperature at initiation of boiling, provided there are heating surface cavities of a wide spectrum in sizes. Each equation, however, requires that the thickness of the heated liquid layer be substituted before it can be used.

Han and Griffith [14] use a model and analysis which is similar to that of Hsu [13] to derive an equation for the maximum and minimum effective cavity radius at a particular superheat temperature. The criterion for bubble initiation in this case is that the superheat temperature in the liquid layer at a distance $\frac{3}{2} \tau_c'$ from the heating surface must be equal to the temperature of the nucleus. The thickness of the liquid layer to be substituted in the equation was evaluated on the assumption that, in free convection heat transfer, the heat is first transferred by unsteady state conduction across this layer. The free convection heat transfer rate may be obtained from either theory or experiment and substituted in the Fourier conduction equation to give the thickness of the layer.

The equations of Hsu [13] and Han and Griffith [14] for the maximum and minimum radius τ_c' , can therefore be used to give the range of effective cavity sizes, provided there is a wide range of cavity sizes on the heating surface (see Section 8. 3.).

This previous work suggests that a theoretical prediction for the incidence of nucleation may be derived, if a characteristic dimension of a heating surface cavity can be related to the critical radius τ_c in Gibbs [3] equation and to the thickness of the thermal layer.

An analysis along these lines is described in Chapter 5 of this study.

2.2. Correlation of nucleate boiling data

A large number of equations have been derived to relate

liquid and surface variables in order to correlate experimental data of nucleate pool boiling. These equations which are intended to apply to saturated liquid, correlate the steep part or "established boiling" region of the boiling curve only. In general, dimensionless analysis is used to relate the variables, and the derivation of two such equations is described here.

Forster and Greif [6] set out to relate the fundamental properties of the boiling liquid, without considering the influence of the boiling surface conditions. A model is proposed, in which the growing bubbles transfer heat by pushing a bubble volume of hot liquid away from the heating surface into the colder bulk liquid. The voids left by the departing bubbles are filled by the bulk liquid, which is then heated and the process repeated. This model was derived after the observation, that only 2% of the heat transferred during boiling was required as latent heat for bubble growth.

The variables are related by the Prandtl number N_{Pr} , and two other groups, which play the part of the Reynolds number N_{Re} and the Nusselt number N_{Nu} in the correlation of forced convection heat transfer data from a solid boundary to a liquid. A coefficient for the growth of a vapour bubble in a highly superheated liquid is inserted in the dimensionless group which represents the Reynolds number, and the critical radius of a nucleus from Gibbs [3] equation in the group representing the Nusselt number. The groups are related in the usual form
$$N_{Nu} = C N_{Re}^m N_{Pr}^n$$
, where C is a constant and has to be evaluated

from one set of experimental results for a particular liquid-surface combination. A value of $\frac{1}{3}$ was chosen for the exponent n , since in many heat transfer problems the Prandtl number to the power $\frac{1}{3}$ correlates the data. The exponent m equal to $\frac{1}{5}$ was derived from an equation of Bonilla and co-workers [15], relating superheat to system pressure at constant heat flux, and for low pressures.

The correlation can, however, be reduced to the form $Q/A = C_1 \Delta T_{sup} \Delta p^{\frac{1}{5}}$, where Q/A is the heat flux at the superheat temperature difference ΔT_{sup} , and Δp the pressure difference corresponding to ΔT_{sup} ; C_1 is a constant which depends on the properties of the liquid and vapour, and on the liquid-surface combination.

Rohsenow [16] claims that most of the transferred heat goes directly from the heating surface to the liquid and that the increased heat transfer rate during boiling is due to the agitation of the liquid by the bubble motion. On this basis, the heat transfer data is correlated by the formulation of a bubble Reynolds number N_{Re} , a bubble Nusselt number N_{Nu} and a Prandtl number N_{Pr} . The bubble diameter at departure, and a mass velocity term, consisting of the product of the mass per bubble, the bubble frequency and the number of bubble sites per square foot of heating surface, define the bubble Reynolds number. The bubble diameter at departure is inserted in the bubble Nusselt number for the characteristic length. These groups are related in the form $N_{Nu} = C N_{Re}^m N_{Pr}^n$, where the constant C has to be evaluated from experimental results for a particular liquid-surface

combination. The variation in the value of C for different liquid-surface combinations is attributed to the omission of the bubble contact angle β from the bubble Reynolds and Nusselt numbers. Constant C is therefore a function of β , and will be determined by the condition of the heating surface and the properties of the fluid. Values of 0.33 and 1.7 for exponents m and n respectively were chosen to fit the final equation to experimental results of Addoms [17]. The equation can be reduced to $Q/A = C_1 \Delta T_{\text{sup}}^{3.03}$, where Q/A is the heat flux at the superheat temperature difference ΔT_{sup} and C_1 a constant which depends on the liquid properties and on the liquid-surface combination.

The equations of Forster and Greif [6] and Rohsenow [16] along with others, are compared with the experimental nucleate boiling results of this work, in Section 8. 1.

CHAPTER 3

Experimental Apparatus

3.1. General description

An apparatus was constructed to enable the experimental study of nucleate pool boiling of water on a metal heating surface, in the pressure range from atmospheric to 1000 lbs./inch² abs., and for a maximum water temperature of 550°F.

The boiler finally decided on takes the form of a stainless steel flanged cruciform (Figure 2), the cruciform shape resulting from the requirements of a vapour condensing surface above the liquid and space for the bulk liquid heaters. The blank flanges allow easy access to the inside of the boiler, and by mounting the test heater on the inside of the bottom flange and the bulk liquid heaters on the inside of the side flanges, their removal for inspection and maintenance is a simple operation. The bulk liquid heaters, together with a heater on the outside wall of the boiler, maintain the liquid temperature at any desired value.

A nitrogen source and pressure control valves supply nitrogen to the boiler and maintain a steady system pressure up to a maximum of 1000 lbs./inch² abs. Water jet pumps and vacuum control valves reduce the pressure within the boiler to a minimum of 1 lb./inch² abs. (see degassing procedure, Section 4. 3. 2.). Windows designed to withstand pressures of over 1000 lbs./inch² are fitted into the opposing side flanges and allow visual study of the bubbles formed on the test heating

surface during nucleate boiling. The boiler and other parts of the apparatus are shown in Figure 3.

3.2. Boiler shell design and fabrication

The boiler shell (Figure 2) was designed for a maximum pressure and temperature of 1000 lbs./inch² abs. and 550°F, in accordance with B.S. 1560 for pressure vessels.

Austenitic stainless steel was specified for the material, and the shell was fabricated by argon-arc welding four short lengths of pipe together to make a cruciform shape. Blank flanges of 8½ inches outside diameter by 1½ inches thick were bolted to the pipe flanges by 8 - ⅜ inch diameter high tensile bolts and nuts, at a pitch circle diameter of 6½ inches.

The complete assembly was stress relieved at 1100°F and then taken apart and the inside walls polished with a rotary wire brush.

3.3. Boiler window design and fitting

Windows were designed to fit into the two opposing blank side flanges and to withstand a maximum boiler pressure of 1000 lbs./inch² absolute (see Figure 4).

A window sight size of ⅜ inch diameter was fixed by the strength of the stainless steel blank flanges. One half of the window frame was machined from the blank flange and the other from a mild steel flange that could be secured to the blank flange by 6 - ⅝ inch diameter studs and nuts. Two 1½ inch diameter by ¼ inch thick "Armourplate" glasses, in complete

contact with each other and each capable of carrying the maximum pressure, were glazed into the metal frame. Pressure seals between the glass and metal, were cut from "Walkerite" jointing and asbestos fibre used to insulate the edges of the glass from the frame. The two halves of the frame were bolted together, taking care that the pressure on the glass was evenly distributed.

3.4. Test heater design and choice of heat supply

A heater having a flat surface in contact with the test liquid was designed to the following requirements:

- (a) A maximum heat flux output that would give established nucleate boiling on the surface.
- (b) Uniform heat flux over the surface area.
- (c) Simple control of the heat flux.
- (d) Accurate assessment of the heat flux and temperature of the surface in contact with the liquid.

Experimental work of Addoms [17] in the pressure range from 14.7 to 2000 lbs./inch² abs. indicates that a heat flux of 2×10^4 B.t.u./ft.² hr. should be sufficient to give "established nucleate boiling" of saturated water in the pressure range from atmospheric to 1000 lbs./inch² abs.

Three different methods of supplying heat to the test surface were considered.

- (1) Steam is supplied at constant pressure and allowed to condense on the surface of the heater, which is away from the test liquid. This has the advantage of constant temperature at the condensing surface. A heat transfer coefficient between

the condensing steam and metal surface has to be estimated, however, before the temperature drop through the wall can be calculated, to give the temperature of the heating surface.

The heat input to the test surface is measured by metering the steam condensate; and the heat output, by measuring the heat taken up by the cooling water, in condensing the vapour generated in the test liquid. Westwater and Santangelo [18] have reported disagreement between these values of the order of 50% for low rates of boiling (6×10^3 B.t.u./ft.² hr.). The accuracy of the temperature measurement is not given, but is probably better than 1%.

(2) Another method which has been used is that of a copper conductor, in which heat is supplied by electrical heaters to a finned end and then conducted through a short length of uniform area to the heating surface. Thermocouples are embedded in the uniform section and the readings extrapolated, to give the temperature of the surface in contact with the liquid. The heat flux can either be calculated from the temperature gradient in the copper conductor, or from the electrical power input to the finned end. One advantage of this system is that the boiling surface can be treated with emery paper to change the nucleation properties.

Claude and Foust [11], using a similar system, estimated that the heat flux measured was accurate to within 22%, and the surface temperature to within 4%, for low rates of boiling.

(3) A third method, which best satisfied the design requirements and was adopted in the present study, consists of generating heat

within the test heater by the passage of electrical current. The heat flux may be calculated directly from the electrical power input to the heater, provided there are no heat losses from the surfaces of the heater that are not in contact with the test liquid (see Section 3. 5.). Difficulty may be experienced in trying to measure the surface temperature, but this is discussed later in Section 3. 7. Control of the heat flux is simple, and since the cross-sectional area of the heater will be small to reduce the power consumption, steady conditions of heat flux and temperature will be reached quickly. Methods (1) and (2) require periods from one to two hours to reach steady conditions after a change in heat input.

The dimensions of the heater were chosen so that the width would be greater than the diameters of the largest bubbles at atmospheric pressure, and that the electrical resistance would be sufficiently large to allow d.c. accumulators to be used as a power supply. Direct current power was selected, because Ellison [19] and Patten [20] noticed that a.c. power caused a 120 cycle/sec. growth and collapse of bubbles. Staniszweski [21], measured bubble diameters of approximately 0.1 inches for saturated liquid at 14.7 lbs./inch² abs. (Figure 29), and these will be the largest bubbles in a pressure range from atmospheric to 1000 lbs./inch² abs.

To satisfy these conditions and bearing in mind the space available within the boiler, a small heater, 0.5 inches wide by 2.0 inches long by 0.003 inches thick in a nickel-chrome material (80% nickel, 20% chrome), was selected. Nickel-chrome

was chosen for its high resistivity, low temperature resistance coefficient and good corrosion resistance.

3.5. Design of heating strip d.c. electrodes, insulation and method of support

The heating strip had to be clamped to d.c. electrodes, fixed horizontally in the plane of the boiler windows, and insulated on the edges and lower surface, so that the heat generated in the strip would be removed at the top surface only. The edges and lower surface were insulated by bonding an insulating material to the strip with adhesive. An insulating material with the following properties was required:

- (a) Good thermal insulation.
- (b) Good electrical insulation.
- (c) Low permeability to liquids.
- (d) Mechanical and thermal stability in water, up to a maximum pressure and temperature of 1000 lbs./inch² abs. and 550°F.
- (e) Good machining properties.

Several plastic materials were considered and tested, and the only material which remained unchanged at a temperature of 550°F. was sintered "Fluon" p.t.f.e., which is manufactured by Imperial Chemical Industries Ltd. The only drawback to using p.t.f.e. is its high rate of expansion with temperature, i.e. a cubic coefficient of thermal expansion of $3.1 \times 10^{-4} \text{ } ^\circ\text{F}^{-1}$ between 68 and 550°F. Because of this, a flexible system was designed for keeping the p.t.f.e. in contact with the lower surface of the strip, so that the p.t.f.e. could expand without

deformation of the strip (see Figure 5).

The heating strip was clamped to the ends of the two nickel plated brass electrodes, which had channel cross sections, to locate the block of p.t.f.e. beneath the lower surface of the strip. The p.t.f.e. block measured 2 inches wide by $2\frac{5}{8}$ inches high by $\frac{3}{4}$ inch thick and was pushed into close contact with the heating strip by nickel plated leaf springs attached to the electrodes. The top of the p.t.f.e. block was machined to a radius of 4 inches, and a channel cut for the strip, so as to locate and thermally insulate the edges of the strip. A silicon adhesive (E.P. 276.) manufactured by I.C.I., that remains tacky up to 550°F ., completed the bond between the p.t.f.e. insulation and heating strip.

The ends of the d.c. electrodes were clamped by nuts to the ends of another pair of circular cross sectioned electrodes, which carry the current through the lower blank flange of the boiler. The circular electrodes were nickel plated and had a flanged section, which, together with mica washers and a screwed follower, electrically insulated the electrodes from the boiler shell and at the same time formed a water seal. The seal could withstand a maximum pressure and temperature of 1000 lbs./inch² abs. and 550°F .. Bushes machined from p.t.f.e. completed the electrical insulation between the electrodes and boiler flange.

3.6. Manufacture of artificial cavities on the heating strip and their measurement

A microscopic examination of the nickel-chrome heating strip

at a magnification of x 1000 showed that the rolling process had produced cavities and grooves, with widths ranging from 200 to 1000×10^{-6} inches. The minimum width which was measured was determined by the resolving powers of the Vickers projection microscope, and it was very likely that cavities and grooves with sizes less than 200×10^{-6} inches were present. These cavities and grooves were not considered satisfactory for the present study, since their boundaries were not clearly defined; and therefore some method of creating artificial cavities was decided upon.

Treatment with emery papers was rejected because this would leave a predominance of grooves on the surface. The groove width could be taken as a representative dimension, but Bankoff [22] believes that grooves are not likely to be good gas or vapour traps, because the gas or vapour can be displaced by the liquid advancing along the groove.

Grit blasting of the strip with a commercial machine was attempted, and although excellent cavities were made, the lack of control of the number and force of the grit particles hitting the strip resulted in distortion of the strip in many cases. To overcome this, a simple paint sprayer was converted into a device for grit blasting. Control of the grit feed was achieved by using different sized nozzles, while the depth of grit penetration was regulated by the air pressure, and by the distance between the grit blasting device and the strip. Tests were carried out to determine the operating conditions, which would produce cavities with diameters of the same size as the

cavities already on the strip, and with a distance between the cavities of approximately 1000×10^{-6} inches.

Several 3 inch lengths of the nickel-chrome strip were polished on one side by No. 3/0 emery paper, followed by No. 4/0 paper, to remove the original cavities; then fixed to a rigid backing plate and grit blasted with a No. 100 carborundum grit, to give the required size and number of cavities. The surface was again polished, but this time on chamois leather with alumina powder suspended in water, to give a bright finish to the metal between the cavities and a clearly defined cavity boundary.

The diameters of the cavities on one strip were measured on the Vickers microscope at a calibrated magnification of $\times 1000$. In many cases the cavities were elliptical in shape, and for these the minor axis dimension was recorded. The microscope was made to scan paths across the strip at random positions along the length, and all cavities which appeared within the screen boundary were measured, until a total of 500 readings had been obtained. The cavity diameters or minor axes were converted to radii in inches and then counted under class sizes with class intervals of 100×10^{-6} inches. The fraction of cavities was plotted against each class mid-mark in the form of a histogram (Figure 6) and approximated by the normal law.

The widths of the strips were measured to an accuracy of 0.001 inches, using a travelling microscope and were found to vary by less than 0.2% along the 3 inch lengths. The thicknesses of the strips were measured to an accuracy of 0.0001 inches, between two $\frac{1}{4}$ inch diameter spherical anvils attached

to a Magna gauge comparator, and were found to vary by less than 3% along the lengths.

Talysurf records of the cavity depths were obtained from the ends of the strips, since the recording stylus produces a slight scratch on a metal surface (see Figure 7).

3.7. Welding technique for fixing a thermocouple to the heating strip

It was considered inadvisable to weld a thermocouple junction to the boiling surface of the test strip, because the thermocouple wires would act in the manner of fins (Figure 8a) and remove heat from the part of the surface where the temperature was being measured. This region would therefore be at a lower temperature than the rest of the surface. The thermocouple junction would also change the nucleation characteristics of the surface.

The alternative was to attach a thermocouple to the lower side of the strip and calculate the temperature drop across the strip. Heat losses from the vicinity of the thermocouple junction by conduction along the wires may be reduced by welding the junction to the centre of the strip area, and leading the wires away from the junction in an isothermal plane, i.e. parallel to the strip surface. See Figure 8b and Jakob [23].

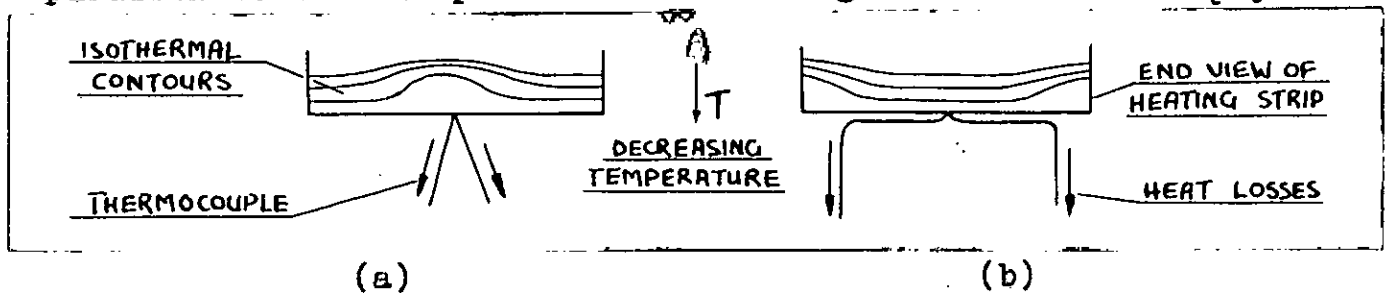


FIGURE 8

This results in the thermocouple wires conducting some heat from the edges of the strip, while leaving the temperature at the junction unchanged.

The main problem in this form of temperature measurement is the knowledge that a thermocouple in electrical contact with a current carrying heating strip will pick up a voltage from the d.c. voltage gradient in the strip. This voltage, which is termed the "pick up", will either add to, or subtract from the voltage generated by the thermocouple. The "pick up" can, however, be reduced to minimum, by making the area of contact between the thermocouple junction and the strip small, at the expense of strength. This can be achieved by using small diameter thermocouple wires and arranging that the wires lie in a constant voltage plane, i.e. at right angles to the current flow (see "Studies in Boiling Heat Transfer" [24]). To make this possible and to reduce heat losses by conduction, chromel and alumel wires of 0.002 inches diameter were selected.

Since a small junction was needed, the wires had to be joined by a discharge welding technique. The ends of the wires to be joined were cut, squared, and placed in clamps, which were part of a jig that allowed the wires to be brought into line and butt-welded. The clamps were manipulated while observing the wires through a microscope. The power for welding the wires was obtained from a capacitor bank, which made available a range of capacitances and discharge voltages (see Figure 10). The best values of capacitance, voltage and gap size were obtained by trial and error, (45 V.d.c. - 16 MFD.). A weld

made in this manner was considered satisfactory, if no change in diameter was noticed when comparing the junction with the wires. Many welds were made and inspected, before several thermocouples were available for welding to the heating strips.

These thermocouples had to be welded to the opposite side of the strips from the boiling side, with the junctions at the centre of the area, and the wires arranged in a plane normal to the current flow. This was done by first marking out the weld positions on the surfaces of the strips with a pencil, and then using the jig to position the thermocouples, prior to making the welds. To make the area of contact as small as possible, the thermocouple was bent sharply at the junction, before fixing in the jig. Figure 11 shows the various stages in making the heating strip thermocouple. The welds were passed as satisfactory if the width of the fillet was equal to the diameter of the wire.

Three strips with thermocouples attached were selected and given a rough check for voltage "pick up". The strips were clamped to electrodes, submerged in water, and a current made to flow in the strips, first in a +ve. direction and then in a -ve. direction, for a d.c. voltage across the strips of 1 volt. The thermocouple e.m.f. was recorded for both current directions, and by the assumption that the heating strip temperature remained constant, the difference between these readings corresponds to twice the "pick up" voltage. For the three strips, the "pick up" was less than 0.04 millivolts for a potential of 1 volt across the strip, and was considered satisfactory. A more detailed

description of the measurement of the "pick up", is given in Section 4. 4.

3.8. Heating surface, bulk liquid and boiler wall temperature measurement

Six thermocouples were made from 0.0076 inch diameter, enamelled chromel and alumel wires, the junctions being formed by twisting the ends of the wires together and silver soldering. The thermocouples were calibrated at the ice point, steam point and freezing point of lead, to check the homogeneity of the thermocouple material. The e.m.f. readings from the six thermocouples agreed at each fixed point to within ± 0.005 millivolts and were considered satisfactory. Four of the thermocouples were to be fixed to the outside wall of the boiler, one used in measuring the bulk liquid temperature, and the other in carrying out a further and more accurate calibration of the chromel-alumel material (see Section 4. 1.).

The thermocouple circuits used in measuring the boiler wall, heating surface and bulk liquid temperatures are now described.

1. Boiler wall thermocouple circuits

These thermocouples were intended for measuring the boiler outside wall temperature and for assisting in positioning the wall heater, to give a uniform temperature over the four limbs of the boiler.

Four 0.0076 inch diameter chromel-alumel thermocouples were bonded now to mid positions on the boiler limbs and the wires

led to the ice point reference, which was removed from the vicinity of the boiler. The ice point reference was constructed by soldering the ends of the thermocouple wires to copper conductors, inserting in glass tubes filled with paraffin, and placing in a vacuum flask filled with finely crushed melting ice. The ends of the copper conductors were soldered to double pole, single throw toggle switches, which were connected in parallel, so that a single pair of conductors could be taken to a portable Cambridge potentiometer. The thermocouple wires and copper conductors were covered with p.v.c. insulating sleeving. A schematic arrangement of the thermocouple circuits is shown in Figure 12.

2. Heating strip thermocouple circuit

A heating strip with thermocouple attached was clamped to the d.c. electrodes and the thermocouple wires arranged so that the heat losses from the junction were minimised (see Section 3. 7.). The arrangement consisted of covering the surface of the strip in the vicinity of the junction with a thin layer of high temperature silicon adhesive, allowing the adhesive to dry, laying the wires on top of the adhesive and applying another layer to fix the wires in position. A small groove was cut in the top of the p.t.f.e. insulating block, a thin film of adhesive applied to the lower surface of the heating strip and the strip pushed into contact with the p.t.f.e. block, making sure that the thermocouple wires fitted into the groove. The remaining lengths of the wires ran down the sides of the p.t.f.e.

block in grooves cut for the purpose and connected with 0.0076 inch diameter chromel and alumel wires, which passed through pressure seals in the boiler lower flange and hence to the cold junction (see Figure 13).

The pressure seals were designed to withstand a maximum pressure and temperature of 1000 lbs./inch² abs. and 550°F, and were constructed by passing each wire through a $\frac{1}{64}$ inch diameter hole, drilled in a $\frac{1}{2}$ inch diameter cylinder of p.t.f.e. and compressing the cylinder by a screwed follower to form the seal (see Figure 14). The cold junction was made in the same manner as described in 1., and the copper conductors connected to terminals on a Croydon precision potentiometer, which had provision for four external circuits. The thermocouple circuit is shown in Figure 12.

3. Bulk liquid thermocouple circuit

Consideration was given to the best position for locating the thermocouple junction, so as to give a representative value of the bulk liquid temperature. Ellison [19] measured a 10°F difference in bulk liquid temperature between a thermometer located $\frac{1}{2}$ inch above the heating surface, and one below and to the side of the heating surface, for a heat flux of 5.2×10^5 B.t.u./ft.² hr.; the thermometer above the strip reading the higher temperature. For this study it was assumed that a position level with the strip and just to one side will record the representative bulk liquid temperature.

To achieve this, a 0.0076 inch diameter chromel-alumel

thermocouple was bonded into grooves cut on the side of the p.t.f.e. block, and a $\frac{1}{2}$ inch length of the thermocouple, terminating in the junction, was bent over at right angles to lie in a plane parallel and slightly lower than the heating surface. The remaining lengths of the thermocouple wires were dealt with in a similar manner to the heating strip thermocouple (see Figure 12).

3.9. Heating strip d.c. supply and power measurement circuits

Two 2-volt Chloride Plante accumulators, with a maximum current rating of 51 amperes for $1\frac{1}{2}$ hours, were arranged in series and connected by heavy copper braid to a 50 ampere double pole, double throw knife switch. A battery charger with a maximum trickle current of 4 amperes, was connected across the accumulators to give an overnight trickle charge. Heavy copper braid carried the current from the knife switch through a circuit, comprising a Zenith carbon plate resistor with an ohmic range from 0.07 to 1.4Ω , a 0.001Ω Croydon standard resistance, and the experimental heating strip. The knife switch allowed the current to flow either in a +ve. or -ve. direction through this circuit. The voltage drop across the heating strip was measured by taking leads from the strip electrodes to a double pole, double throw toggle switch, then to a Croydon volt ratio box, which reduced the voltage by a factor of 150, and hence to the precision potentiometer. The current flow in the heating strip was calculated from the voltage drop across the 0.001Ω standard resistance, leads being taken from voltage terminals

on the standard resistance, to a double pole, double throw toggle switch and then to the potentiometer.

The toggle switches in the voltage and current measuring circuits were operated in conjunction with the knife switch, so that the polarity at potentiometer was the same for both +ve. and -ve. current flow through the heating strip. A schematic arrangement of the d.c. supply and power measurement circuits are shown in Figure 15.

3.10. Bulk liquid and boiler wall a.c. heater circuits

Two 500-watt heating elements were inserted in "Pyrex" glass tubes, which were then bent to a U shape and clamped to the inside surface of the boiler side flanges (see Figure 16). These U-shaped heaters fitted into the horizontal limbs of the boiler when the blank flanges were in position. Electrical leads were taken from the heaters through p.t.f.e. pressure seals in the blank flanges, the heaters connected in series and the leads connected to output no. 1, on a dual output, Zenith "Variac" regulating transformer.

A flat 500-watt "Electrothermal" heating tape, which was later replaced by a 2000-watt "Hot-foil" flat element heating tape, was closely coiled round the boiler limbs, for the complete length of the three shorter limbs and halfway up the longer limb. The heating tape was connected via a Sunvic resistance thermometer temperature controller, to output no. 2 on the "Variac" transformer. The resistance thermometer was held in close contact with the outside wall of the boiler, at the junction

of the limbs. Heat losses from the boiler were reduced by covering the limbs and bottom and side flanges with 1 inch thick glass fibre insulation.

The dual "Variac" provides smooth control of the heater power from zero to the maximum, while the outside wall of the boiler can be maintained at any temperature by adjusting a temperature setting on the controller. A schematic arrangement of the heater circuits are shown in Figure 17.

3.11. Boiler pressure systems

Two pressure systems were required to cover the experimental pressure range from atmospheric to 1000 lbs./inch² abs., and one for low pressure degassing of the heating surface. The systems are described in the following sections.

1. Pressure range from atmospheric to 1 lb./inch² abs.

Two "Speedivac" metal water jet pumps, which reduced the pressure within the boiler, were connected through a stop valve and vacuum gauge to the top flange of the boiler. A fine control needle valve was included in this branch of the system to control the vacuum level in the boiler by allowing air to leak into the system. The vacuum gauge was only used to give a quick indication of the vacuum level. Glass tubing connected the top flange to the vacuum gauge and needle valve, since there was a risk that steam condensing in this part of the circuit might flow back into the boiler when the vacuum was reduced. Copper tube connected the vacuum gauge and stop valve

to the water pumps. A 30-inch mercury manometer was connected to the boiler top flange by glass tubing to complete the system. A schematic arrangement of the system is shown in Figure 18a.

2. Atmospheric pressure

In this case the boiler was open to atmosphere. A water manometer was, however, connected by glass tubing to the boiler top flange, in case of an increase in pressure during vigorous boiling of the test liquid.

3. Pressure range from atmospheric to 1000 lbs./inch² abs.

The pressures in this range were maintained by a nitrogen supply. A pressure regulating valve was attached to a nitrogen bottle and connected by copper tubing to a high pressure stainless steel needle valve, which was in turn connected by stainless steel tubing to the boiler top flange. Three boiler pressure gauges were used to cover the pressure range.

- (a) Bourdon gauge with a range from 0 to 110 lbs./inch², graduated in increments of 2 lbs./inch².
- (b) Dewrance gauge with a range from 0 to 500 lbs./inch², in increments of 2 lbs./inch².
- (c) Budenberg gauge with a range from 0 to 1500 lbs./inch², in increments of 10 lbs./inch².

A stainless steel tube, bent to form a syphon, connected the pressure gauge to the boiler top flange. "Ermeto" high pressure stainless steel couplings connected the nitrogen bottle to the needle valve, and the needle valve and pressure gauge to the top

flange. These couplings can be broken and re-made almost indefinitely, without affecting their efficiency. A safety valve screwed directly into the boiler top flange completed this system. Figure 18b shows a schematic arrangement of the system.

3.12. Auxiliary equipment

A stainless steel condensate shield was designed to fit into the upper limb of the boiler and be located immediately above the liquid level. Steam generated from the test liquid would pass through holes in the shield, but on condensing on the colder top section of the boiler would fall, and be diverted by the shield to the sides of the vessel. The condensate could then be returned to the bulk liquid, without disturbing the temperature of the water in the immediate vicinity of the test surface.

A copper cooling coil was wound on the upper limb of the boiler, immediately below the fixed flange, to cool the top section of the boiler and cause condensation of the steam generated from the test liquid. The cooling coil was only needed when the top section, which was not covered by insulation, was unable to cope with the steam generation. This fact was indicated by a slight increase in the boiler pressure from the test value maintained by the nitrogen supply.

A system of mirrors was erected on one of the side flanges, so that the heating surface could be observed without looking directly into the window. This arrangement was used for

pressures greater than 200 lbs./inch² absolute.

As a further safety measure, a sheet metal panel was erected between the boiler and the recording instruments, which required the attention of the operator. The panel was also used as an instrument panel. Figure 19 shows the recording equipment used in this study.

CHAPTER 4

Experimental Procedure

4.1. Calibration of 0.0076 inch diameter chromel-alumel thermocouple at fixed points on the International Temperature Scale

An accurate calibration of the 0.0076 inch diameter chromel-alumel material was essential, since the heating strip thermocouple described in Section 3. 7. was itself calibrated, by comparing it with the 0.0076 inch diameter chromel-alumel bulk liquid thermocouple described in Section 3. 8. 3.; the water in the pressure vessel being utilised as a constant temperature bath.

A 0.0076 inch diameter thermocouple, whose manufacture has been described in Section 3. 8., was therefore calibrated at the steam point, and at the freezing points of tin and lead, the reference junctions being maintained at the ice point in each case.

The e.m.f. readings at the fixed points were plotted against the corresponding temperatures and the points joined by straight lines to give a calibration curve, which was used for the bulk liquid thermocouple only.

The construction of the fixed points and the method of calibration are described in the following sections.

1. Ice point

The reference junction (commonly called cold junction), is

most easily controlled at a known temperature by placing it in a well designed ice point. The ice point used in the calibration consisted of a vacuum flask filled with finely crushed ice, which was saturated with deionised water. The thermocouple reference junction was constructed by soldering the ends of the wires to copper conductors, inserting them in $\frac{1}{8}$ inch diameter glass tubes filled with paraffin, and pushing the tubes into the crushed ice to a depth of 6 inches. During the calibration, the excess water in the flask was drained off and the flask replenished with ice. The change in the melting point of ice with atmospheric pressure may be neglected.

2. Steam point

The steam point is realised by constructing a hypsometer and, if properly designed, the thermocouple reading should be independent of the rate of heat supply to the boiling water, the length of time the hypsometer has been in operation and the depth of immersion of the thermocouple in the steam.

These conditions were satisfied by using a boiling flask, half filled with deionised water, heated from below, and insulated on the outside wall from above the water line. A water manometer measured the pressure within the flask, which was held constant by allowing steam to escape through a small vent in the flask stopper. The thermocouple entered the flask through a glass capillary inserted in the rubber stopper.

The thermocouple leads from the reference junction were connected to the precision potentiometer and several e.m.f.

readings obtained over a period of time. The steam temperatures corresponding to these readings were calculated from the formula specified in the International Temperature Scale for relating the temperature T_p in $^{\circ}\text{C}$, to the pressure p , in m.m. of Hg, viz.

$$T_p = 100.000 + 0.0367 (p - 760) - 0.000023 (p - 760)^2.$$

3. Freezing point of tin

The e.m.f. developed by a thermocouple at the freezing point of a metal is constant and reproducible, provided that the following conditions are fulfilled:

- (a) The couple is protected from contamination.
- (b) The couple is immersed in the freezing point sample sufficiently far to eliminate heating or cooling of the junction by heat flow along the wires or protection tube.
- (c) The freezing point sample is pure.

The principal apparatus required for carrying out a freezing-point calibration is therefore a suitable furnace, a crucible containing the metal sample and a protection tube for the thermocouple.

In this case, the furnace consisted of a $1\frac{1}{2}$ inch i.d. by 11 inches long refractory tube, wound with a heating element and insulated to a diameter of 7 inches with a suitable heat resisting material. A "Pyrex" glass tube of $1\frac{1}{2}$ inches diameter by 8 inches long was inserted into the refractory tube and filled to a depth of 6 inches, with molten tin having a minimum purity of 99.999%. A sufficient length of the thermocouple wires were insulated from each other with asbestos string, inserted

in a $\frac{1}{4}$ inch diameter "Pyrex" glass tube and immersed to a depth of 5 inches in the molten tin.

The calibration was commenced by maintaining the temperature of the molten tin constant for about 5 minutes and then allowing the furnace to cool slowly, taking readings of the thermocouple e.m.f. at 1 minute intervals. When the freezing point was reached, the e.m.f. remained constant for approximately 10 minutes. Prior to each reading, the tin was stirred by the thermocouple protection tube, to ensure uniform temperature within the metal. The freezing point of pure tin (449.4°F) was obtained from the International Temperature Scale.

4. Freezing point of lead

The thermocouple was calibrated at the freezing point of pure lead using the apparatus and procedure which has been described in Section 4. 1. 3. A freezing point temperature of 621.23°F for pure lead was obtained from the International Temperature Scale (a figure for the percentage purity was not known, and therefore precautions were taken to purify the lead sample).

4.2. Specification for cleaning the heating surface, test liquid and boiling vessel

The importance of maintaining a clean system led to the specification of a cleansing procedure, which was carried out before each experiment. The methods of cleaning the heating surface, test liquid and boiling vessel are described in the following sections.

1. Heating surface

The heating surface was rubbed thoroughly with a paper tissue, soaked in acetone; acetone being preferred to carbon tetrachloride, as the latter deposited a film on the surface. This was followed by rubbing with a tissue, soaked in "deionised" boiling water, and finally dried.

To prevent re-contamination of the cleaned surface, the boiler bottom flange containing the heating strip and its support was bolted to the boiler without delay, the strip support and inside surface of the flange having already been cleaned with acetone.

2. Test liquid

The test liquid was collected by passing water through a Griffin-Raleigh water deioniser until the specific resistance was greater than 5 megohm-cms. A 1400 c.c. charge of water was required to give a water level, which was $\frac{1}{2}$ inch above the heating surface. Both the collecting bottle and measuring jar were carefully cleaned before filling with the deionised water.

3. Boiling vessel

The inside walls of the vessel could only be cleaned with acetone after the blank flanges had been removed. As a result the vertical limbs were cleaned before each test, and the horizontal limbs between every three tests, or when removal of the side flanges was made necessary, for repairs to the bulk liquid heaters or renewal of flange gaskets.

Before filling the boiler with the test liquid, the walls were further cleaned by washing them several times with deionised water.

4.3. Degassing of the heating surface

In any experiment, the aim must be to get reproducible results, for until these are obtained, the true effect of a change in operating conditions cannot be determined.

In nucleate boiling, the ability to reproduce results will be greatly influenced by the size and number of heating surface cavities, which are filled with gas. This number will determine the number of active bubble sites at a particular liquid superheat temperature, which in turn will determine the corresponding heat flux. Degassing is therefore carried out, to reduce the quantity of gas trapped in the heating surface cavities to some equilibrium value which would otherwise be attained after a very long period of boiling.

This result is achieved by vigorous boiling of the test liquid when it is in contact with the heating surface, so that some gas is driven off and gas, which is trapped in the cavities, is then encouraged to diffuse into the degassed liquid. Many cavities will become gas-free, leaving only the cavities which resist degassing because of their favourable geometry and liquid-metal contact angle. These cavities are therefore the sources of bubble nuclei on the heating surface.

The test liquid can be boiled for this purpose, using either auxiliary heaters or the test heating surface. The

latter should accelerate the process, since the departing bubbles will carry away some of the gas from the cavities.

Two different sets of conditions for degassing the heating surface were investigated, by carrying out comparative sets of experiments. A set of experiments consisted of degassing the heating surface, and then taking readings of heat flux and heating surface temperature at atmospheric pressure. The experiments were compared by drawing curves of heat flux versus superheat temperature difference. Before each experiment the heating surface was cleaned, and the boiler charged with fresh deionised water. The two conditions for degassing are described below.

1. Degassing at atmospheric pressure

The heating surface was degassed by boiling the liquid at atmospheric pressure from the bulk liquid heaters and from the test surface ($\frac{Q}{A} = 2 \times 10^4$ B.t.u./ft.² hr. for test surface). A degassing period of $\frac{1}{2}$ hour was allowed in the first instance, and resulted in poor agreement between the boiling curves for successive tests. It was hoped that better agreement would result from an increase in the degassing period from the test surface, the degassing period from the bulk liquid heaters being maintained at $\frac{1}{2}$ hour, which was thought sufficient to degas the liquid. The degassing period from the test surface, was therefore increased in stages of $\frac{1}{2}$ hour up to 2 hours, without showing any real improvement in the agreement between the boiling curves. At this stage method one was abandoned.

2. Degassing at 1 lb./inch² abs.

Method two was carried out by evacuating the boiler (see Section 3. 11.), and maintaining a pressure of 1 lb./inch² abs. above the liquid for $\frac{1}{2}$ hour, the liquid being at room temperature. During this period, a large number of air bubbles formed on both the heating surface and boiler walls, and rose to the liquid surface. At the end of the $\frac{1}{2}$ hour period, the air bubbles having stopped forming, the boiler wall and bulk liquid heaters were switched on to raise the liquid to saturation temperature, corresponding to 1 lb./inch² abs. When saturation temperature was reached, the liquid was boiled both from the bulk liquid heaters and from the test surface ($\frac{Q}{A} = 2 \times 10^4$ B.t.u./ft.² hr.) for $\frac{1}{2}$ hour, to complete the degassing. The vacuum pumps were then stopped, and the boiler pressure raised to atmospheric pressure by introducing nitrogen into the vessel. The boiling tests at atmospheric pressure which followed this procedure showed good agreement. Method two was therefore adopted as standard degassing procedure.

Later in the experimental study this method had to be slightly changed, because, on one occasion, a heat flux of 2×10^4 B.t.u./ft.² hr. from the heating surface was sufficient to cause overheating of the test strip. Overheating was subsequently avoided, by raising the boiler pressure to 3 lbs./inch² abs. at the end of the first $\frac{1}{2}$ hour period of degassing. The boiler wall and bulk liquid heaters were used to raise the liquid to saturation temperature corresponding to 3 lbs./inch² abs. After both heaters were switched off, the boiler pressure was

reduced to 1 lb./inch² abs., causing vigorous boiling from the test surface and the boiler walls. Reducing the boiler pressure from 3 to 1 lb./inch² abs. produces a uniformly superheated liquid of approximately 40°F. When boiling ceased, the pressure was again raised to 3 lbs./inch² abs. and the procedure repeated to give a total degassing time of $\frac{1}{2}$ hour.

4.4. Calibration of the voltage "pick up" by the heating strip thermocouple

At the beginning of this study, the experimental boiling curves were obtained by recording two values of heating surface temperature, at each heat flux level; one, with the current flowing in a +ve. direction and the other with the current flowing in a -ve. direction. The experimental points of heat flux versus heating surface temperature were then plotted, and curves drawn, one through the points for +ve. current and one for -ve. current. The separation of these curves at any one value of heat flux gives the temperature difference, which corresponds to twice the voltage "pick up" of the heating strip thermocouple (see Section 3. 7.). A curve was therefore drawn midway between the first two curves, to give a boiling curve, which corrected the heating surface temperature for thermocouple "pick up".

These preliminary boiling experiments proved that the thermocouple "pick up" was, as expected, proportional to the voltage drop across the heating strip, and that the magnitude of the "pick up" had remained constant throughout several experiments.

The thermocouple "pick up" was therefore calibrated, and the heating surface temperatures in the remaining experiments corrected accordingly.

The calibration was carried out at atmospheric pressure in the following manner. The heating surface, liquid and boiler walls having been cleaned, the heating surface was degassed to give stable boiling. With the liquid held constant at saturation temperature by the bulk liquid heaters, the heating strip thermocouple e.m.f. was recorded, with the current flowing first in a +ve. direction, then in a -ve. direction, and again +ve., for heating strip voltages increasing from 0.2 to 1.6 volts in increments of 0.2 volts. If the second reading with +ve. current flow did not agree with the first, the calibration at that particular voltage was repeated until agreement was obtained.

The difference between the thermocouple e.m.f. values for +ve. and -ve. flow potential were then plotted to a base of heating strip voltage. The straight line determined by the method of least squares was drawn through the points. The thermocouple e.m.f. difference is, however, equal to twice the thermocouple voltage "pick up", and a second line was drawn with a gradient, which was half the gradient of the first line. The thermocouple e.m.f. difference versus heating strip voltage is shown in Figure 20, for the two heating strips used in this study.

It was decided to carry out subsequent tests with a +ve. current flow, the voltage "pick up" being added to, or subtracted from, the thermocouple e.m.f., depending on whether +ve. current

flow gave the lower or higher e.m.f. values for the heating strip used.

4.5. Corrosion of the boiler walls

During a preliminary boiling experiment at 80 lbs./inch² abs., the test water appeared brownish in colour after a boiling time of 4 hours, the discolouration increasing as the test proceeded. On completing the experiment, the boiler was dismantled. Examination revealed corrosion patches on those areas of the boiler walls, which had been in contact with the water. The boiler water had dissolved some of the corrosion products, hence the discolouration of the water.

A check was carried out on the hydrogen-ion concentration of the deionised water, as received from the Griffin-Raleigh water deioniser, and compared with the pH value of the water taken from the boiler after the experiment at 80 lbs./inch² abs. A Pye pH meter, gave a value of 6.6 for water collected from the deioniser, and a value of 4 for the water from the experiment at 80 lbs./inch² abs. This means that the boiler water is slightly acidic initially (pH = 7 for pure water), and that dissociation of the water towards greater acidity had taken place, as the temperature increased to the value corresponding to the pressure of 80 lbs./inch² abs.

Corrosion of the stainless steel boiling tube was reported in studies on forced boiling heat transfer at the University of California [24]. A separate study was devoted to this problem and the main conclusions were that the corrosion of the stainless

steel was due to surface reaction with water at elevated temperatures, and that the corrosion could be reduced considerably by maintaining the pH of the water between 9.5 and 10.0.

Evans [25] in his chapter on boilers and condensers recommends a practice of making the water alkaline, if it is not already so. He refers to various authors who believe that the boiler water should have an initial pH value of 10.5 at ordinary temperatures. He draws attention to the fact that alkalinity maintained by means of sodium (or potassium) hydroxide is only effective on those parts of the surface directly contacted by the boiler water. To prevent corrosion on other parts of the circuit a volatile alkali is required, and ammonia is suggested.

On the basis of these recommendations, it was decided to raise the pH of the boiler water to 10.0 by the addition of ammonia. The ammonia must be added after the degassing at 1 lb./inch² abs., otherwise it will be removed during this process. An experiment was therefore carried out to determine the volume of water remaining in the boiler after degassing, since it was this volume for which a pH value of 10.0 was specified. Of the original charge of 1400 c.c. about 1350 c.c. remained after degassing; 4 c.c. of 0.5% ammonia solution were required to raise the pH of the 1350 c.c. volume from 6.0 to 10.0.

The experiment at 80 lbs./inch² abs. was then repeated with the boiler water treated with ammonia, and showed no signs of corrosion. A test at atmospheric pressure was carried out to

determine whether the addition of ammonia had an effect on the nucleation properties, and hence the heat transfer rate from the test surface. Comparison of the test with previous tests at atmospheric pressure showed excellent agreement, thus proving that the ammonia did not affect the nucleation properties of the heating surface.

Thereafter ammonia was added to the boiler water for each experiment, with the result that the system remained free of corrosion throughout the complete pressure range.

4.6. Effect of pressure and bulk liquid subcooling on nucleate boiling

The experimental procedure is described for tests designed to study the effect of pressure and bulk liquid subcooling on nucleate boiling in the pressure range from atmospheric to 1000 lbs./inch² abs.

The heating surface and inside walls of the boiler were first cleaned (see Section 4. 2.) and the bottom flange bolted to the boiler. Lagging was replaced on the boiler flanges, the d.c. power supply connected to the heating strip electrodes and the thermocouple leads connected to the potentiometer. A fresh supply of "deionised" water was collected (see Section 4. 2.), the inside walls of the boiler washed several times with "deionised" water and the boiler charged with 1400 c.c. of "deionised" water. The condensate shield was fixed in position above the heating surface and the top flange bolted to the boiler.

The top flange was now connected to the low pressure system

(see Section 3. 11. 1.), and the heating surface degassed at 1 lb./inch² abs. by the method described in Section 4. 3. 2. of this chapter. After degassing, 4 c.c. of 0.5% ammonia solution were added to the boiler water, to prevent corrosion of the boiler walls when the water temperature was raised during the experiment (see Section 4. 5.). The boiler top flange was next connected to the high pressure system (see Section 3. 11. 3.) and the boiler pressurised with nitrogen to the desired test pressure (except for those tests at atmospheric pressure). The boiler wall and bulk liquid heaters were switched on to raise the water to the saturation temperature corresponding to the test pressure. When saturation temperature was attained, the liquid was boiled from the heating surface for $\frac{1}{2}$ hour at a heat flux of 2×10^4 B.t.u./ft.² hr., to ensure stable boiling conditions before taking readings of heat flux and heating surface temperature. During this time, the water was maintained at saturation temperature by boiling from the bulk liquid heaters, the boiler wall heater being controlled by the temperature controller to give an outside wall temperature a few degrees above saturation.

At the end of this $\frac{1}{2}$ hour period the heating strip power was reduced to zero. After a delay of 5 minutes, the heating strip thermocouple was calibrated against the bulk liquid thermocouple, the boiling water itself acting as a constant temperature bath. A calibration for the bulk liquid thermocouple was already available, since a thermocouple made from the same reel of material had been calibrated at fixed points

on the International Temperature Scale (see Section 4. 1.).

The bulk liquid heaters were now reduced in power until boiling from them ceased, in order to avoid obscuring boiling from the test surface. For the subcooling experiments, the heater power was reduced further to give the required degree of subcooling.

When the bulk liquid temperature was steady, the heating strip current was increased to 4 amps corresponding to a heat flux of 5×10^2 B.t.u./ft.² hr. The current was increased by stages of 1 amp to 26 amps (heat flux of 2×10^4 B.t.u./ft.² hr.). At each current value the heating strip voltage, current and temperature, together with the bulk liquid temperature, were determined, using the precision potentiometer. Any reading which fluctuated was recorded as a mean value plus the limits of the fluctuation (fluctuation was apparent in the case of the heating strip temperature readings). Whenever possible, the heating strip temperature was recorded when the first bubble site appeared on the surface, and when increase occurred in the number of sites. The number of sites was counted visually, a method which restricted the maximum to about five.

During these boiling experiments, the output from the bulk liquid heaters was reduced in steps, to counteract the increase in heat flux from the test surface and maintain the bulk liquid temperature constant to within $\pm \frac{1}{2}^{\circ}$ F. The boiler pressure was maintained constant throughout by controlling the pressure of the nitrogen blanket.

On completing the test, the heating strip voltage and

current were converted from millivolts to volts and amps, and the heating surface flux calculated from the equation,

$$Q/A = \frac{C_4 VI}{A} \dots \dots \dots (4.6.1.)$$

- where
- Q/A = heat flux (B.t.u./ft.² hr.),
 - V = heating strip voltage (volts),
 - I = " " current (amps),
 - A = heating surface area (ft.²),
 - C_4 = conversion factor (3.41).

The readings of heating strip temperature, i.e. the temperature at the lower surface of the strip, were corrected for the thermocouple voltage "pick up" (see Section 4. 4.) and converted to °F. The temperature at the boiling surface was computed, by subtracting the temperature drop across the strip from the temperature at the lower surface. By making the assumptions that heat is generated uniformly throughout the strip by the steady flow of electrical current, and that the strip is ideally insulated except for the boiling surface, the temperature drop across the strip was calculated by the equation,

$$\Delta T = \frac{Q/A \times x}{2k} \dots \dots \dots (4.6.2.)$$

- where
- ΔT = temperature drop across strip (°F),
 - Q/A = heat flux (B.t.u./ft.² hr.),
 - x = thickness of strip (ft.),
 - k = mean coefficient of thermal conductivity of strip (B.t.u./ft.² hr. °F/ft.).

At the completion of each alternate boiling experiment, the heating strip thermocouple voltage "pick up" was measured for



one value of heating strip voltage, to guard against a change in the "pick up" with time.

The accuracies of the heating surface temperature, bulk liquid temperature and heat flux values are given in the appendices.

CHAPTER 5

Nucleate Boiling Theory

5.1. Bubble initiation

It is assumed that two conditions have to be satisfied before a vapour bubble will form and grow in a pure liquid.

- (a) The liquid must be superheated with respect to the saturation temperature, corresponding to the external pressure acting upon the liquid.
- (b) A nucleus of vapour must be present within the liquid, and in stable equilibrium with the superheated liquid.

The relationship between the size of this nucleus and the degree of superheat is given by an equation derived by Gibbs [3] for the mechanical equilibrium of a spherical vapour bubble in a liquid, and takes the form,

$$p_v - p_l = \frac{2\sigma}{r} \dots \dots \dots (5.1.1.)$$

where p_v is the vapour pressure within the nucleus, p_l the liquid pressure in the plane of the nucleus, σ the surface tension of the vapour-liquid boundary and r the radius of the boundary.

It is seen from this equation that for a particular value of $p_v - p_l$ only one value of radius r will give stable equilibrium, and we denote this value by the critical radius r_c . For variations in r , it is a case of unstable equilibrium, i.e. if $r < r_c$, the nucleus will collapse, and if $r > r_c$, it will expand indefinitely while surrounded by superheated liquid.

It is known from measurements of the temperature in a liquid above a heated surface (see Jakob [26]) that only a thin layer of

liquid adjacent to the surface is sufficiently superheated to initiate boiling, while the rest of the liquid is at some temperature near saturation or less, depending on the history of the liquid. It is then in this region that a nucleus will be found, and since Westwater [12] observed that bubbles grow from imperfections in the metal surface, it seems reasonable to apply Equation (5.1.1.) to the cavities in the experimental heating surface, with radius τ above replaced by the critical radius τ_c .

After the manner of Claude and Foust [11] an ideal vapour filled surface cavity is postulated, with the vapour-liquid interface concave to the liquid (Figure 21), where τ_c is the radius of the interface, τ_c' the radius of the cavity where the vapour-liquid boundary contacts the cavity wall, θ the cavity cone angle and β the contact angle between the liquid and metal, being measured between metal wall and vapour-liquid interface.

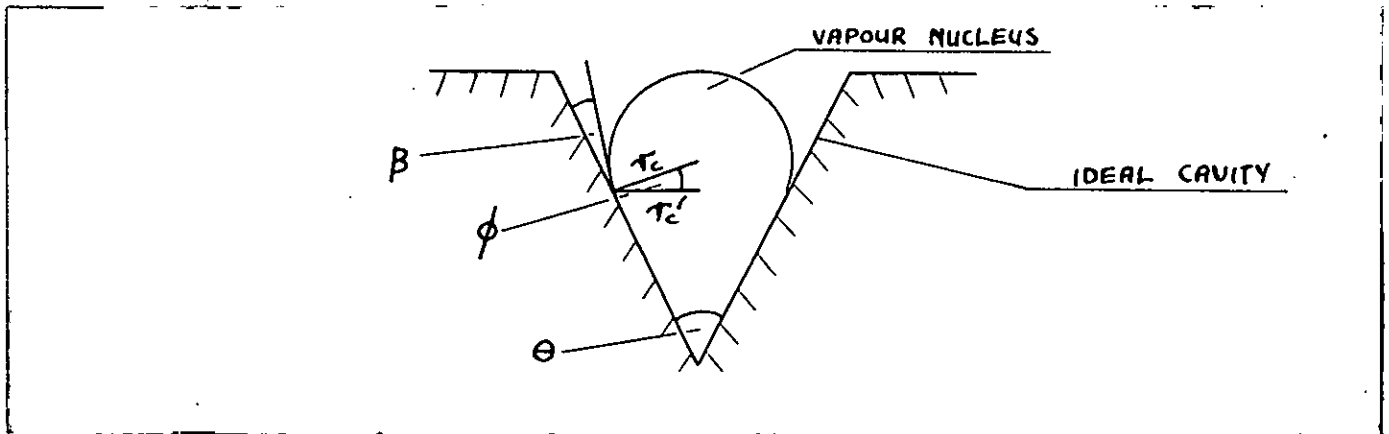


FIGURE 21

From Equation (5.1.1.),

$$p_v - p_L = \frac{2\sigma}{\tau_c} \dots \dots \dots (5.1.2.)$$

where τ has been replaced by τ_c .

If ϕ is the angle included by r_c and r'_c this becomes,

$$p_v - p_L = \frac{2\sigma}{r'_c} \cos \phi \dots (5.1.3.)$$

But $\phi = \frac{\theta}{2} - \beta$

$$\dots p_v - p_L = \frac{2\sigma}{r'_c} \cos \left(\frac{\theta}{2} - \beta \right) \dots (5.1.4.)$$

where the magnitude of $\left(\frac{\theta}{2} - \beta \right)$ is such that, $0 < \cos \left(\frac{\theta}{2} - \beta \right) < 1$. It is assumed that $\frac{\theta}{2} = \beta$, because for the measured cavities on test surface, $\frac{\theta}{2}$ was approximately equal to the average contact angle of 40° , which was measured by Griffith and Wallis [27] for water on a clean metal surface at atmospheric pressure and saturation temperature. Records of the cavity profiles are shown in Figure 7.

Equation (5.1.4.) is rewritten with $\cos \left(\frac{\theta}{2} - \beta \right) = 1$ and becomes,

$$p_v - p_L = \frac{2\sigma}{r'_c} \dots (5.1.5.)$$

The pressure difference $p_v - p_L$ across the nucleus vapour-liquid boundary may be converted to the superheat temperature difference in the liquid, by the Clausius-Clapeyron equation,

$$\frac{dp}{dT} = \frac{LJ}{T(v_v - v_L)} \dots (5.1.6.)$$

where L is the latent heat of vaporisation, v_v the specific volume of the vapour, v_L the specific volume of the liquid, T the saturation temperature of the two phases and J Joule's equivalent.

For pressures up to 1000 lbs./inch² abs. $v_L \ll v_v$ and may be neglected; therefore Equation (5.1.6.) becomes,

$$\frac{dp}{dT} = \frac{LJ}{T v_v} \dots (5.1.7.)$$

If it is assumed that the vapour behaves as a perfect gas

according to the law $p_v v_v = RT$, where R is the perfect gas constant, then substituting for v_v in Equation (5.1.7.) gives,

$$\frac{dp}{dT} = \frac{p v L J}{R T^2} \quad (5.1.8.)$$

Rearranging, and integrating from the vapour pressure corresponding to the liquid pressure p_L to the vapour pressure p_v within the nucleus, at their saturation temperatures we have,

$$\int_{p_L}^{p_v} \frac{dp}{p} = \frac{LJ}{R} \int_{T_1}^{T_2} \frac{dT}{T^2} \quad (5.1.9.)$$

$$\text{and} \quad \log_e \frac{p_v}{p_L} = \frac{LJ}{R} \left[\frac{1}{T_1} - \frac{1}{T_2} \right] \quad (5.1.10.)$$

Substituting Equation (5.1.5.) in Equation (5.1.10.) becomes,

$$\left[\frac{1}{T_1} - \frac{1}{T_2} \right] = \frac{R}{LJ} \log_e \left[1 + \frac{2\sigma}{\tau_c' p_L} \right] \quad (5.1.11.)$$

$$\text{and} \quad T_2 - T_1 = \frac{RT_1 T_2}{LJ} \log_e \left[1 + \frac{2\sigma}{\tau_c' p_L} \right] \quad (5.1.12.)$$

where T_2 is the temperature of the saturated vapour within the nucleus, and for equilibrium across the nucleus boundary it must be equal to the temperature of the superheated liquid surrounding the nucleus; T_1 is the temperature of the saturated liquid at pressure p_L .

If T_2 is denoted by the superheat temperature T_{sup} and T_1 by the saturation temperature T_{sat} , substitution in Equation (5.1.12.) provides,

$$T_{\text{sup}} - T_{\text{sat}} = \frac{R T_{\text{sup}} T_{\text{sat}}}{LJ} \log_e \left[1 + \frac{2\sigma}{\tau_c' p_L} \right] \quad (5.1.13.)$$

Equation (5.1.13.) gives the liquid superheat temperature difference ($T_{\text{sup}} - T_{\text{sat}}$), which is required to initiate bubble growth from a vapour filled conical cavity of characteristic radius r_c , in contact with a uniformly superheated liquid.

It is shown in Section 7.4. that for the heating surface arrangement used in the present study, the thickness of the superheated layer at pressures of 14.4 and 30 lbs./inch² abs. for saturated liquid is very much greater than the radii of the largest surface cavities. It can be assumed, therefore, that for initiation purposes the liquid is uniformly superheated and T_{sup} may be replaced by the heating surface temperature T_{sur} in Equation (5.1.13.) to give,

$$T_{\text{sur}} - T_{\text{sat}} = \frac{R T_{\text{sur}} T_{\text{sat}}}{L_j} \log_e \left[1 + \frac{2\sigma}{r_c' p_L} \right] \quad (5.1.14.)$$

In order to apply Equation (5.1.14.), it is necessary to assume that the largest radius of a cavity, i.e. the cavity mouth radius, will determine the initiation superheat temperature, since it would be impossible to predict how far the liquid will penetrate into a cavity, without a more exact knowledge of the cavity geometry and metal-liquid contact angle.

Equation (5.1.14.) is compared in Figure 22 with experimental measurements of the superheat temperature difference required to initiate bubble growth at the first bubble site. The value of r_c' inserted in Equation (5.1.14.) is 360×10^{-6} inches. This value corresponds to the mouth radius of the largest heating surface cavity, and compares favourably with the value of 550×10^{-6} inches, recorded for the radii of the largest cavities on the experimental heating surface (see Section 8.3.).

5.2. Bubble site density

Consider a metal heating surface, the sizes of cavities in which are distributed normally. As the superheat temperature is increased, the large-sized cavities will initiate first and further superheating will initiate the lesser sized cavities in turn, the total number of active cavities being the summation of the number of cavities for each particular size range.

Sufficient experimental evidence has been obtained by Claude and Foust [11] to indicate that this is in fact what happens, since they have been able to vary the rate of increase in bubble sites with increase in superheat, by changing the surface roughness.

Equation (5.1.14.) is now applied to the range of cavity sizes on the test heating surface, with r_c' becoming the mouth radius of any cavity. Equation (5.1.14.) is

$$T_{\text{sur}} - T_{\text{sat}} = \frac{R T_{\text{sur}} T_{\text{sat}}}{LJ} \log_e \left[1 + \frac{2\sigma}{r_c' h} \right]$$

and may be written in an approximate form, provided that

$$(T_{\text{sur}} - T_{\text{sat}}) \text{ is small and that } \log_e \left[1 + \frac{2\sigma}{r_c' h} \right] \approx \frac{2\sigma}{r_c' h}$$

to give,

$$T_{\text{sur}} - T_{\text{sat}} = \frac{2R T_{\text{sat}}^2 \sigma}{LJ r_c' h} \quad (5.2.1.)$$

Let the superheat temperature difference ($T_{\text{sur}} - T_{\text{sat}}$) be ΔT_{sup} , so that Equation (5.2.1.) becomes,

$$\Delta T_{\text{sup}} = \frac{B}{r_c'} \quad (5.2.2.)$$

where $B = \frac{2R T_{\text{sat}}^2 \sigma}{LJ h}$

Rearranging and differentiating gives,

$$\frac{d\tau_c'}{d(\Delta T_{\text{sup}})} = - \frac{B}{\Delta T_{\text{sup}}^2} \quad (5.2.3.)$$

The distribution of cavity sizes on the experimental heating surface (Figure 6) was approximated by the normal law,

$$\frac{dN}{N} = \frac{1}{\sqrt{2\pi} \epsilon} e^{-\frac{1}{2} \left(\frac{\tau_c' - M}{\epsilon} \right)^2} d\tau_c' \quad (5.2.4.)$$

where $\frac{dN}{N}$ is the fraction of the cavity population N , with radii between τ_c' and $(\tau_c' + d\tau_c')$, M the arithmetic mean value of τ_c' in the whole population and ϵ the standard deviation of the population from the mean.

Rewriting Equation (5.2.4.) provides,

$$dN = C_5 e^{-\frac{1}{2} \left(\frac{\tau_c' - M}{\epsilon} \right)^2} d\tau_c' \quad (5.2.5.)$$

where $C_5 = \frac{N}{\sqrt{2\pi} \epsilon}$

Substituting Equations (5.2.2.) and (5.2.3.) in (5.2.5.) gives,

$$dN = - \frac{BC_5}{\Delta T_{\text{sup}}^2} e^{-\frac{1}{2} \left(\frac{\frac{B}{\Delta T_{\text{sup}}} - M}{\epsilon} \right)^2} d(\Delta T_{\text{sup}}) \quad (5.2.6.)$$

Integrating Equation (5.2.6.) from ΔT_{sup_1} to ΔT_{sup_2} provides,

$$\int_1^2 dN = - BC_5 \int_{\Delta T_{\text{sup}_1}}^{\Delta T_{\text{sup}_2}} \frac{1}{\Delta T_{\text{sup}}^2} e^{-\frac{1}{2} \left(\frac{\frac{B}{\Delta T_{\text{sup}}} - M}{\epsilon} \right)^2} d(\Delta T_{\text{sup}}) \quad (5.2.7.)$$

$$\text{and } N_2 - N_1 = - BC_5 \int_{\Delta T_{\text{sup}_1}}^{\Delta T_{\text{sup}_2}} \frac{1}{\Delta T_{\text{sup}}^2} e^{-\frac{1}{2} \left(\frac{\frac{B}{\Delta T_{\text{sup}}} - M}{\epsilon} \right)^2} d(\Delta T_{\text{sup}}) \quad (5.2.8.)$$

The integration of the right hand side has to be carried out by a graphical method and if this is done from $\Delta T_{\text{sup}_1} = 0$, then $N_1 = 0$ and Equation (5.2.8.) can be rewritten, viz.,

$$N_2 = -BC_5 \int_0^{\Delta T_{\text{sup}_2}} \frac{1}{\Delta T_{\text{sup}}^2} e^{-\frac{1}{2} \left(\frac{B}{\Delta T_{\text{sup}}} - M \right)^2} d(\Delta T_{\text{sup}}) \quad (5.2.9.)$$

Equation (5.2.9.) therefore predicts the number of cavities N_2 , which are active bubble sites at any superheat temperature difference ΔT_{sup_2} .

The number of bubble sites was calculated from Equation (5.2.9.) (see Section 8.3.) for increasing values of ΔT_{sup_2} , and compared with the number of bubble sites on the test heating surface, which were counted visually. The comparison showed that the number of sites predicted by Equation (5.2.9.) was greater than the experimental number by a factor of 10^4 . If the theory is assumed correct, this means that only a very small fraction of the available cavity population are bubble sites (this applies to the early stage of boiling only).

To correct for this a multiplying constant D is introduced. Constant D is defined as the ratio of the active cavity population N^1 to the available cavity population N, such that

$$N^1 = DN \quad (5.2.10.)$$

where $D = 10^{-4}$

Replacing N by N^1 in constant C_5 gives,

$$C_5^1 = \frac{N^1}{\sqrt{2\pi} \epsilon} \quad (5.2.11.)$$

Equation (5.2.9.) now becomes,

$$N_2 = -BC_5' \int_0^{\Delta T_{sup_2}} \frac{1}{\Delta T_{sup}^2} e^{-\frac{1}{2} \left(\frac{B}{\Delta T_{sup} - M} \right)^2} d(\Delta T_{sup}) \quad (5.2.12.)$$

Equation (5.2.12.) is plotted in Figure 23 against the superheat temperature difference ΔT_{sup_2} , for liquid pressures of 14.3, 30 and 122 lbs./inch² abs., and compared with the experimental count of the number of bubble sites at pressures of 14.3 and 29 lbs./inch² abs. Equation (5.2.12.) shows some agreement with experiment, despite the difficulties experienced when counting the number of bubble sites on the experimental heating surface (see Section 8.3.). Figure 23 also shows that Equation (5.2.12.) predicts that the effect of an increase in pressure is to increase the rate at which bubble sites appear. This would seem to agree with experimental results in that, the effect of an increase in pressure on the boiling curve is to decrease the region of weak boiling and bring about "established nucleate boiling" at a lower value of superheat temperature difference (see Section 8.1.).

5.3. Bubble frequency

A study of the bubble frequency at one bubble site revealed large time intervals between successive bubbles at initiation, and a decrease in these intervals as the superheat temperature was increased.

Hsu and Graham [28] define the frequency of bubble formation at a given site by two time periods: namely, the bubble growth period t_g and the bubble waiting period t_w . The waiting period is the time between the departure of one bubble from the heating

surface and the appearance of the next bubble; and the growth period, the time that the bubble grows while remaining attached to the surface. Hsu and Graham [28] measured the waiting and growth periods for twenty bubbles, from high-speed pictures of boiling at atmospheric pressure, for a superheat temperature difference ($T_{\text{sur}} - T_{\text{sat}}$) of 2°F and a bulk liquid subcooling ($T_{\text{sat}} - T_{\text{bulk}}$) of 16°F . These times show an average ratio $\frac{t_w}{t_g} = 9$, the waiting time being quite large with respect to the growth time. The subcooling of 16°F will have some effect on these times, although in this case their graphs of bubble radius versus time is typical of saturated boiling, i.e. the bubble radius remains constant after growing to a maximum size. A possible explanation is that some mistake has been made in estimating the superheat and subcooling temperature differences which make up the measured temperature difference ($T_{\text{sur}} - T_{\text{bulk}}$) of 18°F , since the superheat temperature difference of 2°F seems rather low for nucleate boiling at atmospheric pressure. The ratio of $\frac{t_w}{t_g} = 9$ indicates that the bubble frequency may be estimated by considering the waiting period only, for low rates of boiling (small values of superheat temperature difference).

A simplified model similar to the models used by Hsu [13] and Han and Griffith [14] is proposed to enable a prediction of the waiting time, and hence the bubble frequency. In this model, the waiting time is associated with the time required to raise the temperature of the liquid layer adjacent to the heating surface from bulk liquid temperature to a temperature which will initiate bubble growth at a site. The growth of the bubble

removes a section of the heated layer and allows liquid at bulk temperature to move in and take its place, so that the cycle is repeated.

To enable a solution to be arrived at for the waiting time, it is assumed that the liquid layer is heated by conduction only, that the layer is of constant thickness and that heat is supplied at one side at a constant rate, while the other side is held constant at bulk liquid temperature. The problem is one of transient conduction of heat in a slab, in one dimension x , with a prescribed heat flux Q/A at one side and a constant temperature T_{bulk} , at the other (see Figure 24).

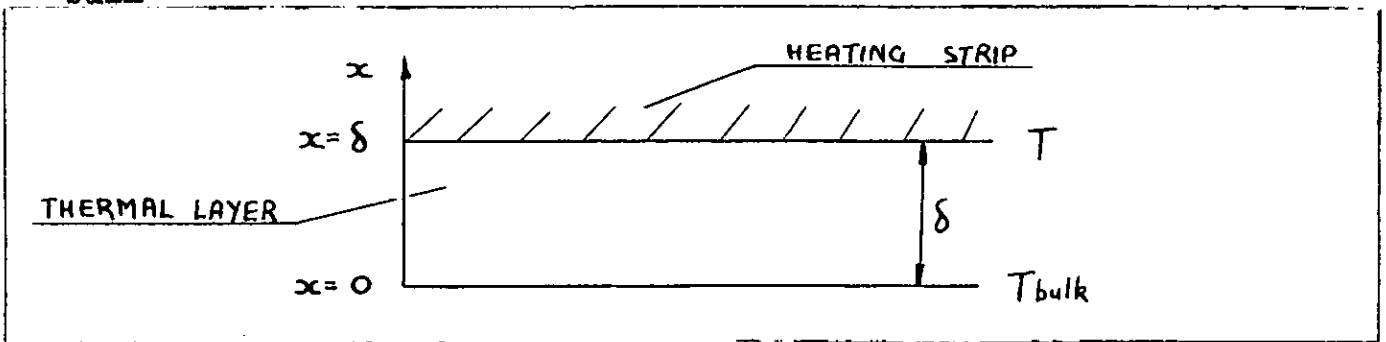


FIGURE 24

Let δ be the thickness of the liquid layer and T be the temperature at $x > 0$, so that $T - T_{\text{bulk}} = \Delta T$.

The one dimensional transient conduction equation is,

$$\mathcal{L} \left(\frac{\delta^2 \Delta T}{\delta x^2} \right) = \frac{\delta \Delta T}{\delta t} \quad (5.3.1.)$$

where \mathcal{L} is the thermal diffusivity and t the time.

The boundary conditions are,

$$\Delta T = 0, \text{ at } t = 0, \text{ for } 0 < x < \delta$$

$$\Delta T = 0, \text{ at } x = 0, \text{ for } t > 0$$

$$-\left(k A \frac{\delta \Delta T}{\delta x}\right)_{x=\delta} = Q = \text{constant, for } t > 0$$

The solution of Equation (5.3.1.) from Carslaw and Jaeger [29], is

$$\Delta T = T - T_{\text{bulk}} = \frac{2 \frac{Q}{A} (\alpha t)^{\frac{1}{2}}}{k} \sum_{n=0}^{\infty} (-1)^n \left\{ \text{ierfc} \frac{(2n+1)\delta - x}{2(\alpha t)^{\frac{1}{2}}} - \text{ierfc} \frac{(2n+1)\delta + x}{2(\alpha t)^{\frac{1}{2}}} \right\} \quad (5.3.2.)$$

If it is assumed, as in Section 5. 1., that the superheat temperature can be replaced by the heating surface temperature for initiation purposes, then Equation (5.3.2.) has to be solved for T at x equal to δ only. Therefore time t is equal to the waiting time t_w , when the temperature T at x equal to δ is equal to the heating surface temperature required for initiation.

Substituting for T, t and x in Equation (5.3.2.) gives,

$$T_{\text{sur}} - T_{\text{bulk}} = \frac{2 \frac{Q}{A} (\alpha t_w)^{\frac{1}{2}}}{k} \sum_{n=0}^{\infty} (-1)^n \left\{ \text{ierfc} \frac{(2n+1)\delta - \delta}{2(\alpha t_w)^{\frac{1}{2}}} - \text{ierfc} \frac{(2n+1)\delta + \delta}{2(\alpha t_w)^{\frac{1}{2}}} \right\} \quad (5.3.3.)$$

Consider the first bubble site at some pressure p_L . The heating surface temperature for initiation from the first site is obtained from Equation (5.1.14.), which is plotted in Figure 22, and gives the initiation superheat temperature difference ($T_{\text{sur}} - T_{\text{sat}}$) versus liquid pressure p_L . If the heating surface temperature T_{sur} and heat flux Q/A corresponding to initiation are substituted in Equation (5.3.3.), it can be solved for t_w . The waiting times t_w , at increasing values of T_{sur} , can be obtained by substituting

the corresponding values of heat flux Q/A in Equation (5.3.3.).

The waiting periods were therefore obtained by this method for the first eight bubble sites at pressures of 14.3, 30 and 122 lbs./inch² abs. The heating surface temperature for initiation at each site was obtained from Equation (5.2.12.), as shown in Figure 23. Figure 23, which gives the number of bubble sites at a superheat temperature difference ΔT_{sup_2} , can be interpreted as the superheat temperature difference that is required to initiate the first bubble site and each site in turn. Experimental measurements of the layer thickness δ (see Chapter 7), at pressures of 14.4 and 30 lbs./inch² abs. for saturated liquid, were substituted in Equation (5.3.3.) in the solution of the waiting periods at the pressures of 14.3 and 30 lbs./inch² abs. A layer thickness of 0.030 inches was assumed for saturated liquid at a pressure of 122 lbs./inch² abs. Experimental values of the free convection heat flux corresponding to the heating surface temperatures T_{sur} were also substituted in Equation (5.3.3.).

The bubble frequencies given by $\frac{1}{t_w}$ were calculated for the liquid pressures of 14.3, 30 and 122 lbs./inch² abs. The bubble frequencies f , for eight bubble sites at the pressure of 14.3 lbs./inch² abs. are plotted in Figure 25 against the superheat temperature difference $(T_{sur} - T_{sat})$. Similar graphs were drawn for the bubble frequencies at the pressures of 30 and 122 lbs./inch² abs. so that the bubble flux ψ , i.e. the number of bubbles, per unit area of heating surface, per unit time, could be computed by summing the bubble frequencies at the bubble sites, for increasing values of $(T_{sur} - T_{sat})$.

Figure 26 shows curves of bubble flux ψ against the superheat temperature difference $(T_{sur} - T_{sat})$, at the pressures of 14.3, 30 and 122 lbs./inch² abs. This is a theoretical prediction only, because it was not found possible to measure the bubble frequencies at each site with the present experimental apparatus.

5.4. Weak nucleate boiling heat flux

In the region of weak nucleate boiling, the heat flux may be determined by the summation of the free convection heat flux, and the heat flux associated with bubble growth at the heating surface. The heat flux in this region is therefore given by,

$$Q/A \text{ weak boiling} = Q/A \text{ free convection} + Q/A \text{ bubble growth} \quad (5.4.1.)$$

Consider first the heat flux associated with bubble growth. This will equal the heat removed from the heating surface by the growth of one bubble, multiplied by the number of bubbles per unit area and unit time, corresponding to the specified heating surface temperature.

The heat removed by a bubble may be estimated with the aid of the model described in Section 5. 3. In this, it was assumed that the growth of a bubble removes a section of the heated liquid layer (thermal layer) from the vicinity of the heating surface. If T_{sur} is the heating surface temperature and T_{bulk} the bulk liquid temperature, then the heat q_b , removed by the growth of a bubble may be written as,

$$q_b = a \times \delta \times \rho \times C_p \times \frac{(T_{sur} - T_{bulk})}{2} \quad (5.4.2.)$$

where a = area of thermal layer removed by the bubble (ft.²),
 δ = thickness of thermal layer at the temperature difference ($T_{\text{sur}} - T_{\text{bulk}}$) (ft.),
 ρ_L = liquid density (lbs./ft.³),
 C_p = specific heat at constant pressure (B.t.u./lb. °F),
 $\frac{T_{\text{sur}} - T_{\text{bulk}}}{2}$ = mean temperature ^{difference} of thermal layer (°F).

It is assumed that the area of the thermal layer removed by the bubble is characterised by a diameter D_2 , which is proportional to the maximum bubble diameter, such that

$$D_2 = E D_{\text{max}} \quad (5.4.3.)$$

where E is a constant.

The area of the displaced thermal layer then becomes,

$$a = \frac{\pi}{4} (E D_{\text{max}})^2 \quad (5.4.4.)$$

Substituting Equation (5.4.4.) in (5.4.2.) gives,

$$q_b = \frac{\pi}{4} \cdot E^2 \cdot D_{\text{max}}^2 \cdot \delta \cdot \rho_L \cdot C_p \cdot \frac{(T_{\text{sur}} - T_{\text{bulk}})}{2} \quad (5.4.5.)$$

Equation (5.4.5.) can now be multiplied by the bubble flux ψ , corresponding to the heating surface temperature T_{sur} to give the heat flux associated with bubble growth. Multiplying by ψ in units of ft.⁻² hr.⁻¹ gives,

$$\frac{Q}{A} \text{ bubble growth} = \frac{\pi}{4} \cdot E^2 \cdot D_{\text{max}}^2 \cdot \delta \cdot \rho_L \cdot C_p \cdot \psi \cdot \frac{(T_{\text{sur}} - T_{\text{bulk}})}{2} \quad (5.4.6.)$$

The free convection heat flux has been correlated successfully in many cases by the Newton Equation,

$$\frac{Q}{A} \text{ free convection} = h (T_{\text{sur}} - T_{\text{bulk}})$$

where h is the heat transfer coefficient.

The coefficient h is derived from dimensional analysis of the free convection problem (see Equation (8.2.2.))

In this case, however, the Newton equation predicted heat flux values, which were less than the experimental ones by as much as 50%. For this reason, experimental values of free convection heat flux were used in Equation (5.4.1.) (see Section 8. 2.).

Equation (5.4.1.) is compared in Figures 27 and 28 with the experimental results in the region of weak boiling for pressures of 14.3 and 30 lbs./inch² abs. respectively. The theoretical curve (Equation (5.4.1.)) was drawn by first drawing an experimental curve of free convection heat flux, calculating the heat flux associated with bubble growth from Equation (5.4.6.) at increments of heating surface temperature T_{sur} , and then adding these values to the free convection curve at the corresponding values of T_{sur} , to give the final curve. The value of constant E required for Equation (5.4.6.) is referred to below.

Experimental values of maximum bubble diameter D_{max} by Staniszweski [21] at pressures of 14.7 and 28 lbs./inch² abs. for saturated liquid were substituted in Equation (5.4.6.) to calculate the heat flux at the pressures of 14.3 and 30 lbs./inch² abs. These values, plotted in Figure 29, show that D_{max} remains constant for increasing values of heat flux. A mean value of maximum bubble diameter was therefore used in Equation (5.4.6.), and assumed constant over the weak boiling region. Because of the scatter in the experimental values in Figure 29,

a negligible error will occur in using a maximum bubble diameter obtained at 28 lbs./inch² abs. and at saturation temperature for a pressure of 30 lbs./inch² abs. and 2.5°F subcooling (see Figure 28). The diameters used in Equation (5.4.6.) were 0.11 and 0.08 ins. for 14.3 and 30 lbs./inch² abs. respectively.

Thermal layer thicknesses δ , of 0.036 and 0.034 inches were substituted in Equation (5.4.6.) for pressures of 14.3 and 30 lbs./inch² abs. respectively and assumed constant over the weak boiling region. These were measured at pressures of 14.4 and 30 lbs./inch² abs. by a thermocouple method, which is described in Chapter 7 of this work. A theoretical value of δ might have been used here, since good agreement has been shown between the "boundary film" thickness from an equation by Chang [33] and the thermal layer thickness measured in Chapter 7 (see Section 7. 4. 2.). The bubble flux ψ was obtained from Figure 26.

The value of constant E was chosen to give the best fit between experiment and theory, and was equal to 1.5 in each case. If the model is correct, this implies that the growth of a bubble disturbs an area whose diameter is 1.5 times the maximum diameter of the bubble. This is to be compared with the work of Hsu and Graham [28], who observed that the growth of a bubble disturbed an area whose diameter was twice the maximum diameter of the bubble.

CHAPTER 6

Shadowgraph Measurement of the Thermal Layer Thickness

6.1. Introduction

The Shadowgraph technique, based on the refraction of light rays as a result of density changes in a medium, is a relatively simple way of observing the density change and, by deduction, the corresponding temperature change in a heated liquid.

In this work the shadowgraph technique was used to measure the thickness of the thermal layer adjacent to the heating surface.

The growth of the layer thickness with increase in heating surface temperature was recorded on film at various stages of free convection and boiling heat transfer. The thickness of the layer was measured from these photographs and compared, at one value of heating surface temperature, with the thickness obtained by traversing the liquid with a thermocouple (see Chapter 7).

The thickness of the thermal layer was measured at liquid pressures of 14.2 and 30 lbs./inch² abs.

With the shadowgraph method, light is projected from a point source so that uniformly divergent or parallel light (using an auxiliary lens) is passed through the thermal layer and is refracted to form a shadow on a translucent screen placed behind the heating surface. The screen allows both visual study of the shadow and photographic recording.

6.2. Application of the shadowgraph method

The application of the shadowgraph method to the study of the temperature distribution in the layer adjacent to a heating surface has been described by Jakob [30]. Figure 30, which is reproduced from his work, shows in a schematic manner what happens when a cylindrical heating surface, in contact with air, receives light at grazing incidence.

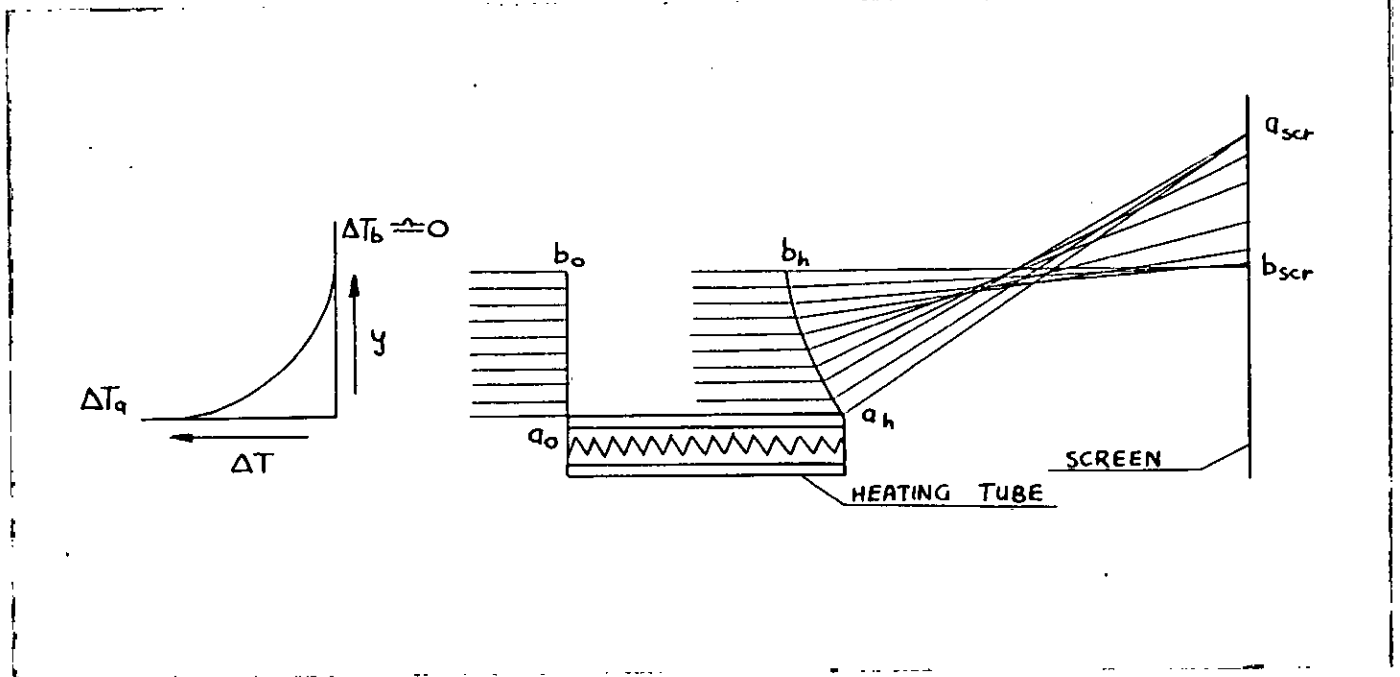


FIGURE 30

The arrows between a_0 and b_0 represent the velocities of parallel rays which arrive at the leading edge of the heating tube and have a plain wave front a_0 , b_0 . At the left of Figure 30, the temperature distribution in the heated layer is indicated by the curve ΔT_a , ΔT_b , where ΔT is the temperature excess over the bulk air temperature.

According to Jakob [30], the temperature drop and corres-

ponding density increase in the y direction will cause the velocity of the rays to change in such a manner that the wave front takes the curved shape b_h , a_h on leaving the heated layer. The light now travels in straight lines to meet the screen, since light propagation is always perpendicular to the wave front. Because of the small curvature of the ends of line ΔTa , ΔTb , the ends of a_h , b_h are also nearly straight, and therefore light is concentrated in bundles close to a_h , a_{scr} and b_h , b_{scr} (termed caustic bundles). Since no light falls below b_{scr} , a deep shadow is formed inside the caustic line at b_{scr} .

Although air has been the fluid considered in the previous discussion, the principle also applies for water.

The most important feature of this technique, however, as far as this work is concerned, is that no light falls below b_{scr} . For this reason, the vertical distance between b_{scr} and the projection of the heating surface on the screen corresponds to the thickness of the heated layer.

It was this fact that suggested the method, which is about to be described, for measuring the thickness of the thermal layer.

6.3. Experimental apparatus

The need for a point source of sufficient brightness to give satisfactory shadowgraphs was satisfied by the illuminating unit from a Vickers projection microscope. The unit consisted of a mercury vapour lamp, condenser lens and iris, positioned to produce uniformly divergent light from a secondary light source.

Because of a stop on the iris this source could not by itself be made sufficiently small. This was corrected by placing an adjustable slit in the light path and using both the slit and iris to regulate the source size.

Refraction irregularities in the boiler windows were prevented from appearing on the shadowgraph screen by making the plane of the secondary light source coincide with the plane of the first window, and by placing the translucent screen close to the second window. The magnification of irregularities in the first window is so great that they are blurred and not readily visible, while irregularities in the second window have no distance in which to build up a separation of the light rays (see "Techniques of Flow Visualisation" by W.F. Hilton [31]). An additional advantage of this arrangement is a magnification of $x.2$.

Several translucent screens were tried, and best contrast with sufficient illumination was obtained using a plain glass covered with a uniform layer of magnesium oxide.

The shadowgraphs were photographed with a 35 mm. single reflex camera using Kodak Tri-X fast film, the pictures being taken at an angle of 15° to the optical axis, to avoid fogging of the film by the light source, which was otherwise slightly visible through the screen.

In the layout of the shadowgraph optical bench shown in Figure 31, the distances between the various optical components are indicated.

6.4. Experimental procedure

Preliminary experiments were carried out to determine the best settings for the illuminating unit iris and the adjustable slit, to give shadowgraphs of good contrast and definition. A camera shutter speed of $\frac{1}{100}$ second and an aperture setting of 2.8 were required to give a bright shadowgraph and to freeze the movement of the thermal layer during boiling.

Before commencing a shadowgraph experiment the heating surface, inside walls of the boiler and test liquid were cleaned (Section 4. 2.), and the heating surface degassed at 1 lb./inch² abs. (Section 4. 3. 2.). When degassing was completed the bulk liquid temperature was maintained constant by the boiler wall heater only, since the internal heaters would have caused unwanted density gradients in the light path. This resulted in a greater degree of bulk liquid subcooling than for those tests in which the internal heaters operated (e.g. series designed to study the effect of pressure and subcooling).

The first picture of the screen was taken at zero heat flux to fix the datum position for the heating surface, since in shadowgraphs the dark areas corresponding to the heating strip and thermal layer are indistinguishable. Further pictures were then taken at various stages of free convection and boiling heat transfer, the heating strip voltage, current and temperature, and the bulk liquid temperature being recorded for each picture.

The shadowgraph pictures were printed with a magnification of x 5, giving a total magnification of x 10, since the actual shadowgraph represents a magnification of x 2 (Section 6. 3.).

The thickness of the thermal layer was obtained, after transferring the position of the heating surface from the datum photograph to the remaining photographs, and measuring the thickness of the dark layer above this position.

Five such records are presented in Figures 32 (b - f), in which the broken white lines represent the position of the heating surface.

6.5. Results and discussion

Shadowgraph photographs of part of the heating surface and liquid are shown in Figures 32 (a - f); the outside diameters of the pictures correspond to the boiler window diameter.

Figure 32a, taken at zero heat flux, gives the datum position for the heating surface; the dark columns indicate two pins which were located in the plane of the heating surface, at a fixed distance apart, to check the photograph enlargement.

Figures 32 (b - d), taken at increasing values of heat flux, show the growth of the thermal layer thickness for free convection heat transfer; the broken white lines represent the position of the heating surface (see Section 6. 4.).

Caustic lines (bright lines) can be seen along the top edge of the thermal layer in Figures 32b and c, and correspond to the caustic line at position b_{scr} in Figure 30. According to Figure 30, a second set of caustic lines corresponding to a_{scr} should be visible in Figures 32b and c, but since these do not appear it is concluded that the temperature distribution adjacent to the heating surface is different from that in

Figure 30. This is confirmed in Figure 37, which represents the temperature measured in the thermal layer using a traversing thermocouple (see Chapter 7), and shows that the temperature distribution adjacent to the heating surface is a straight line.

The thickness of the thermal layer from Figures 32 (b - f) is plotted against the heating surface temperature in Figure 33, and it is seen that the layer thickness reaches a maximum at a temperature of 213.5°F (corresponding to Figure 32d). At a heating surface temperature of 216.8°F boiling is initiated, and at 218.7°F (corresponding to Figure 32e) the average layer thickness is still a maximum. The fluctuations of the layer thickness in Figure 32e may be due to bubble growth at other parts of the heating surface. At 227.2°F (corresponding to Figure 32f) the average layer thickness is less than the maximum, and may be attributed to the increase in the number of nucleation sites and the resulting displacement of the layer by the growing bubbles.

The thickness of the layer, measured at a heating surface temperature of 216°F using a traversing thermocouple (see Figure 37), is plotted in Figure 33 and shows some agreement with the thickness measured from the photographs.

An interesting feature of Figure 32d is the wave form which can be seen at the upper boundary of the thermal layer. Since this motion appeared just prior to bubble initiation, a further experiment was carried out to study this phenomena in the absence of boiling. In this experiment, employing a greater subcooling of the bulk liquid, the layer thickness varied as

follows:

- (a) As the temperature difference between the heating surface and bulk liquid ($T_{\text{sur}} - T_{\text{bulk}}$) was increased from 0 to 15°F, the layer thickness increased uniformly (similar to Figures 32b and c).
- (b) At a temperature difference ($T_{\text{sur}} - T_{\text{bulk}}$) of 15°F, the layer thickness reached a maximum and a wave motion developed at the upper boundary (similar to Figure 32d).
- (c) With a further increase in temperature difference the wave frequency and amplitude increased, until the upper half of the layer became completely turbulent at a temperature difference ($T_{\text{sur}} - T_{\text{bulk}}$) of 20°F.

This means that for free convection heat transfer to water from a flat, horizontal surface (the experimental strip had a radius of 4 inches in the longitudinal direction), the thermal layer develops in three distinct stages as the temperature difference between the heating surface and bulk liquid is increased.

In stage one, the layer is laminar and increases in thickness with temperature difference, reaching a maximum thickness at a temperature difference ($T_{\text{sur}} - T_{\text{bulk}}$) of 15°F. Stage two represents a transition stage from laminar to turbulent flow, in which a wave motion develops at the upper boundary of the layer and increases in amplitude and frequency with temperature difference. Finally is reached stage three, in which the upper half of the layer becomes fully turbulent at a temperature difference ($T_{\text{sur}} - T_{\text{bulk}}$) of 20°F; the lower half of the layer, however, probably remains laminar.

Figure 34 shows the thickness of the thermal layer obtained by the shadowgraph method for a pressure of 30 lbs./inch² abs. The increase in layer thickness with heating surface temperature closely resembles that of Figure 33.

Figures 33 and 34 also show that a temperature difference ($T_{\text{sur}} - T_{\text{bulk}}$) of 15 and 10^oF respectively is required before the layer reaches a maximum thickness. It follows, therefore, that for saturated water at pressures of 14.2 and 30 lbs./inch² abs. (corresponding to Figures 33 and 34) the layer thickness will only be 75% and 65% of the maximum respectively when boiling is initiated, provided the layer growth rate remains the same. This may be an important point when determining the thickness of the thermal layer (or superheated layer) at the initiation of boiling for pressures greater than 100 lbs./inch² abs., i.e. when initiation temperature differences ($T_{\text{sur}} - T_{\text{bulk}}$) are less than 1^oF. On the other hand, the rate of growth of the layer thickness may well increase with liquid pressure.

The shadowgraph method has given some information on the development and thickness of the thermal layer in free convection heat transfer, and would seem particularly suited to determining the regions of laminar and turbulent flow. It is of interest to note that in Jakob [32] the experimental results of free convection heat transfer from a horizontal surface were correlated by the equation in dimensionless variables $Nu = C (Gr \cdot Pr)^{\frac{1}{3}}$, where the exponent $\frac{1}{3}$ is characteristic of turbulent flow.

The experimental boiler of this study was not designed

primarily for the application of the shadowgraph technique, and several design factors, such as the large extent of water in the light path which reduced the transmitted light to a low value initially, prevented greater use of this method. However, if these limitations were avoided in an experimental apparatus, the combination of the shadowgraph technique and high-speed photography should yield even more information on the behaviour of the thermal layer, especially in the nucleate boiling region.

CHAPTER 7

Thermocouple Measurement of the Thermal Layer Thickness

7.1. Introduction

A thermocouple probe was also used to measure the thickness of the thermal layer, by measuring the temperature distribution in the liquid above the heating surface. The thickness of the layer was required specifically for the following reasons:

- (a) To justify the assumption, in Sections 5. 1. and 5. 3., that the thickness of the superheated layer at the initiation of boiling is very much greater than the radii of the largest surface cavities.
- (b) To solve for the waiting time t_w , in Equation (5.3.3.) (by substituting the measured thermal layer thickness for δ).
- (c) To determine whether the shadowgraph technique described in Chapter 6 can be used to predict the thickness of the thermal layer.

The thickness of the thermal layer was measured first at a pressure of 14.7 lbs./inch² abs., and compared in Figure 33 with the thickness measured by the shadowgraph method. The thickness of the layer was next measured at pressures of 14.4 and 30 lbs./inch² abs., and the values obtained, assumed to be the thickness at the initiation of boiling for liquid at saturation temperature.

Two methods of predicting the thickness of the thermal layer were tried: the first, where it is assumed that heat is transferred across the layer by conduction only, and the second by Chang [33], which assumes a wave motion inside the layer, stable

in the lower part and unstable in the upper. The lower part is termed the "boundary film", where heat is transferred by conduction only, and the upper is termed the "wave layer", where heat is transferred by laminar and turbulent flow. The theory of Chang [33] is in best agreement with the experimental results presented here.

7.2. Experimental apparatus

The apparatus consisted of a thermocouple probe and a device, both for moving the probe perpendicular to the heating surface and for indicating the distance of the thermocouple junction from the surface.

1. Thermocouple probe

A 0.002 inch diameter chromel-alumel thermocouple was held in tension by a spring across the ends of a "Fluon" p.t.f.e. insert, which protruded from a stainless steel bridge (see Figure 35a).

The thermocouple junction was formed by butt-welding the ends of the wires, using the discharge welding technique described in Section 3. 7. The bridge position was fixed so that the thermocouple wires lay in the plane of the heating strip longitudinal axis, and the junction was above the centre of the strip area (Figure 36).

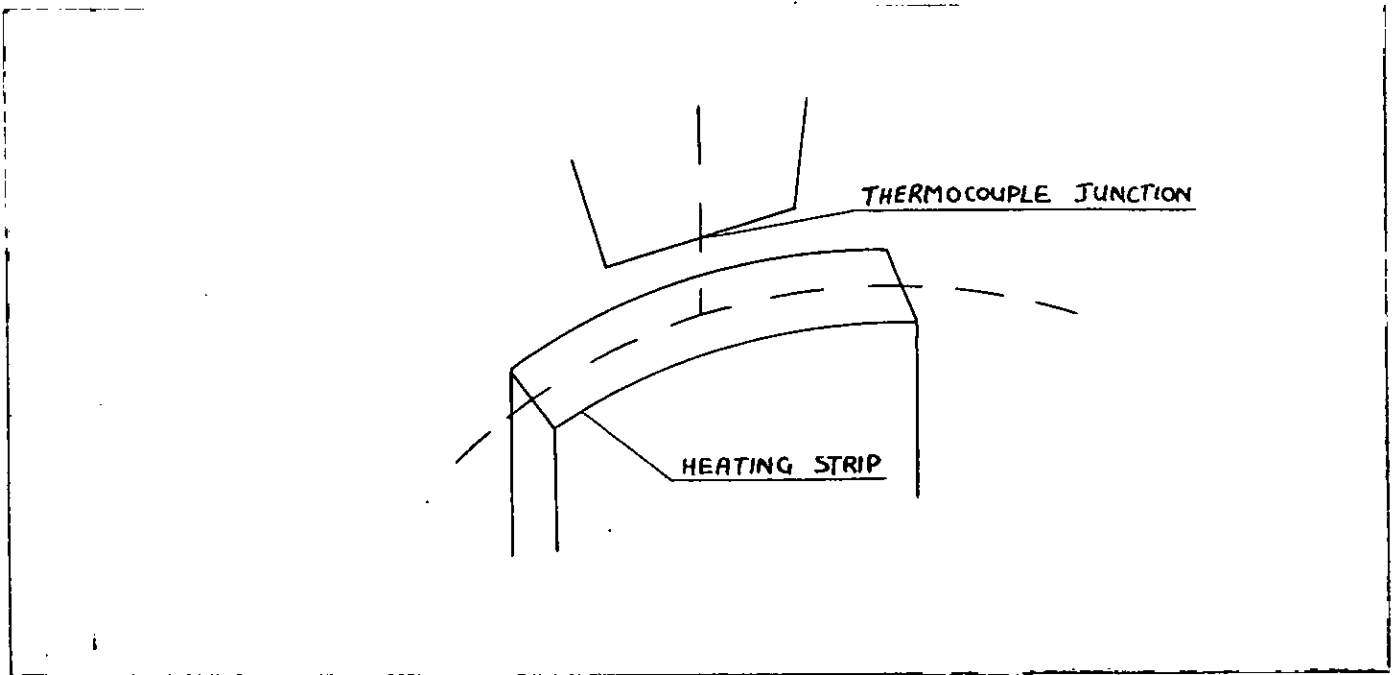


FIGURE 36

Starting from this position, the probe was lowered until the thermocouple junction contacted the heating surface to give a datum height of 0.001 inches (it is assumed that the thermocouple measures the mean temperature of a layer of 0.002 inches thickness). The heat losses from the thermocouple junction by conduction along the wires are minimised by this arrangement, since the thermocouple wires close to the junction are in a near-isothermal plane.

The tensile force on the thermocouple was applied by a metal coil spring and a p.t.f.e. leaf spring arranged in series. This method was preferred to bonding the thermocouple wires to the bridge, since the bonds had proved unreliable at temperatures exceeding 212°F. Tension was applied initially by pulling the wires through several $\frac{1}{64}$ inch diameter holes in the p.t.f.e.

leaf spring, the wires being prevented from slipping by the friction force between the wires and p.t.f.e.

The ends of the 0.002 inch diameter chromel and alumel wires were silver soldered to 0.0076 inch diameter chromel and alumel wires respectively. The 0.0076 inch diameter wires were passed through several holes in a p.t.f.e. ring attached to the $\frac{1}{4}$ inch diameter rod of the probe. This prevented an external force from being applied to the spring system by the 0.0076 inch diameter wires when the probe was raised or lowered. The wires were then passed through a p.t.f.e. pressure seal in the boiler top flange to the cold junction; the pressure seal (Figure 35b) was similar to the pressure seal described in Section 3. 8. 2. Connections between the cold junction and potentiometer were of copper.

"Fluon" p.t.f.e. was used in all cases to insulate the thermocouple wires from the metal parts.

2. Probe mechanism

The mechanism (Figure 35c) included a brass body, a micrometer head and a coupling to connect the micrometer anvil to the $\frac{1}{4}$ inch diameter nickel plated rod of the probe. A pin, located in slots in the brass body, prevented the transmission of rotary movement from the micrometer anvil to the $\frac{1}{4}$ inch diameter rod. The clearance in the coupling resulted in a backlash of 0.001 inches. A mild steel adaptor connected the brass body to the boiler top flange, and at the same time compressed a p.t.f.e. ring to form a pressure seal on the vertical rod. With this

arrangement the vertical movement of the thermocouple probe was limited to $\frac{1}{2}$ inch.

7.3. Experimental procedure

When a d.c. voltage is applied to the heating strip electrodes, a d.c. field will be established in the water between the electrodes, being strongest near the heating surface. A thermocouple measuring the liquid temperature in this region will therefore be expected to "pick up" a voltage from this d.c. field. This "pick up" will either add to, or subtract from, the thermocouple e.m.f. corresponding to the liquid temperature.

For this reason a preliminary test was carried out to determine whether the probe thermocouple would "pick up" a voltage from the d.c. field. This was done by simply replacing the probe thermocouple with a chromel wire of similar dimensions, to eliminate the e.m.f. corresponding to the liquid temperature. A d.c. voltage was then applied to the heating strip electrodes and it was noted whether or not a voltage appeared across the ends of the chromel wire. The test was repeated for various heights of the probe and in each case the voltage "pick up" was zero.

Before commencing an experiment to measure the thickness of the thermal layer, the heating surface, inside walls of the boiler and test liquid were cleaned (Section 4. 2.), and the heating surface degassed at 1 lb./inch² abs. (Section 4. 3. 2.). After degassing, the probe and heating strip thermocouples were

calibrated under conditions of boiling of the test liquid from the bulk liquid heaters, the boiler wall heater maintaining the outside boiler wall temperature a few degrees above the saturation temperature corresponding to the test pressure.

The output from the bulk liquid heaters was reduced until they operated in the free convection region, and a period allowed for the bulk liquid temperature to become steady. The probe was lowered towards the heating surface, and the reading on the micrometer noted when the thermocouple junction touched the surface. Contact between the junction and surface was indicated on an avometer, by the sudden drop in resistance between one of the heating strip electrodes and one of the probe thermocouple wires. Several readings of the contact position were obtained, the probe being raised and then lowered each time so as to eliminate backlash. The readings agreed to within ± 0.00025 inches.

When the bulk liquid temperature was steady, the probe was raised to a starting position of about 0.1 inches above the heating surface. At this position a voltage was applied to the heating strip and regulated to give the desired heating surface temperature. The heating strip, probe and bulk liquid temperature, together with the heating strip voltage and current, and probe position, were recorded. All these readings, with the exception of the heating strip voltage and current, were repeated while the probe was lowered in varying increments towards the heating surface until contact was made. The heating strip and bulk liquid temperatures were maintained

constant throughout. At the completion of the test, the heating strip voltage and current and probe contact position were again recorded, and the contact position found to agree with the initial readings to within the tolerance limits of ± 0.00025 inches.

Since it was assumed in Section 7. 2. that the probe thermocouple measures the mean temperature of a layer of 0.002 inches thickness, the micrometer readings of probe height were therefore corrected by adding the datum height of 0.001 inches to them. With this apparatus, it was thus possible to measure the temperature in the liquid to within approximately 0.0015 inches of the heating surface with an accuracy of ± 0.00025 inches (the backlash was eliminated by rotating the micrometer thimble in one direction only when lowering the probe).

7.4. Results and discussion

Figure 37 shows the temperature distribution in the liquid above the heating surface at a pressure of 14.7 lbs./inch² abs., the bulk liquid and heating surface temperatures being 202 and 216°F, respectively. The experimental points were fitted by two straight lines drawn in by eye. The first line, drawn through the points in the proximity of the heating surface, shows the large decrease in temperature across the thermal layer. The second line, drawn through the points above this region, shows that the bulk liquid temperature is maintained almost constant by the mixing effect of convective currents. A thermal

layer thickness of 0.020 inches was obtained from the temperature distribution by extrapolating both lines until they intersected. The height at which the intersection takes place is assumed to be the thickness of the layer.

Between the regions of thermal layer and bulk liquid, however, there must be a transition zone to correlate the two regions, without an abrupt change in temperature. A broken line is therefore drawn in Figure 37 to represent the temperature distribution across the transition zone, giving a smooth change in temperature from the thermal layer to the bulk liquid. The thickness of the thermal layer is still determined, however, by the intersection of the full lines, since a transition zone does not give a clear indication of the thickness of the layer.

The thermal layer thickness of 0.020 inches from Figure 37 is compared in Figure 33 with the thickness measured by the shadowgraph method. The heating surface temperature of 216°F in Figure 37 was selected to correspond with the maximum layer thickness in Figure 33 (without boiling). The bulk liquid temperature of 202°F in Figure 37 is 3.5°F higher than the bulk temperature in Figure 33, but this is considered unlikely to affect the comparison. Figure 33 shows good agreement between the two methods of measuring the thickness of the layer, when it is realized that the presence of a transition zone makes it difficult to define the thickness of the thermal layer. It is more than likely that the shadowgraph method (Chapter 6) measures the thickness of the layer at the boundary between the transition zone and the bulk liquid region. If this is the case, then the

thickness of the thermal layer in Figure 37 is nearer 0.030 inches and is in better agreement with the thickness obtained by the shadowgraph method in Figure 33.

Figure 37 also shows that the temperature of the bulk liquid above the thermal layer is greater than the temperature of the bulk liquid, which is measured by the bulk liquid thermocouple, i.e. 202°F. The bulk liquid thermocouple was located level with the heating surface and just to one side (see Section 3. 8. 3.). This position was chosen to measure the bulk liquid temperature, on the basis of an assumed overall liquid flow pattern for free convection and the early stage of nucleate boiling. The assumed flow pattern of Figure 38 shows the colder bulk liquid moving in from the side to the heating surface, where it is heated, rising and returning to complete the cycle.

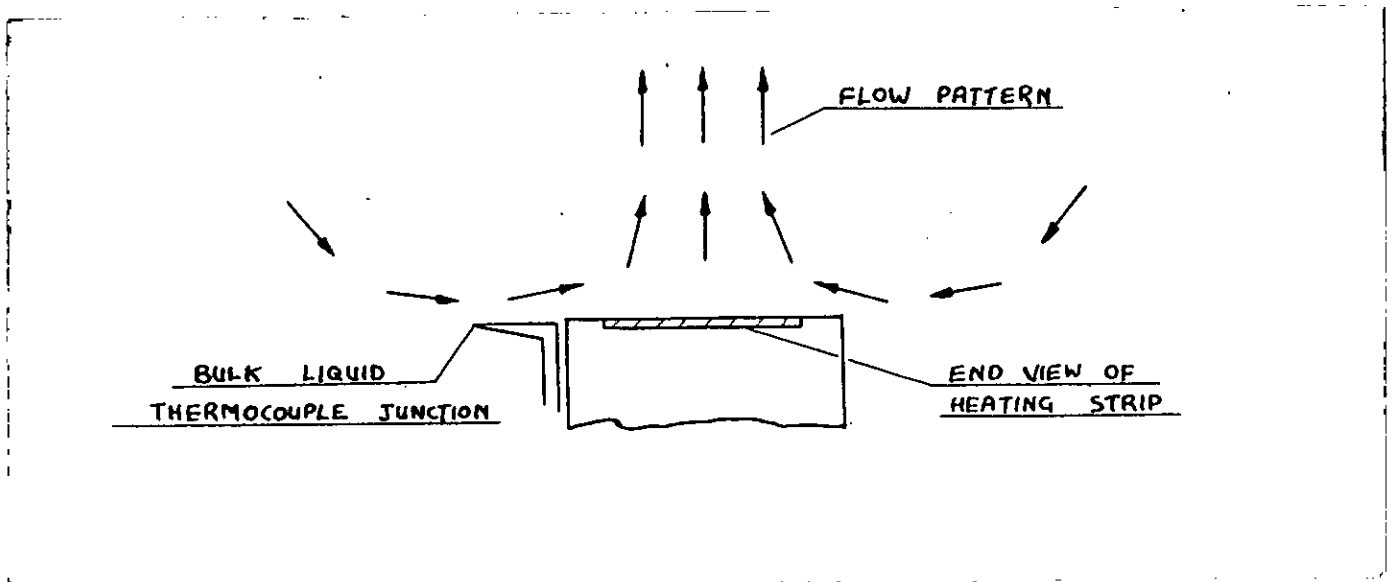


FIGURE 38

The bulk liquid thermocouple, therefore, measures the temperature of the assumed colder bulk liquid, to the side of the heating surface. This temperature is considered representative of the bulk liquid temperature to which heat is being transferred.

Figures 39 and 40 show the temperature distribution above the heated surface at pressures of 14.4 and 30 lbs./inch² abs., for bulk liquid temperatures of 206.5 and 245.5°F, and heating surface temperatures of 215.5 and 253.5°F respectively. Lines were drawn through the experimental points as for Figure 37, and the thickness of the thermal layer again obtained by extrapolating the straight lines. Figures 39 and 40 indicate a thickness for the thermal layer of 0.036 and 0.034 inches respectively. These values were assumed to be the thickness at the initiation of boiling for saturated liquid, in order to satisfy the requirements of (a) and (b) in Section 7. 1. In actual fact, the heating surface temperatures in Figures 39 and 40 are less than the initiation values by 2.2 and 0.3°F respectively, since bubble growth at the first site would have caused unwanted temperature fluctuations in the thermal layer. The bulk liquid temperatures in Figures 39 and 40 are less than the saturation temperatures by 4.5 and 5.0°F respectively, as a result of operating the bulk liquid heaters in the free convection region only (the heating surface and probe would have been obscured by boiling from the bulk liquid heaters). These factors are considered unlikely to produce a significant change between the measured thermal layer thickness and the thickness at the initiation of boiling for saturated liquid.

ALCRA HI-SPEED 11x14

DOCUMENT CUE LISTING , NORM[M4C2 : LP00 ON 16/11/70

CONSOLIDATED BY XPCK 10C DATE 16/11/70 TIME 18/14/4

PROGRAM M4C2
EXTENDED DATA (22AM)
COMPACT PROGRAM (DBM)
CORE 2240

SEG COLLAPSPRESS
ENT FTRAP
ENT FRESET

LAST BUCKET USED OF PROGRAM FILE(0) IS 20

The superheated layer thickness is the part of the thermal layer thickness between the heating surface temperature T_{sur} and the saturation temperature T_{sat} corresponding to the liquid pressure. The thickness of the superheated layer in Figures 39 and 40, corresponding to the pressures of 14.4 and 30.0 lbs./inch² abs., is therefore 0.024 and 0.018 inches respectively. These values prove that the thickness of the superheated layer, at pressures of 14.4 and 30 lbs./inch² abs. for saturated liquid, is very much greater than the radii 550×10^{-6} inches of the largest cavities on the experimental heating surface (see Figure 6).

Two methods of predicting theoretically the thickness of the thermal layer were tried and are described below.

1. Conduction equation

It is assumed that the heating surface heat flux is transferred first by conduction only across the thermal layer. The thickness of the layer is accordingly given by the Fourier equation for steady state conduction written in the form,

$$\delta = \frac{k(T_{sur} - T_{bulk})}{Q/A} \quad (7.4.1.)$$

where δ = thermal layer thickness (ft.),

k = mean coefficient of thermal conductivity of the layer/B.t.u./ft.² hr. °F/ft.),

T_{sur} = heating surface temperature (°F),

T_{bulk} = bulk liquid temperature (°F),

Q/A = heating surface heat flux (B.t.u./ft.² hr.).

The experimental values of T_{sur} , T_{bulk} and Q/A are substituted in Equation (7.4.1.), which yields a thermal layer thickness of 0.019 inches as compared with the measured thickness of 0.020 inches in Figure 37, and a layer thickness of 0.022 inches as compared with 0.036 inches in Figure 39. Figures 37 and 39, corresponding to pressures of 14.7 and 14.4 lbs./inch² abs., are reproduced in Figure 41 with the temperature gradients according to Equation (7.4.1.) shown as broken lines. Figure 41 shows that Equation (7.4.1.) predicts the thickness of the thermal layer quite accurately for a bulk liquid subcooling of 10°F (Figure 37), but much less so for a subcooling of 4.5°F (Figure 39). It would seem that a process other than conduction determines the thickness of the thermal layer at atmospheric pressure when the bulk liquid temperature approaches saturation temperature.

2. Chang's equation

Chang [33] proposes a mechanism for non-boiling convection from a horizontal heating surface. It is assumed that, near the heating surface, heat is transferred by conduction only resulting in a steep temperature gradient; further from the surface, in the bulk of the liquid, convection alone is operative and the fluid is so well stirred up to be at a constant temperature. These two regions are termed the "boundary film" and the "convective core" respectively, and between them there is a transition zone, part of which is termed the "wave layer". A stable wave is assumed to exist in the

"boundary film", and the wave motion in the "wave layer" changes from stable wave to full turbulence. This means that as a result of wave motion, considerable periodic motion of fluid parallel to the boundary surface may exist, and therefore the fluid in the "boundary film" of a horizontal surface is not in stagnation. Because of the wave motion the layer will not be of uniform thickness, and therefore the average thickness of the "boundary film" is designated by δ_w . The thickness of the "wave layer" is denoted by a , and a and δ_w are related by $a = \chi \delta_w$.

The heat transfer problem is solved by determining the amplitude of the wave in the upper stratum of the "wave layer", which in turn determines the thickness of the "boundary film" δ_w . The thickness of the "wave layer" is given by,

$$a = \left[\frac{8\pi^2\chi}{1+\chi} \right]^{\frac{1}{3}} \left[\frac{\mu k_a}{g \rho_c (\rho_c - \rho_a) C_{Pa}} \right]^{\frac{1}{3}} \quad (7.4.2.)$$

where μ = dynamic viscosity (lbs./ft. hr.) (evaluated at mean temperature of gross layer $a + \delta_w$),

k_a = coefficient of thermal conductivity (B.t.u./ft.² hr. °F/ft.) (evaluated at mean temperature of wave layer),

g = acceleration of gravity (ft./hr.²),

ρ_a = density (lbs./ft.³) (evaluated at mean temperature of wave layer),

ρ_c = density (lbs./ft.³) (evaluated at convective core temperature),

C_{p_a} = specific heat at constant pressure (B.t.u./lb. °F)
 (evaluated at mean temperature of wave layer),

χ = constant ≈ 1 .

With the relationship $a = \chi \delta_w$, the thickness of the "boundary film" δ_w is therefore,

$$\delta_w = \left[\frac{8\pi^2}{\chi^2(1+\chi)} \right]^{\frac{1}{3}} \left[\frac{\mu k_a}{9\rho_a(\rho_c - \rho_a)C_{p_a}} \right]^{\frac{1}{3}} \quad (7.4.3.)$$

If ΔT_{sa} is the temperature difference across the "boundary film" and ΔT_{ac} the temperature difference across the "wave layer", then a relationship between ΔT_{sa} and ΔT_{ac} is obtained by the consideration that the temperature gradient of the "boundary film" must be the same as that of the "wave layer" at their common boundary. This relationship together with $\Delta T_{sc} = \Delta T_{sa} + \Delta T_{ac}$ gives,

$$\Delta T_{sa} \approx \frac{4}{4 + \sqrt{\pi\chi}} \Delta T_{sc} \quad (7.4.4.)$$

Chang [33] assumed a value of $\chi \approx 1$. The assumption of $\chi \approx 1$ is justified by the observation that the "boundary film" and the transition zone here can be compared with the laminar sublayer and buffer zone in fluid dynamics. Nikuradse's experiments (see Bakhmetoff [34]) show that the thickness of the buffer zone is about four times that of the sublayer, and since the "wave layer" occupies one quarter of the transition zone in this case, then the "wave layer" will have the same thickness as the "boundary film".

The thickness of the "boundary film" δ_w , and "wave layer" a , were calculated from Equations (7.4.2.), (7.4.3.) and (7.4.4.) for

the experimental conditions in Figures 37 and 39. The corresponding temperature gradients are plotted in Figure 41 as broken lines for comparison with the temperature gradients measured by the probe thermocouple. The comparison shows good agreement between the thickness of the "boundary film" δ_w from Equation (7.4.3.), and the thickness of the thermal layer δ from the measured temperature gradients at pressures of 14.7 and 14.4 lbs./inch² abs. for bulk liquid subcooling of 10 and 4.5°F respectively (corresponding to Figures 37 and 39). An assumed shape for the temperature distribution corresponding to the "wave layer" thickness a is shown in Figure 41. There would seem to be some disagreement between the thickness of the "wave layer" a , from Equation (7.4.2.), and the corresponding thickness of the transition zone, which was assumed and drawn in Figure 37 as a broken line. Since Chang [33] assumed conduction only in the "boundary film", the value of δ_w from Equation (7.4.3.) may be inserted in the Fourier Equation (7.4.1.) to determine the flux Q/A corresponding to Figures 37 and 39. Equation (7.4.1.) gives heat flux values of 2.03×10^3 and $1.04 \times 10^{2.3}$ B.t.u./ft.² hr., compared with the experimental values of 3.55×10^3 and 2.04×10^3 B.t.u./ft.² hr. in Figures 37 and 39 respectively.

Apart from this disagreement, the mechanism proposed by Chang [33] is very important because of the agreement between the "boundary film" thickness from Equation (7.4.3.) and the thickness of the thermal layer measured by the probe thermocouple. It has been shown, therefore, that this method may be used to predict the thickness of the thermal layer at the

initiation of boiling for saturated and slightly subcooled liquid, at atmospheric pressure.

CHAPTER 8

Results and Discussion

8.1. Effect of liquid pressure and subcooling on heat flux

Figures 42 to 48 show the experimental curves of heat flux versus heating surface temperature at liquid pressures of 14.3, 122, 201, 279, 401, 549 and 749 lbs./inch² abs., the curves having been drawn in by eye to fit the points. (During the experiment at 1000 lbs./inch² abs. the boiler wall heater "burned out" and it was not possible to repeat the experiment.) The degree of subcooling ($T_{\text{sat}} - T_{\text{bulk}}$), increases with pressure from 0°F at 14.3 lbs./inch² abs. to 13°F at 749 lbs./inch² abs. This results from restricting the bulk liquid heaters to the region of free convection heat transfer only during the experiments. Some of these experiments have been repeated and in each case reproduce the results. (see Tables 1 to 12 in the Appendices).

Figure 42, which refers to a pressure of 14.3 lbs./inch² abs., shows that heat is transferred firstly by free convection as the heating surface temperature is raised above the bulk liquid temperature. The free convection curve was assumed to be linear for this and other experimental curves. The equation

$N_{Nu} = 0.16 (N_{Gr} \cdot N_{Pr})^{\frac{1}{3}}$, suggested by Jakob [32] for a horizontal heating surface, did not satisfactorily correlate the experimental points (Section 8. 2.). At a heating surface temperature of 217.3°F boiling is initiated at the first site. With a further increase in temperature, the number of sites and bubble frequency at each site increase, so that the heat flux associated with

nucleate boiling increases, and the curve bends upwards. The curve becomes linear again after a temperature of 228.5°F, this linear portion corresponding to "established nucleate boiling". In the region of transition from free convection to "established nucleate boiling" (weak boiling), the quantities of heat transferred by both free convection and nucleate boiling are of the same order, and both must be considered when computing the heat flux theoretically (see Section 5. 4.). The "established nucleate boiling" region is characterised by a very steep slope, and here the heat transfer due to boiling increases so rapidly that the heat transfer due to free convection may be neglected. Only the beginning of the "established nucleate boiling" regions were examined experimentally in this study.

The effect of pressure and subcooling on the free convection, weak boiling and "established boiling" regions can be seen in Figures 42 to 48. The extent of weak boiling or the knee of the curve diminishes with increase in pressure and subcooling until in Figure 48, corresponding to 749 lbs./inch² abs., it appears that only the free convection and "established nucleate boiling" regions remain. This decrease in the weak boiling region has the effect of moving the steep part of the curve to the left, which is more easily seen if the effect of subcooling is neglected and Figures 42 and 43, corresponding to 14.3 and 122 lbs./inch² abs., are compared on a basis of the superheat temperature difference ($T_{sur} - T_{sat}$).

In Figure 42, the free convection region extends until boiling is initiated at the first site for a temperature

difference ($T_{\text{sur}} - T_{\text{sat}}$) of 6.7°F , while in Figure 43 the convection region extends for ($T_{\text{sur}} - T_{\text{sat}}$) equal to 0.9°F . The temperature difference ($T_{\text{sur}} - T_{\text{sat}}$) for the first bubble site or the initiation temperature difference is given in Figure 22, which shows the large decrease in ($T_{\text{sur}} - T_{\text{sat}}$) from 6.7 to 0.9°F , for a pressure increase from 14.3 to 122 lbs./inch² abs. The temperature range corresponding to the region of weak boiling will range from the initiation temperature for the first bubble site to a temperature at which the total heat flux is attributed to boiling. The heat flux in this region has been correlated successfully for pressures of 14.3 and 30 lbs./inch² abs. by Equation (5.4.1.) (see Figures 27 and 28). Equation (5.4.1.) is a summation of the heat flux associated with free convection and with nucleate boiling. The nucleate boiling heat flux has been shown in Equation (5.4.6.) to be proportional to such terms as the temperature difference between the bulk liquid and heating surface ($T_{\text{sur}} - T_{\text{bulk}}$), the square of the maximum bubble diameter D_{max}^2 , the thickness of the thermal layer δ and the bubble flux ψ , which is derived from the number of nucleation sites and the bubble frequency at each site. The weak boiling region in Figures 42 and 43 requires a temperature range of 11 and 7°F respectively, and this value, when added to the temperature difference ($T_{\text{sur}} - T_{\text{sat}}$) corresponding to free convection, i.e. 6.7 and 0.9°F respectively, gives the temperature difference ($T_{\text{sur}} - T_{\text{sat}}$) at the start of the "established boiling" region. The resulting temperature difference ($T_{\text{sur}} - T_{\text{sat}}$) of 17.7 and 7.9°F respectively shows that the effect of an increase in

pressure, i.e. 14.3 to 122 lbs./inch² abs., is to reduce the temperature difference ($T_{\text{sur}} - T_{\text{sat}}$) at the start of the "established boiling" region. In other words, an increase in pressure will move the steep part of the curve to the left if a vertical line through the saturation temperature is taken as the datum axis. This movement to the left with increase in pressure can be inferred from Figures 42 to 48 if the saturation line is taken as a datum axis in each case. This agrees with the experimental results of Addoms [17].

It has been shown that the extent of the temperature difference ($T_{\text{sur}} - T_{\text{sat}}$), corresponding to free convection, is determined by the temperature difference at initiation of the first bubble site, and that the temperature range for the transition or weak boiling region is a function of the number of nucleation sites (the number of sites is included in ψ in Equation 5.4.6.). Since both the initiation temperature difference ($T_{\text{sur}} - T_{\text{sat}}$) and the number of nucleation sites N_2 have been correlated by the size and distribution of heating surface cavities (Figures 22 and 23), it may be concluded that the distance of the steep part of the boiling curve ("established boiling" region) from the saturation line is a function of the heating surface cavities. Therefore an equation intended to predict the "established boiling" region must include a term which takes account of the heating surface cavities.

The equations from other sources which have been derived to correlate "established boiling" all involve Q/A the heat flux as a function of the superheat temperature difference ΔT_{sup} , or in

some cases of Δp the pressure difference corresponding to ΔT_{sup} . In general, the function is $Q/A \propto \Delta T_{sup}^m$ or $Q/A \propto \Delta p^m$, where m is the index of superheat temperature difference or pressure difference. To enable a comparison to be made between the slopes of the "established boiling" regions in Figures 42 to 48 with the slopes predicted by some of the better known equations, the indices m of superheat temperature difference ΔT_{sup} were obtained from the "established boiling" regions of Figures 42 to 48 (see Table 8.1.).

TABLE 8.1.

Indices of ΔT_{sup} for "established boiling"

FIGURES 42 to 48		CICHELLI and BONILLA [37]	
PRESSURE lbs./inch ² abs.	INDEX (m)	PRESSURE lbs./inch ² abs.	INDEX (m)
14.3	3	22	3
122	2.4	60	3
201	1.5	115	3
279	1.3	215	3
401	0.7	315	2.7
549	0.7	415	1.7
749	0.6		

For $Q/A \propto \Delta T_{sup}^m$, Rohsenow [16] gives m equal to 3.03, and Kutateladze [35] m equal to 2.5. If $\Delta p \propto \Delta T_{sup}$ is assumed, then Forster and Zuber [36] give m equal to 2.0, and Forster and

Greif [6] n equal to 2.4. The derivations of the Rohsenow [16] and Forster and Greif [6] equations are described in Section 2. 2. of this work.

Table 8.1. shows that the indices of ΔT_{sup} for the "established boiling" regions in Figures 42 to 48 do not, however, remain constant but decrease from 3 to 0.6 for a pressure increase from 14.3 to 749 lbs./inch² abs. This means that the equations of Rohsenow [16], etc., which are for all pressures, predict the index n satisfactorily for the pressure range from 14.3 to 201 lbs./inch² abs. in this case, but are in error for pressures exceeding this. It should be remembered that only part of the "established boiling" region was recorded in this study, and that the index n of the superheat temperature difference ΔT_{sup} may change at higher heat flux values. A similar effect of an increase in pressure, causing a decrease in the index n of the "established boiling" curves, can be seen to some extent in the experimental curves of Cichelli and Bonilla (see McAdams [37]), for the boiling of n-pentane (90% pure) on a clean, chromium plated horizontal surface (Table 8.1.). The indices n were calculated over a heat flux range similar to that in Figures 42 to 48.

Before the change in position of the "established boiling" curve with change in pressure can be shown exactly, the effect of liquid subcooling must be ascertained. McAdams et al. [38] were able to correlate experimental results of forced convection boiling, by an equation of the form $Q/A \propto \Delta T_{\text{sup}}^{3.86}$, where ΔT_{sup} is the superheat temperature difference. With this

correlation the experimental results were independent of the degree of subcooling (20 - 150°F), the water velocity (1 - 36 ft./sec.), the liquid pressure (30 - 90 lbs./inch² abs.) and the heating tube diameter (0.17 - 0.48 inches). Forster and Greif [6] used a model of nucleate boiling to show why the data of McAdams et al. [38] should be insensitive to liquid subcooling. Briefly, the model is that when a bubble grows to a maximum radius R_{\max} and then collapses, it causes the exchange of a volume of liquid proportional to R_{\max}^3 between the heated layer adjacent to the heating surface and the colder bulk liquid; the amount of heat withdrawn from the heating surface by each bubble growth-collapse cycle is therefore proportional to $R_{\max}^3 (T_{\text{sur}} - T_{\text{bulk}})$, where $(T_{\text{sur}} - T_{\text{bulk}})$ is the temperature difference between the heating surface and bulk liquid. If the period of the bubble growth-collapse cycle is t_g , then the amount of heat transferred by each bubble per second is proportional to $R_{\max}^3 (T_{\text{sur}} - T_{\text{bulk}}) \frac{1}{t_g}$. The insensitivity of heat flux to subcooling may therefore be attributed to the reduction of R_{\max} with subcooling, which compensates for the increase in $(T_{\text{sur}} - T_{\text{bulk}})$ and $\frac{1}{t_g}$. It is noted that the number of bubble sites is a function of the superheat temperature difference $(T_{\text{sur}} - T_{\text{sat}})$ only. A table was compiled by Forster and Greif [6] from the data of Ellison [19], showing that the product $R_{\max}^3 (T_{\text{sur}} - T_{\text{sat}}) \frac{1}{t_g}$ was independent of subcooling.

The main difference between the model of Forster and Greif [6] and the model used in this study, on which Equation (5.4.6.) is based, is in the derivation of the bubble frequency. The bubble

frequency incorporated in the bubble flux ψ in Equation (5.4.6.) was calculated from the bubble waiting time t_w , the bubble growth time t_g being neglected for the early stage of nucleate boiling. Forster and Greif [6], who are concerned with "established boiling", are probably correct in deriving the bubble frequency from the bubble growth-collapse period t_g , since the bubble waiting period will decrease with increasing heat flux and may reach a value which is several times smaller than the growth period. Figure 25, in which the bubble frequency was calculated from the waiting time for individual bubble sites, shows a rapid increase in frequency or decrease in waiting time, with increase in superheat temperature difference and corresponding heat flux. Examination of the experimental results from this study suggests that, although Forster and Greif [6] may have explained why subcooling does not seem to affect boiling data, nevertheless some effect does exist, and unless the experiments are carefully controlled, the scatter of points will obscure this effect.

Figures 49 and 50 show the effect of liquid subcooling on the experimental curves of heat flux versus superheat temperature difference ($T_{sur} - T_{sat}$). Figure 49 shows curves at liquid pressures of 122 and 126 lbs./inch² abs. for subcooling ($T_{sat} - T_{bulk}$) of 5 and 10°F respectively, and Figure 50, pressures of 201 and 204 lbs./inch² abs. for subcoolings of 6 and 12°F respectively. It is evident that the complete curves are not independent of subcooling when plotted to a base of superheat temperature difference, and cannot, therefore, be correlated by an equation of the form $Q/A \propto \Delta T_{sup}^m$. The effect of an

increase in subcooling in both Figures 49 and 50 is to move the steep part of the curve to the left in a manner similar to an increase in pressure.

Some method is therefore needed to find a relation between the position of these curves with respect to a datum axis and the degree of subcooling. With the help of such a relationship the experimental values can then be extrapolated to give the position of the boiling curve for zero subcooling.

It is assumed here that if the boiling curves are plotted to a base of superheat temperature difference, the effect of an increase in subcooling is to move the "established boiling" part of the curve to the left, the distance moved being directly proportional to the degree of subcooling. A vertical line at saturation temperature was therefore taken as a datum, and the steep part of the experimental curves in Figures 49 and 50 extrapolated until they intersected the $(T_{sur} - T_{sat})$ axis. The values of $(T_{sur} - T_{sat})$ at the intersections were then plotted in Figure 51 against the subcoolings of the corresponding curves, and the points for the same pressure joined by straight lines. The straight lines were next extrapolated to zero subcooling. The values of $(T_{sur} - T_{sat})$ at zero subcooling were now used to draw curves parallel to the existing "established boiling" curves in Figures 49 and 50. The positions of the "established boiling" curves at pressures of 124 and 203 lbs./inch² abs. (mean pressures of experimental curves in Figures 49 and 50 respectively) for zero subcooling are assumed to be known, and are reproduced in Figure 52, together with the experimental "established boiling" curve at

14.3 lbs./inch² abs. (also for zero subcooling (Figure 42)).

The equations of Rohsenow [16], etc., which were mentioned earlier, were compared with the experimental curves in Figure 52 and it was found that the equation of Forster and Greif [6] was in best agreement. This equation was derived from a model of nucleate boiling and the variables related by three dimensionless groups, which replace the Nusselt, Reynolds and Prandtl numbers, in the correlation of forced convection heat transfer; the derivation is discussed in greater detail in Section 2. 2.

The Forster and Greif [6] equation is,

$$\frac{Q}{A} = \frac{C_1' k \Delta P \Delta T_{\text{sub}}}{2 \sigma} \left(\frac{\rho_L}{\mu} A_1 \right)^{\frac{1}{5}} \left(\frac{\mu C_p}{k} \right)^{\frac{1}{3}} \quad (8.1.1.)$$

$$\text{where } A_1 = \frac{C_p \rho_L (\pi d)^{\frac{1}{2}} T_{\text{sat}} \Delta P}{(L \rho_V)^2 J}$$

and C_1' a constant which has to be determined from an experimental value of heat flux, at one pressure, for a particular heating surface-liquid combination.

Curves of heat flux Q/A versus $(T_{\text{sur}} - T_{\text{sat}})$, from Equation (8.1.1.), are compared in Figure 52 with the experimental curve at 14.3 lbs./inch² abs. and the curves at 124 and 203 lbs./inch² abs., which were obtained by extrapolating the experimental curves to zero subcooling. Constant C_1' was chosen, to fit Equation (8.1.1.) to the experimental curve at 14.3 lbs./inch² abs., and in this case was 3.35×10^{-3} , which is quite different from the value of 7×10^{-3} used by Forster and Greif [6] to correlate experimental results of others. This discrepancy may result

from a difference in cavity sizes and distribution.

8.2. Free convection heat transfer

Equation (5.4.1.), which has been derived to correlate the weak nucleate boiling region or "knee" of the boiling curve, requires the free convection heat flux to be known. This may be given by the Newton equation,

$$Q/A = h(T_{\text{sur}} - T_{\text{bulk}}) \quad (8.2.1.)$$

where Q/A = free convection heat flux,

$(T_{\text{sur}} - T_{\text{sat}})$ = temperature difference between heating surface
_{bulk} and bulk liquid,

h = heat transfer coefficient.

The results of free convection experiments by Jakob [32] and co-workers have been correlated by the following equation in dimensionless variables:

$$N_{Nu} = C (N_{Gr} \cdot N_{Pr})^{1/3} \quad (8.2.2.)$$

where $N_{Nu} = \frac{h D_1}{k}$ = Nusselt number; h the heat transfer coefficient, D_1 a characteristic length and k the coefficient of thermal conductivity.

$N_{Gr} = \frac{g D_1^3 \beta_1 \Delta T}{\nu^2}$ = Grashof number; g the gravitational acceleration, β_1 the cubic coefficient of thermal expansion, $\Delta T = (T_{\text{sur}} - T_{\text{bulk}})$ and ν the kinematic viscosity.

$N_{Pr} = \frac{\nu}{\alpha}$ = Prandtl number; and α the thermal diffusivity.

C = constant = 0.16 for a horizontal heating surface.

The exponent $\frac{1}{3}$ in equation (8.2.2.) eliminates the effect of any characteristic length which might be chosen for N_{Nu} and N_{Gr} .

The heat transfer coefficient h was calculated from Equation (8.2.2.) for a liquid pressure of 14.3 lbs./inch² abs., the liquid properties being evaluated at saturation temperature. Then it was substituted in Equation (8.2.1.), which is compared in Figure 53 with the free convection results taken from the free convection region of the boiling curve in Figure 42 (14.3 lbs./inch² abs.), and from another free convection experiment at 14.3 lbs./inch² abs. with a subcooling of 25°F. This latter experiment was carried out for two purposes:

- (a) To obtain a free convection curve with a temperature difference range ($T_{sur} - T_{bulk}$), which would extend beyond the free convection region in Figure 42.
- (b) To estimate the percentage heat loss from the heating strip by conduction along the d.c. electrodes.

The heat losses were estimated on the assumption that the d.c. electrodes transfer heat in a similar manner to fins. A thermocouple was inserted into one of the electrodes to measure a representative fin root temperature. The heat transfer coefficient in the approximate fin equation was calculated from Equation (8.2.2.), with C equal to 0.61 for a vertical surface. The heat losses were estimated to be 3.5% of the free convection heat flux, which is not sufficient to account for the difference between Equation (8.2.1.) and the experimental results in Figure 53.

Because of this discrepancy, the experimental curve in Figure 53 was used to evaluate the free convection part of

Equation (5.4.1.), which correlates the weak boiling region in Figure 27.

The free convection regions from the experimental boiling curves at 30 (Figure 28) and 122 lbs./inch² abs. (Figure 43), are compared with the theoretical curves from Equation (8.2.1.) in Figures 54 and 55 respectively. These also show a discrepancy between theory and experiment, with the result that the experimental curve in Figure 54 was extrapolated and used in Equation (5.4.1.) to correlate the weak boiling region of Figure 28.

The experimental free convection points in Figures 53 to 55 were fitted by straight lines drawn in by eye.

8.3. Nucleation properties of the heating surface

Figure 22 shows good agreement between the experimental measurements of the superheat temperature difference for initiation from the first site, and the theoretical prediction of Equation (5.1.14.). The initiation temperature was not recorded for pressures greater than 122 lbs./inch² abs. for the following reasons:

- (a) The bubbles were not clearly distinguishable by the naked eye.
- (b) The rate of increase of bubble sites with temperature was so great, that it was found impossible to control the heating surface temperature to give only one bubble site.
- (c) The initiation superheat temperature difference was less than 1°F and approached the accuracy with which the heating surface temperature could be measured ($\pm 0.5^\circ\text{F}$).

A value of 360×10^{-6} inches was substituted for τ' , the

mouth radius of the largest cavity, in Equation (5.1.14.) to correlate the experimental results in Figure 22. This compares with a value of 550×10^{-6} inches, which was measured to an accuracy of 25×10^{-6} inches, for the mouth radii of the largest cavities on the experimental heating surface (see Figure 6). A discrepancy of this order is not considered to be excessive in the light of the assumptions made in the derivation of Equation (5.1.14.) (see Section 5. 1.). This discrepancy may possibly be reduced if accurate values of θ , the cavity cone angle and β , the solid-liquid contact angle, were included in Equation (5.1.14.). Reliable information on solid-liquid contact angles has not been made available to date, because of difficulties in the measurements of contact angles (see Addoms [17] and Griffith and Wallis [27]). The measurement of cavity radius and cone angle would be facilitated if some method of producing uniformly shaped cavities had been used, e.g. a microscopic forming tool made of some hardened material.

Hsu [13] derived an equation for the limiting sizes of effective cavities (Section 2. 1.) as a function of subcooling, liquid pressure, physical properties and the thickness of the thermal layer. The equation for the limiting sizes of cavity mouth radius in these parameters is,

$$\tau_c' = \frac{\delta}{2C_2} \left[1 - \frac{(T_{sat} - T_{bulk})}{(T_{sur} - T_{bulk})} + \sqrt{\left(1 - \frac{(T_{sat} - T_{bulk})}{(T_{sur} - T_{bulk})}\right)^2 - \frac{4 A' C_3}{\delta(T_{sur} - T_{bulk})}} \right]$$

(8.3.1.)

where $C_2 = \text{constant} = 2,$

$C_3 = \text{constant} = 1.6,$

$$A^1 = \frac{2 \sigma T_{\text{sat}}}{L \rho V J},$$

$\delta = \text{thermal layer thickness},$

$(T_{\text{sat}} - T_{\text{bulk}}) = \text{temperature difference between saturation and bulk liquid temperatures},$

$(T_{\text{sur}} - T_{\text{bulk}}) = \text{temperature difference between heating surface and bulk liquid temperature.}$

Equation (8.3.1.) can be used to draw a curve of maximum cavity radius r_c' max, and a curve of minimum cavity radius r_c' min, versus superheat temperature difference $(T_{\text{sur}} - T_{\text{sat}})$. These two curves form the boundary of a region of effective cavity radii. A cavity with a mouth radius which is outside this region will not be an active bubble site.

The measured thermal layer thickness of 0.036 inches (Figure 39), for a pressure of 14.4 lbs./inch² abs. and a subcooling of 4.5°F, was therefore substituted in Equation (8.3.1.) to obtain the curves of maximum and minimum r_c' for a pressure of 14.4 lbs./inch² abs. and a subcooling of 4.5°F. The curve for maximum r_c' was, however, outside the size range of cavities on the experimental heating surface of this study. Therefore, only the curve of minimum r_c' is shown in Figure 56 for cavity mouth radii ranging from 100 to 1200 x 10⁻⁶ inches. This curve can be used to predict the initiation of boiling for the size range of cavities of this study (r_c' from 0 to 550 x 10⁻⁶ inches), since boiling will not occur until a heating surface temperature is reached, such that

the maximum cavity radius of 550×10^{-6} inches is on the r_c' min curve. The curve of r_c' min from Equation (8.3.1.) is therefore compared, in Figure 56, with the curve of cavity mouth radius versus initiation superheat temperature ($T_{sur} - T_{sat}$) from Equation (5.1.14.) of this study. Figure 56 shows these two curves to be almost identical. This means that when a thermal layer thickness of the order of 0.036 inches is substituted, Equation (8.3.1.) becomes similar to Equation (5.1.14.), which was derived for the case of a uniformly superheated liquid (this only applies to the curve of r_c' min by Equation (8.3.1.)). The thermal layer thickness substituted in Equation (8.3.1.) would therefore have to be very much less than 0.036 inches, before the curve of r_c' min diverges from the curve of r_c' versus initiation superheat temperature difference predicted by Equation (5.1.14.).

The previous argument would also apply to the equation of Han and Griffith [14], since their equation is very similar to that of Hsu [13] (see Section 2. 1.).

The theoretical prediction of the number of bubble sites (Equation (5.2.12.)) versus superheat temperature difference at pressures of 14.3, 30 and 122 lbs./inch² abs. is shown in Figure 23, along with the number recorded in experiments at pressures of 14.3 and 29 lbs./inch² abs. In Equation (5.2.12.) were substituted values of 200 and 114×10^{-6} inches for the population parameters η and ϵ respectively of the normalised cavity distribution (see Figure 6). The properties appearing in constant B were evaluated at the saturation temperature corresponding to the pressure p_L . Constant C_s' was evaluated, with N the cavity

population equal to 1.2×10^5 cavities/inch² and ϵ equal to 114×10^{-6} inches. The cavity population was counted, by moving the Vickers projection microscope across the heating surface at random positions along the heating strip length, and then taking an average of the readings.

Figure 23 shows some agreement between Equation (5.2.12.) and experiment. No check could be carried out for pressures greater than 30 lbs./inch² abs., because of the rapid increase in the number of sites with increase in superheat temperature. Figure 23 also shows that Equation (5.2.12.) predicts a decrease in the rate of increase with temperature difference of the number of bubble sites, when the superheat temperature difference reaches 12°F at a pressure of 14.3 lbs./inch² abs., and 6°F for 30 lbs./inch² abs. It is unlikely that this happens experimentally, and is probably due to inaccuracy in the cavity distribution for the smaller cavity sizes. This is quite possible, since it was mentioned earlier (Section 3. 6.) that the Vickers projection microscope could only record a minimum cavity size of 200×10^{-6} inches, whereas it was most likely that cavities with sizes of less than this were present. It will be necessary, therefore, in extending this work, to be able to resolve and to measure accurately much smaller surface cavities, i.e. less than 200×10^{-6} inches.

Figure 25 shows the theoretical curves of bubble frequency versus superheat temperature difference for the first eight bubble sites at a pressure of 14.3 lbs./inch² abs. The initiation superheat temperature difference for these sites is obtained from

Equation (5.1.14.). Equation (5.3.3.), which predicts the bubble frequency, is based on the assumption that the thermal layer is heated by transient conduction only (see Section 5. 3.), although it is realised that conduction alone is not a complete description of the heat transfer process in the thermal layer. It is shown in Section 7. 4. 1. of this work that if conduction only is assumed, then the thickness of thermal layer predicted by the Fourier equation is in better agreement with the measured thickness for a subcooling of 10°F than for a subcooling of 4.5°F (see Figure 41). It may be expected, therefore, that when comparing Equation (5.3.3.) with experiment, the largest discrepancy will occur at saturation temperature and tend to disappear as the subcooling increases. This fact could not be substantiated in the present study, since the experimental pressure vessel was unsuited to the high-speed photographic technique necessary to determine high frequencies. A search of existing literature for experimental records of bubble frequency which could be applied to this work revealed very little experimental work on bubble frequency. In no case had the frequency been measured at one bubble site for increases in the heating surface temperature.

Figures 27 and 28 show the correlation of the weak boiling region at pressures of 14.3 and 30 lbs./inch² abs. respectively by Equation (5.4.1.). Equation (5.4.1.) is the summation of the free convection heat flux (experimental values were used here) and the theoretical heat flux associated with bubble growth, which is given by Equation (5.4.2.) (see Section 5. 4.). These

figures show that Equation (5.4.2.) does predict the heat flux associated with bubble growth in the weak boiling region. The correlation is not so good near the "established boiling" region, and this may be due to the decrease in the rate of increase of bubble sites with increase in superheat temperature at the higher values of superheat temperature, according to Equation (5.2.12.).

Some success has therefore been achieved in the correlation of the weak nucleate boiling region in terms of the nucleation characteristics of the heating surface, viz. the initiation of boiling, the bubble site density, the bubble frequency, and of the energy associated with the growth of a bubble in a superheated liquid. It now seems possible to predict the start of the "established boiling" region from a knowledge of the heating surface cavity distribution.

CHAPTER 9

Conclusions and Remarks

By applying the Gibbs and Clausius-Clapeyron equations to conditions in an ideal vapour-filled surface cavity, an equation has been derived which predicts the superheat temperature at the initiation of boiling. Calculations based on this equation agree with experimental measurements of the initiation superheat temperature for a pressure range from atmospheric to 122 lbs./inch² abs., provided that the value of the cavity mouth radius which is substituted in this equation is 360×10^{-6} inches.

The heating surface cavity distribution is measured with the aid of a projection microscope, approximated to a normal curve and used with the previous equation to predict the increase in the number of bubble sites with increase in superheat temperature at pressures of 14.3, 30 and 122 lbs./inch² abs. The increase in the number of bubble sites with increase in superheat temperature has been measured by experiment at pressures of 14.3 and 29 lbs./inch² abs., and is in fair agreement with the theoretical prediction. However, this agreement is only obtained when a multiplying constant of 10^{-4} is introduced into this equation to account for the fact that only a very small fraction of the heating surface cavity population are effective bubble sites for the early stage of nucleate boiling.

An equation is derived for the bubble frequency, and the frequency calculated for the first eight bubble sites at pressures of 14.3, 30 and 122 lbs./inch² abs. (the initiation

superheat temperature for these sites was obtained from the rate of increase in bubble sites with superheat temperature, predicted by the previous equation). The derivation of the frequency equation uses a simplified model of the thermal layer, and the assumption that the layer is heated by unsteady state conduction only. The bubble frequency is not determined experimentally. Curves of bubble frequency for a pressure of 14.3 lbs./inch² abs. are presented, and from these have been determined the increase in the number of bubbles per unit area of heating surface per unit diameter with increase in superheat temperature, i.e. the bubble flux. The bubble flux is shown for pressures of 14.3, 30 and 122 lbs./inch² abs.

The experimental weak boiling curves at pressures of 14.3 and 30 lbs./inch² abs. are correlated successfully by an equation, which takes account of both the free convection heat flux and the heat flux associated with bubble growth. Experimental values of free convection heat flux are substituted in this equation, and the heat flux associated with bubble growth derived from a model, which assumes that the growth of a bubble removes a section of the thermal layer from the vicinity of the heating surface. An empirical constant of 1.5 introduced in the equation, which predicts the heat flux associated with bubble growth, to improve the correlation, is interpreted as showing that when a bubble grows it removes a section of the thermal layer whose diameter is 1.5 times the maximum diameter of the bubble.

The thermal layer thickness is measured by a shadowgraph

technique at pressures of 14.2 and 30 lbs./inch² abs. with bulk liquid subcooling of 11.5 and 10⁰F respectively. The maximum layer thicknesses are 0.030 and 0.032 inches respectively. These experiments reveal that the thermal layer develops in three distinct stages: (i) a laminar stage, (ii) a transition stage from laminar to turbulent flow and (iii) a stage where the upper half of the layer is fully turbulent. The thickness of the layer is also obtained by direct measurement of the temperature distribution in the liquid above the heating surface. These measurements are carried out at pressures of 14.7, 14.4 and 30 lbs./inch² abs. with subcoolings of 10, 4.5 and 5⁰F respectively. The thicknesses obtained in this manner are 0.020, 0.036 and 0.034 inches respectively. The corresponding layer thicknesses are 0.020 inches by direct measurement of temperature, and 0.030 inches by the shadowgraph method, for similar experimental conditions. These values indicate the extent of agreement between the two methods of measuring the thermal layer thickness.

An equation by Chang [33], which predicts the thickness of a "boundary film", shows good agreement with the thickness of the thermal layer measured from the temperature distribution in the liquid at atmospheric pressure for subcoolings of 10 and 4.5⁰F.

Experimental boiling curves at pressures of 14.3, 122, 201, 279, 401, 549 and 745 lbs./inch² abs., showing the regions of free convection, weak nucleate boiling and the start of "established nucleate boiling", are presented. These curves give new information on the beginning of nucleate pool boiling

of water.

The "established boiling" regions of experimental curves at pressures of 122 and 126 lbs./inch² abs. with subcoolings of 5 and 10°F respectively, and at 201 and 204 lbs./inch² abs. with subcooling of 6 and 12°F respectively, are extrapolated to give "established boiling" curves at pressures of 124 and 203 lbs./inch² abs. (mean pressures of 122 and 126, and of 201 and 204 lbs./inch² abs. respectively) with zero subcooling.

The "established boiling" curves at 124 and 203 lbs./inch² abs. with zero subcooling, together with the experimental "established boiling" curve at 14.3 lbs./inch² abs. (experiment conducted at zero subcooling), are correlated with some success by an equation of Forster and Greif [6].

The experimental free convection results of this study are not correlated by the equation $N_{Nu} = 0.16 (N_{Gr} \cdot N_{Pr})^{\frac{1}{3}}$, which Jakob [32] and co-workers used to correlate their experimental results from a horizontal heating surface.

A P P E N D I C E S

ACCURACY OF RESULTS

Heating surface temperature

The final accuracy of the heating surface temperature measurement depends on the following items, for which the accuracy is given systematically in brackets.

- (1) The calibration of the heating strip thermocouple against the bulk liquid thermocouple ($\pm 0.15^{\circ}\text{F}$).
- (2) The calibration of the heating strip thermocouple voltage "pick up" ($\pm 0.1^{\circ}\text{F}$).
- (3) The fluctuation of the heating strip thermocouple reading ($\pm 0.2^{\circ}\text{F}$).
- (4) The calculated temperature drop across the heating strip ($\pm 0.01^{\circ}\text{F}$).
- (5) The precision potentiometer ($\pm 0.04^{\circ}\text{F}$).

The final accuracy of the heating surface temperature measurement is therefore $\pm 0.5^{\circ}\text{F}$.

Bulk liquid temperature

The bulk liquid temperature measurement depends on the following:

- (1) the calibration of the bulk liquid thermocouple against fixed points on the International Temperature Scale ($\pm 0.1^{\circ}\text{F}$),

- (2) the fluctuation of the bulk liquid thermocouple reading ($\pm 0.1^{\circ}\text{F}$) and
- (3) the change in bulk liquid temperature during an experiment ($\pm 0.5^{\circ}\text{F}$).

The final accuracy of the bulk liquid temperature measurement is therefore $\pm 0.7^{\circ}\text{F}$.

Heat Flux

The final percentage accuracy of the heating surface heat flux depends on the following items and their respective accuracies:

- (1) the heating strip voltage ($\pm 0.04\%$),
- (2) the heating strip current ($\pm 0.03\%$),
- (3) the heating strip surface area ($\pm 0.6\%$) and
- (4) the estimated heat losses of 3.5% which were not subtracted from the heat flux values.

The final accuracy of the heat flux is therefore + 0% - 5%.

NOMENCLATURE

<u>Symbol</u>	<u>Definition</u>	<u>Units</u>
A	Heating surface area	ft. ²
A ₁	$\frac{C_p \rho_L (\pi d)^{\frac{1}{2}} T_{sat}}{(L \rho_V)^2 J}$	ft./hr. ^{$\frac{1}{2}$}
A ¹	$\frac{2 \sigma T_{sat}}{L \rho_V J}$	ft. °F
a	Area of thermal layer removed by bubble	ft. ²
a	Thickness of "wave layer"	ft.
B	$\frac{2RT_{sat}^2 \sigma}{LJ \rho_L}$	ft. °F
C, C ₁ , C ₁ '	Constants	
C ₂	Constant = 2	
C ₃	Constant = 1.6	
C ₄	Conversion factor = 3.41	B.t.u./watts hr.
C ₅	$\frac{N^1}{\sqrt{2\pi \epsilon}}$	1/ft. ³
C ₅ ¹	$\frac{N^1}{\sqrt{2\pi \epsilon}}$	1/ft. ³
Cp	Specific heat at constant pressure	B.t.u./lb. °F
Cp ₂	" " " " " (evaluated at mean temperature of "wave layer")	B.t.u./lb. °F
D	Constant = 10 ⁻⁴	
D max	Maximum bubble diameter	ft.
D ₁	Characteristic length	ft.
D ₂	Diameter of thermal layer section removed by bubble	ft.
E	Constant = 1.5	
f	Bubble frequency	1/hr.

g	Gravitational acceleration	ft./hr. ²
h	Heat transfer coefficient	B.t.u./ft. ² hr. °F
I	Current	amps
J	Joule's equivalent	ft. lbs./B.t.u.
k	Mean coefficient of thermal conductivity	B.t.u./ft. ² hr. °F/ft.
k _a	Coefficient of thermal conductivity (evaluated at mean temperature of "wave layer")	B.t.u./ft. ² hr. °F/ft.
L	Latent heat of vaporisation	B.t.u./lb.
m	Exponent of Reynolds number	
N	Cavity population	1/ft. ²
N ¹	Active cavity population	1/ft. ²
N ₂	Number of bubble sites	1/ft. ²
n	Exponent of Prandtl number	
n ₁	Any whole number	
p	Vapour pressure	lbs./ft. ²
p	Liquid pressure	lbs./ft. ²
Δp	Pressure difference (p _v - p _l) corresponding to ΔT _{sup}	lbs./ft. ²
Q	Heat flow rate	B.t.u./hr.
$\frac{Q}{A}$	Heat flux	B.t.u./ft. ² hr.
q _b	Heat content associated with bubble growth	B.t.u.
R _{max}	Maximum bubble radius	ft.
R	Perfect gas constant	ft. lbs./lb. °F
r	Radius of nucleus boundary	ft.
r _c	Critical radius of nucleus boundary	ft.
r _c '	Cavity mouth radius	ft.
T	Temperature	°F or °FAbs.

ΔT	Temperature difference or temperature drop	$^{\circ}F$
t	Time	hr.
t _g	Bubble growth period	hr.
t _w	Bubble waiting period	hr.
V	Voltage	volts
V_v	Specific volume of vapour	ft. ³ /lb.
V_L	Specific volume of liquid	fr. ³ /lb.
x	Thickness of heating strip	ft.

Greek letters

α	Thermal diffusivity $\frac{k}{\rho C_p}$	ft. ² /hr.
β	Solid-liquid contact angle	
β_1	Cubic coefficient of thermal expansion	1/ $^{\circ}F$
δ	Thermal layer thickness	ft.
δ_w	Thickness of "boundary film"	ft.
ϵ	Standard deviation of cavity population	ft.
η	Arithmetic mean of τ_c'	ft.
θ	Cavity cone angle	
μ	Dynamic viscosity	lbs./ft. hr.
π	3.142	
ρ	Vapour density	lbs./ft. ³
ρ_L	Liquid density	lbs./ft. ³
ρ_0	Density (evaluated at mean temperature of "wave layer")	lbs./ft. ³
ρ_c	Density (evaluated at mean temperature of convective core)	lbs./ft. ³

σ	Vapour-liquid surface tension	lbs./ft.
ν	Kinematic viscosity	ft. ² /hr.
ϕ	Angle included by τ_c and τ_c'	
χ	Constant ≈ 1	
ψ	Bubble flux	1/ft. ² hr.

Dimensionless Groups

N_{Nu}	Nusselt number	= $\frac{hD}{k}$
N_{Gr}	Grashof number	= $\frac{gD^3 \beta \Delta T}{\nu^2}$
N_{Pr}	Prandtl number	= $\frac{\nu}{\alpha}$

Subscripts

sat	Saturation
sur	Heating surface
sup	Superheat
bulk	Bulk liquid
ac	"Wave layer"
sa	"Boundary film"
sc	("Boundary film" + "wave layer")
min	Minimum
max	Maximum

TABLE 1 (Data for Figure 42).

System pressure:- 14.3 lbs/inch² abs.

Saturation temperature:- 210.6°F

Bulk liquid temperature:- 210.6°F

Heating Strip Temp. (bottom surface) (°F)	Temp. drop across Heating Strip. ΔT (°F)	Heating Strip Temp. (top surface) T _{sur} (°F)	Heating Strip Voltage V (volts)	Heating Strip Current I (amps)	Heat Flux Q/A (Btu/ft ² hr)
213.7	0.01	213.7	0.275	4.181	546
214.4	0.01	214.4	0.333	5.084	804
216.4	0.02	216.4	0.402	6.083	1160
215.3	0.02	215.3	0.464	7.095	1560
218.9	0.03	218.9	0.530	8.100	2070
219.7	0.04	219.7	0.588	9.036	2522
222.6	0.05	222.5	0.664	10.146	3200
222.1	0.05	222.0	0.721	11.035	3790
224.8	0.06	224.7	0.789	12.074	4520
226.1	0.08	226.0	0.852	13.060	5290
227.4	0.09	227.3	0.927	14.171	6240
228.1	0.10	228.0	0.987	15.084	7060
228.7	0.11	228.6	1.050	16.077	8010
230.1	0.13	230.0	1.122	17.196	9160
230.7	0.14	230.6	1.182	18.137	10200
230.6	0.16	230.4	1.246	19.109	11300
231.3	0.18	231.1	1.308	20.060	12430
231.2	0.20	231.0	1.374	21.085	13770
231.7	0.21	231.5	1.438	22.059	15050
233.9	0.23	233.7	1.503	23.059	16470
233.5	0.25	233.2	1.568	24.063	17920
238.8	0.28	238.5	1.639	25.094	19550
238.7	0.30	238.4	1.698	26.049	21000

TABLE 2 (data for Figures 43 and 49).

System pressure:- 122 lbs/inch² abs.

Saturation temperature:- 342.5°F

Bulk liquid temperature:- 337.8°F

Heating Strip Temp. (bottom surface) (°F)	Temp.drop across Heating Strip ΔT (°F)	Heating Strip Temp. (top surface) T _{sur} (°F)	Heating Strip Voltage V (volts)	Heating Strip Current I (amps)	Heat Flux $\frac{Q}{A_2}$ (Btu/ft ² .hr)	Superheat Temperature Difference (T _{sur} -T _{sat})°F
339.3	0.01	339.3	0.263	4.087	510	3.7
340.3	0.01	340.3	0.325	5.139	790	2.2
341.3	0.02	341.3	0.383	6.095	1108	1.2
341.9	0.02	341.9	0.439	7.027	1460	0.6
344.2	0.03	344.2	0.506	8.076	1940	1.7
344.6	0.03	344.6	0.571	9.094	2460	2.1
346.9	0.04	346.9	0.633	10.072	3020	4.4
347.6	0.05	347.5	0.696	11.079	3660	5.0
348.8	0.06	348.7	0.759	12.071	4340	6.2
349.2	0.07	349.1	0.819	13.052	5060	6.6
349.8	0.08	349.7	0.880	14.041	5860	7.2
350.6	0.10	350.5	0.947	15.101	6770	8.0
351.1	0.11	351.0	1.008	16.080	7660	8.5
351.4	0.12	351.3	1.073	17.119	8700	8.8
352.2	0.14	352.1	1.139	18.097	9760	9.6
352.1	0.15	352.1	1.198	19.092	10820	10.4 9.4
352.6	0.17	352.4	1.257	20.041	11920	9.9
352.8	0.19	352.6	1.329	21.162	13300	10.1
353.2	0.21	353.0	1.387	22.135	14520	10.5
353.6	0.22	353.4	1.446	23.108	15800	10.9
353.9	0.24	353.7	1.506	24.063	17170	11.2
354.4	0.26	354.1	1.570	25.076	18650	11.2
354.8	0.29	354.5	1.625	26.036	20080	11.6

TABLE 3 (data for Figure 49).

System pressure:- 126 lbs/inch² abs.
 Saturation temperature:- 345.0°F
 Bulk liquid temperature:- 335.4°F

Heating Strip Temp. (bottom surface) (°F)	Temp. drop across Heating Strip ΔT (°F)	Heating Strip Temp. (top surface) T _{sur} (°F)	Heating Strip Voltage V (volts)	Heating Strip Current I (amps)	Heat Flux Q/A ₂ (Btu/ft ² .hr)	Superheat Temperature Difference (T _{sur} -T _{sat})°F
340.0	0.02	340.0	0.468	7.890	1745	
344.0	0.04	344.0	0.575	9.715	2640	1.4
346.5	0.06	346.4	0.673	11.370	4020	3.6
348.7	0.07	348.6	0.783	13.210	4880	5.7
350.8	0.09	350.7	0.894	15.135	6400	7.3
352.4	0.12	352.3	1.010	17.101	8150	7.8
352.8	0.14	352.8	1.131	19.103	10200	8.5
353.7	0.18	353.5	1.246	21.031	12360	9.0
354.2	0.21	354.0	1.363	23.017	14800	8.0
353.3	0.25	353.0	1.478	25.018	17440	8.4
353.7	0.34	353.4	1.721	29.083	23650	7.6
352.8	0.24	352.6	1.461	24.596	16960	6.9
352.1	0.20	351.9	1.316	22.175	13760	7.4
352.6	0.16	352.4	1.193	20.153	11350	5.7
350.8	0.11	350.7	0.967	16.290	7440	4.6
349.7	0.08	349.6	0.847	14.246	5700	2.5
347.6	0.06	347.5	0.733	12.329	4270	1.3
346.4	0.05	346.3	0.636	10.747	3225	
342.7	0.03	342.7	0.514	8.644	2100	

TABLE 4 (data for Figures 44 and 50).

System pressure:- 201 lbs/inch² abs.
 Saturation temperature:- 382.2°F
 Bulk liquid temperature:- 376.2°F

Heating Strip Temp. (bottom surface) (°F)	Temp.drop across Heating Strip ΔT (°F)	Heating Strip Temp.(top surface) T _{sur} (°F)	Heating Strip Voltage V (volts)	Heating Strip Current I (ampe)	Heat Flux Q/A (Btu/ft ² .hr)	Superheat Temperature Difference (T _{sur} -T _{sat})°F
378.9	0.01	378.9	0.265	4.164	524	
379.4	0.01	379.4	0.319	5.081	769	
380.6	0.02	380.6	0.383	6.096	1108	
380.9	0.02	380.9	0.445	7.114	1502	
382.2	0.03	382.2	0.512	8.149	1980	
383.5	0.04	383.5	0.571	9.143	2480	1.3
384.0	0.04	384.0	0.631	10.141	3060	1.8
384.9	0.05	384.8	0.692	11.088	3630	2.6
385.5	0.07	385.4	0.758	12.093	4650	3.2
385.9	0.07	385.8	0.825	13.157	5140	3.6
386.4	0.08	386.3	0.885	14.143	5930	4.1
387.0	0.10	386.9	0.949	15.136	6810	4.7
387.4	0.11	387.3	1.014	16.159	7760	5.1
387.7	0.12	387.6	1.072	17.133	8700	5.4
387.7	0.14	387.6	1.134	18.147	9750	5.4
388.0	0.15	387.8	1.191	19.051	10750	5.6
388.2	0.18	388.0	1.256	20.077	12340	5.8
388.8	0.19	388.6	1.320	21.135	13200	6.4
389.3	0.20	389.1	1.377	22.063	14400	6.9
389.7	0.22	389.5	1.443	23.120	15800	7.3
390.1	0.24	389.9	1.504	24.108	17200	7.7
390.5	0.26	390.2	1.565	25.086	18610	8.0
390.8	0.29	390.5	1.627	26.078	20120	8.3

TABLE 5 (data for Figure 50).

System pressure:- 20 1/2 lbs/inch² abs.

Saturation temperature:- 383.5°F

Bulk liquid temperature:- 372.0°F

Heating Strip Temp. (bottom surface) (°F)	Temp.drop across Heating Strip ΔT (°F)	Heating Strip Temp.(top surface) T _{sur} (°F)	Heating Strip Voltage V (volts)	Heating Strip Current I (amps)	Heat Flux Q/A (Btu/ft ² .hr)	Superheat Temperature Difference (T _{sur} -T _{sat})°F
372.4	0.01	372.4	0.222	3.752	393	
377.0	0.02	377.0	0.406	6.806	1320	
379.8	0.03	379.8	0.552	9.324	2433	
383.0	0.06	382.9	0.700	11.819	3910	
384.5	0.07	384.4	0.771	12.974	4730	0.9
386.2	0.08	386.1	0.820	13.803	5340	2.6
385.8	0.09	385.7	0.877	14.778	6116	2.2
386.2	0.11	386.1	1.002	16.904	8000	2.6
388.2	0.14	388.1	1.121	18.855	9980	4.6
387.9	0.18	387.7	1.245	21.003	12350	4.2
388.4	0.21	388.2	1.364	23.002	14830	4.7
389.1	0.25	388.8	1.487	25.224	17730	5.3
390.2	0.33	389.9	1.711	28.878	23350	6.4
388.5	0.24	388.3	1.446	24.408	16650	4.8
388.1	0.20	387.9	1.316	22.227	13800	4.4
388.0	0.16	387.8	1.173	19.828	11000	4.3
387.5	0.13	387.4	1.078	18.171	9240	3.9
385.5	0.08	385.4	0.850	14.313	5800	1.9
384.5	0.06	384.4	0.750	12.624	4465	0.9

TABLE 6 (data for Figure 45).

System pressure:- 279 lbs/inch² abs.
 Saturation temperature:- 410.8°F
 Bulk liquid temperature:- 399.7°F

Heating Strip Temp. (bottom surface) (°F)	Temp. drop across Heating Strip ΔT (°F)	Heating Strip Temp. (top surface) T _{sur} (°F)	Heating Strip Voltage V (volts)	Heating Strip Current I (amps)	Heat Flux Q/A (Btu/ft. ² hr)
404.1	0.02	404.1	0.365	6.173	1063
407.8	0.04	407.8	0.561	9.474	2510
409.3	0.05	409.2	0.662	11.096	3470
409.3	0.05	409.2	0.660	11.239	3510
410.0	0.06	409.9	0.710	12.600	4020
412.2	0.06	412.1	0.753	12.719	4520
412.5	0.07	412.4	0.789	13.300	4960
412.3	0.08	412.2	0.841	14.147	5610
413.5	0.10	413.4	0.901	15.161	7160
414.0	0.11	413.9	0.972	16.375	7520
415.1	0.12	415.0	1.010	17.000	8100
415.1	0.13	415.0	1.073	18.027	9130
416.0	0.16	415.8	1.192	20.012	11250
416.1	0.18	416.9	1.258	21.120	12540
416.6	0.21	416.4	1.369	23.000	14860
417.3	0.23	417.1	1.431	23.987	16200
417.4	0.28	417.1	1.582	26.533	19800
417.8	0.31	417.5	1.650	27.652	21550
418.4	0.37	418.0	1.808	30.198	25800

TABLE 7 (data for Figure 46).

System pressure:- 401 lbs/inch² abs.

Saturation temperature:- 444.9°F

Bulk liquid temperature:- 434.8°F

Heating Strip Temp. (bottom surface) (°F)	Temp. drop across Heating Strip. ΔT (°F)	Heating Strip Temp. (top surface) T _{sur} (°F)	Heating Strip Voltage V (volts)	Heating Strip Current I (amps)	Heat Flux Q/A (Btu/ft. ² .hr)
437.5	0.02	437.5	0.387	6.444	1177
439.6	0.03	439.6	0.480	8.003	1816
442.3	0.04	442.3	0.619	10.266	3005
444.2	0.07	444.1	0.799	13.178	4960
445.7	0.08	445.6	0.848	14.130	5660
445.1	0.09	445.0	0.894	14.928	6310
445.8	0.10	445.7	0.964	16.068	7310
446.7	0.12	446.6	1.027	17.116	8310
447.7	0.13	447.6	1.072	17.851	9030
448.6	0.15	448.4	1.149	19.101	10370
448.8	0.16	448.6	1.196	19.919	11240
449.0	0.19	448.8	1.295	21.552	13180
448.8	0.20	448.6	1.338	22.226	14050
449.7	0.21	449.5	1.387	23.107	15120
450.1	0.24	449.9	1.475	24.525	17070
450.2	0.25	449.9	1.503	25.011	17730
451.5	0.28	451.2	1.573	26.168	19420
451.8	0.30	451.5	1.630	27.098	20860
452.2	0.34	451.9	1.765	29.000	24150

TABLE 8 (data for Figure 47).

System pressure:- 549 lbs/inch² abs.

Saturation temperature:- 476.7°F

Bulk liquid temperature:- 464.8°F

Heating Strip Temp. (bottom surface)	Temp. drop across Heating Strip.	Heating Strip Temp. (top surface)	Heating Strip Voltage	Heating Strip Current	Heat Flux Q/A (Btu/ft ² .hr.)
(°F)	ΔT (°F)	Tsur (°F)	V (volts)	I (amps)	
467.3	0.01	467.3	0.262	4.276	531
470.0	0.02	470.0	0.443	7.213	1510
472.2	0.04	472.2	0.569	9.299	2501
474.3	0.05	474.2	0.689	11.279	3670
476.1	0.07	476.0	0.811	13.513	5100
476.6	0.08	476.5	0.858	14.058	5700
478.0	0.09	477.9	0.918	15.065	6530
477.7	0.10	477.6	0.969	15.887	7270
478.2	0.12	478.1	1.040	17.058	8360
479.2	0.13	479.1	1.098	17.964	9320
479.5	0.15	479.3	1.159	18.966	10400
480.6	0.17	480.4	1.231	20.138	11720
481.3	0.18	481.2	1.288	21.020	12800
481.7	0.20	481.5	1.350	22.055	14080
481.2	0.22	481.0	1.405	22.968	15260
482.6	0.24	482.4	1.472	24.061	16760
483.1	0.26	482.8	1.535	25.090	18220
482.3	0.29	482.0	1.623	26.472	20320
482.7	0.31	482.4	1.691	27.598	22080

TABLE 9 (data for Figure 48).

System pressure:- 749 lbs/inch² abs.
 Saturation temperature:- 510.5°F
 Bulk liquid temperature:- 497.7°F

Heating Strip Temp. (bottom surface) (°F)	Temp. drop across Heating Strip Δ T (°F)	Heating Strip Temp. (top surface) T _{sur} (°F)	Heating Strip Voltage V (volts)	Heating Strip Current I (amps)	Heat Flux Q/A ² (Btu/ft. ² .hr)
498.5	0.01	498.5	0.273	4.339	561
501.6	0.02	501.6	0.469	7.539	1677
504.7	0.04	504.7	0.580	9.388	2587
508.8	0.06	508.7	0.714	11.529	3905
510.5	0.07	510.4	0.825	13.360	5220
510.7	0.08	510.6	0.864	14.011	5730
510.5	0.10	510.4	0.940	15.241	6790
510.9	0.11	510.8	0.981	15.952	7420
511.3	0.12	511.2	1.052	17.074	8510
511.8	0.14	511.7	1.127	18.290	9770
512.7	0.16	512.5	1.195	19.383	10980
513.5	0.17	513.3	1.251	20.274	12040
513.2	0.19	513.0	1.313	21.257	13210
512.9	0.20	512.7	1.365	22.114	14300
513.2	0.22	513.0	1.437	23.255	15810
513.7	0.24	513.5	1.492	24.162	17100
513.6	0.28	513.3	1.595	25.852	19550
513.5	0.31	513.2	1.685	27.304	21800

TABLE 10 (data for Figure 28).

System pressure:- 30 lbs/inch² abs.
 Saturation temperature:- 250.1°F
 Bulk liquid temperature:- 247.6°F

Heating Strip Temp. (bottom surface)	Temp. drop across Heating Strip.	Heating Strip Temp. (top surface).	Heating Strip Voltage.	Heating Strip Current.	Heat Flux Q/A (Btu/ft ² hr)
(°F)	ΔT (°F)	T _{sur} (°F)	V (volts)	I (amps)	
250.6	0.01	250.6	0.318	5.076	755
250.4	0.02	250.4	0.382	6.076	1099
252.3	0.02	252.3	0.446	7.070	1493
253.2	0.03	253.2	0.509	8.067	1950
254.1	0.03	254.1	0.569	9.035	2440
255.7	0.04	255.7	0.633	10.267	3005
256.7	0.05	256.6	0.704	11.151	3720
258.7	0.06	258.6	0.760	12.100	4360
257.8	0.07	257.7	0.821	13.136	5115
259.3	0.08	259.2	0.884	14.092	5900
259.6	0.10	259.5	0.951	15.125	6820
261.1	0.11	261.0	1.013	16.149	7750
261.1	0.12	261.0	1.071	17.289	8670
262.4	0.14	262.3	1.135	18.127	9760
262.9	0.15	262.7	1.198	19.130	10850
262.7	0.17	262.5	1.268	20.211	12140
265.0	0.19	264.8	1.322	21.105	13220
264.8	0.21	264.6	1.385	22.090	14500
266.4	0.22	266.2	1.445	23.056	15800
268.2	0.24	268.0	1.505	24.019	17130
268.9	0.26	268.6	1.568	25.014	18600
270.8	0.29	270.5	1.632	26.033	20160
273.4	0.31	273.1	1.694	27.034	21720

TABLE 11 (additional data).

System pressure:- 30 lbs/inch² abs.

Saturation temperature:- 250.1°F

Bulk liquid temperature:- 248.5°F

Heating Strip Temp. (bottom surface).	Temp. drop across Heating Strip.	Heating Strip Temp. (top surface).	Heating Strip Voltage	Heating Strip Current	Heat Flux Q/A (Btu/ft ² hr)	
(°F)	ΔT (°F)	T _{sur} (°F)	V (volts)	I (amps)		
268.9	0.29	268.6	18.5	1.648	26.200	20470
268.4	0.27	268.1	18.0	1.581	25.107	18800
266.4	0.23	266.2	16.1	1.456	23.150	15970
265.1	0.19	264.9	14.8	1.326	21.038	13220
263.1	0.15	262.9	12.8	1.198	19.062	10820
261.6	0.12	261.5	11.4	1.074	17.176	8750
260.0	0.10	259.9	9.8	0.954	15.131	6840
259.2	0.07	259.1	9.0	0.831	13.154	5190
257.4	0.05	257.3	7.2	0.701	11.113	3690
256.6	0.04	256.6	6.5	0.571	9.146	2480
254.2	0.02	254.2	4.1	0.447	7.105	1508
252.5	0.01	252.5	2.3	0.324	5.157	794
251.6	0.01	251.6	1.5	0.268	4.232	539
251.1	0.02	251.1	4.0	0.393	6.200	1156
255.7	0.03	255.7	5.6	0.530	8.242	2070
256.8	0.04	256.8	6.7	0.637	10.086	3046
258.0	0.06	257.9	7.8	0.775	12.301	4520
258.7	0.08	258.6	8.5	0.893	14.130	5980
260.0	0.11	259.9	9.8	1.010	16.042	7680
262.5	0.14	262.4	12.3	1.144	18.153	9850
262.9	0.17	262.7	12.6	1.272	20.165	12150
264.7	0.21	264.5	14.4	1.392	22.080	14500
265.5	0.25	265.2	15.1	1.514	24.068	17300
266.0	0.27	265.7	15.5	1.587	25.297	19000

TABLE 12 (additional data).

System pressure:- 401 lbs/inch² abs.
 Saturation temperature:- 444.9°F
 Bulk liquid temperature:- 434.2°F

Heating Strip Temp. (bottom surface) (°F)	Temp. drop across Heating Strip. ΔT (°F)	Heating Strip Temp. (top surface). T _{sur} (°F)	Heating Strip Voltage V (volts)	Heating Strip Current I (amps)	Heat Flux Q/A ₂ (Btu/ft ² hr)
436.4	0.02	436.4	0.398	6.636	1250
439.4	0.03	439.4	0.511	8.521	2062
441.6	0.05	441.5	0.648	10.820	3315
445.3	0.08	445.2	0.861	14.983	5860
443.8	0.07	443.7	0.770	12.910	4710
446.3	0.10	446.2	0.920	15.460	6730
446.4	0.11	446.3	0.969	16.221	7440
447.2	0.12	447.1	1.025	17.116	8300
447.6	0.13	447.5	1.086	18.154	9310
447.1	0.14	447.0	1.130	18.878	10070
447.6	0.17	447.4	1.216	20.275	11670
448.1	0.19	447.9	1.296	21.585	13230
450.0	0.21	449.8	1.354	22.561	14440
449.7	0.23	449.5	1.434	23.925	16210
450.1	0.25	449.8	1.503	25.016	17800
450.3	0.29	450.0	1.600	26.580	20100
451.4	0.31	451.1	1.657	27.606	21630
451.4	0.37	451.0	1.820	30.288	26100

REFERENCES

1. McAdams, W.H., "Heat Transmission", 3rd edition, McGraw-Hill, New York, 1954, p. 370.
2. Westwater, J.W., "Petroleum Management", No. 10, Vol. 33, Sept. 1961, pp. 219-226.
3. Gibbs, J.W., Scientific Papers, "Thermodynamics", Vol. 1, Longmans, Green and Co., London, 1906, pp. 252-258.
4. Blake, Jr., F.G., "The Tensile Strength of Liquids: A Review of the Literature", Office of Naval Research, Contract N5 ori -76, Project Order X, Technical Memorandum No. 9: Acoustics Research Laboratory, Harvard University, Cambridge, Massachusetts, June 11, 1949.
5. "Boiling Heat Transfer: Proceedings of a Meeting at NEL, 9th January 1963", NEL Report No. 97, National Engineering Laboratory, DSIR, July, 1963.
6. Forster, K., and Greif, R., "Heat Transfer to a Boiling Liquid: Mechanism and Correlations", ASME Journal of Heat Transfer and Basic Engineering, 81, 1959, pp. 43-53.
7. Kenrick, F.B., Gilbert, C.S., and Wismer, K.L., "The Superheating of Liquids", Journal of Physical Chemistry, 28, 1924, pp. 1297-1307.
8. Fisher, J.C., "The Fracture of Liquids", Journal of Applied Physics, 19, 1948, pp. 1062-1067.
9. Dean, R.B., "The Formation of Bubbles", Journal of Applied Physics, 15, 1944, pp. 446-451.
10. Clark, H.B., Strenge, P.S., and Westwater, J.W., "Active Sites for Nucleate Boiling", Heat Transfer - Chicago, Chemical Engineering Progress Symposium Series, No. 29, Vol. 55, 1959, pp. 103-110.
11. Claude, Corty, and Foust, A.S., "Surface Variables in Nucleate Boiling", Heat Transfer - St. Louis, Chemical Engineering Progress Symposium Series, No. 17, Vol. 51, 1955, pp. 1-12.
12. Westwater, J.W., "Boiling Heat Transfer", American Scientist, 47, September, 1959, pp. 427-446.
13. Hsu, Y.Y., "On the Size Range of Active Nucleation Cavities on a Heating Surface", ASME Journal of Heat Transfer and Basic Engineering, 84, 1962, pp. 207-216.

14. Han, C.Y., and Griffith, P., "The Mechanism of Heat Transfer in Nucleate Pool Boiling", Contract NONR - 1841 (39), Report No. 7673 - 19: Department of Mechanical Engineering, MIT, Cambridge, Massachusetts, March 30, 1962.
15. Bonilla, C.F., and Perry, C.H., "Heat Transmission to Boiling Binary Liquid Mixtures", Trans. AIChE, Vol. 37, 1941, p. 685.
16. Rohsenow, W.M., "A Method of Correlating Heat-Transfer Data for Surface Boiling of Liquids", Trans. ASME, Vol. 74, 1952, pp. 969-976.
17. Addoms, J.N., "Heat Transfer at High Rates to Water Boiling Outside Cylinders", D.Sc. Thesis, MIT, Cambridge, Massachusetts, 1948.
18. Westwater, J.W., and Santangelo, J.G., "Photographic Study of Boiling", Industrial and Engineering Chemistry, Vol. 47, No. 8, 1955, pp. 1605-1610.
19. Ellion, M.E., "A Study of the Mechanism of Boiling Heat Transfer", ORDCIT Project, Contract No. DA-04-495-Ord 18, Dept. of the Army, Ordnance Corps, Memorandum No. 20-88: JPL, California Institute of Technology, California, March 1, 1954.
20. Patten, T.D., "Studies in Nucleate Boiling", McGill University, GDL Report R49, August, 1958.
21. Staniszweski, B.E., "Nucleate Boiling Bubble Growth and Departure", Office of Naval Research, Contract NONR - 1841 (39), DSR Project No. 7 - 7673, Division of Sponsored Research, MIT, Cambridge, Massachusetts, August, 1959.
22. Bankoff, S.G., "The Prediction of Surface Temperatures at Incipient Boiling", Heat Transfer - Chicago, Chemical Engineering Progress Symposium Series, No. 29, Vol. 55, 1959, pp. 87-94.
23. Jakob, M., "Heat Transfer", Vol. 11, Wiley, New York, 1957, p. 151.
24. "Studies in Boiling Heat Transfer", Contract No. AF-11-1-Gen-9, The United States Atomic Energy Commission: Dept. of Engineering, University of California, Los Angeles, California, March, 1951.
25. Evans, U.R., "The Corrosion and Oxidation of Metals", Edward Arnold, London, 1960.
26. Jakob, M., "Heat Transfer", Vol. 1, Wiley and Sons, Inc., New York, 1949, p. 621.

27. Griffith, P., and Wallis, J.D., "The Role of Surface Conditions in Nucleate Boiling", Contract No. N5 ori - 07894, NONR - 1848 (39), DSR Project No. 7 - 7673, Technical Report No. 14: MIT, Division of Industrial Co-operation, Cambridge, Massachusetts, December 1, 1958.
28. Hsu, Y.Y., and Graham, R.W., "An Artificial and Experimental Study of the Thermal Boundary Layer and Ebullition Cycle in Nucleate Boiling", NASA TN D-594, Technical Note D-594: National Aeronautics and Space Administration, Washington, May, 1961.
29. Carslaw, H.S., and Jaeger, J.C., "Conduction of Heat in Solids", 2nd edition, Clarendon, Oxford, 1959, p. 113.
30. Reference (26), p. 573 and p. 575.
31. Hilton, W.F., "Techniques of Flow Visualisation", Research and Development for Industry, No. 8, April, 1962.
32. Reference (26), p. 640.
33. Chang, Y.P., "A Theoretical Analysis of Heat Transfer in Natural Convection and in Boiling", Trans. ASME, Vol. 79, 1957, pp. 1501-1513.
34. Bakhmetoff, B.A., "The Mechanics of Turbulent Flow", Princeton University Press, Princeton, N.J., 1936.
35. Kutateladze, S.S., "Heat Transfer in Condensation and Boiling", 2nd edition, Translation from a Publication of the State Scientific and Technical Publishers of Literature on Machinery, Moscow - Leningrad, 1952, p. 129: United States Atomic Energy Commission, Technical Information Service.
36. Forster, H.K., and Zuber, N., "Dynamics of Vapour Bubbles and Boiling Heat Transfer", AIChE Journal, 1, 1955, pp. 531-535.
37. Reference (1), p. 381.
38. McAdams, W.H., et al., "Heat Transfer at High Rates with Surface Boiling", Industrial and Engineering Chemistry, Vol. 41, July - Dec., 1949, pp. 1945-1953.

REGIMES OF BOILING

(NUKIYAMA [1] IN 1934)

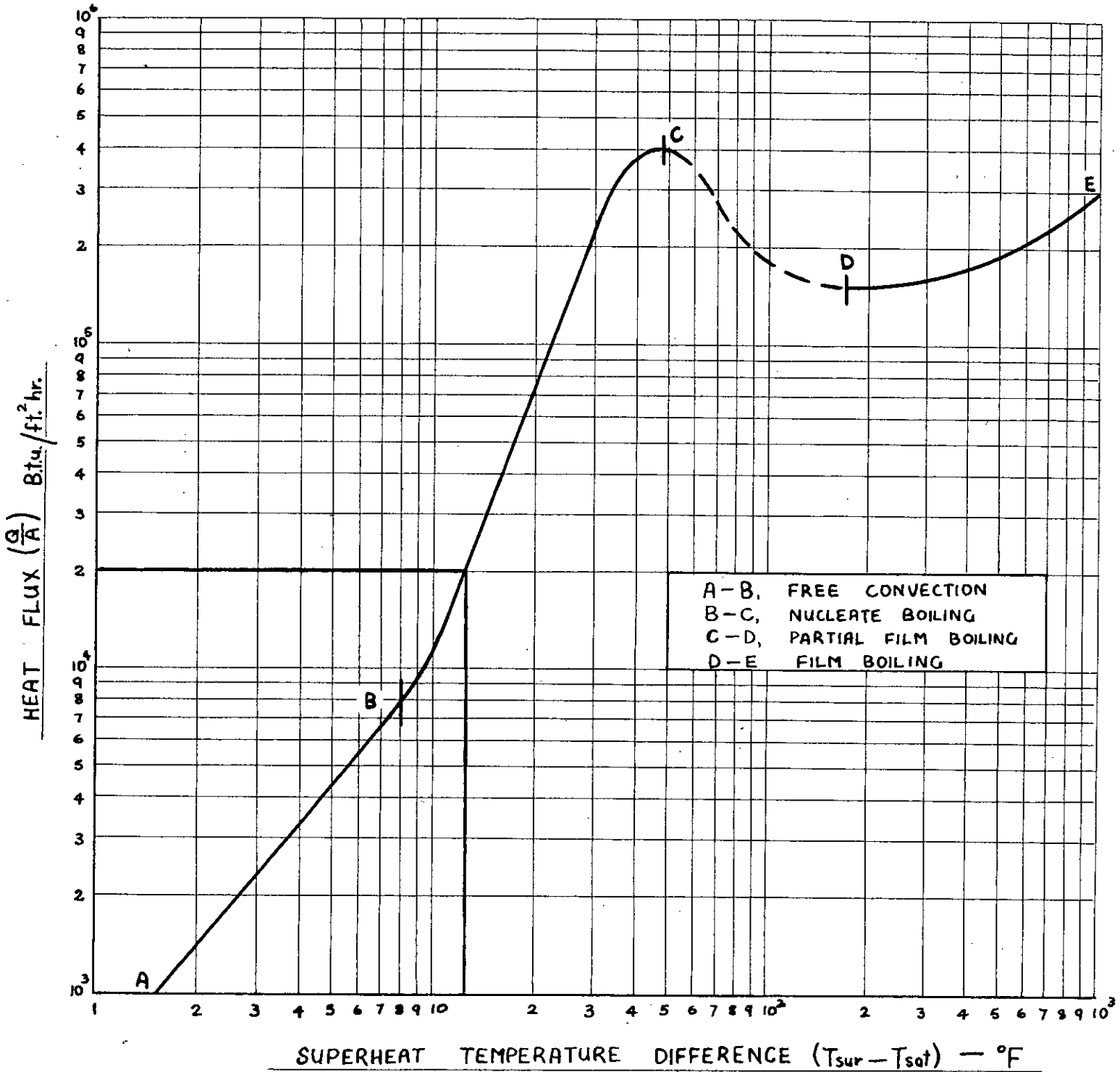


FIG. 1

HALF SECTIONAL VIEW OF BOILER SHELL

SCALE:- HALF FULL SIZE

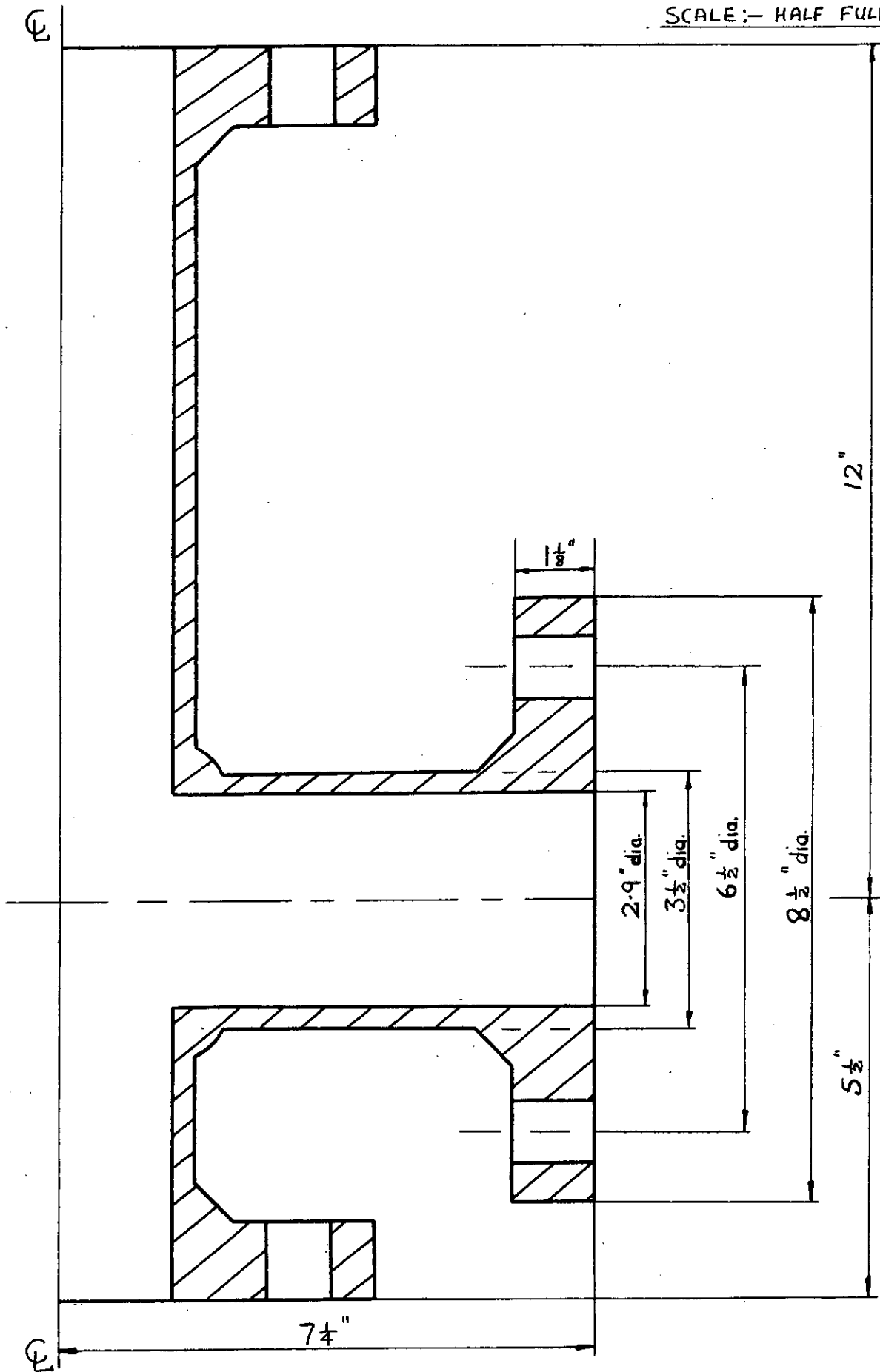
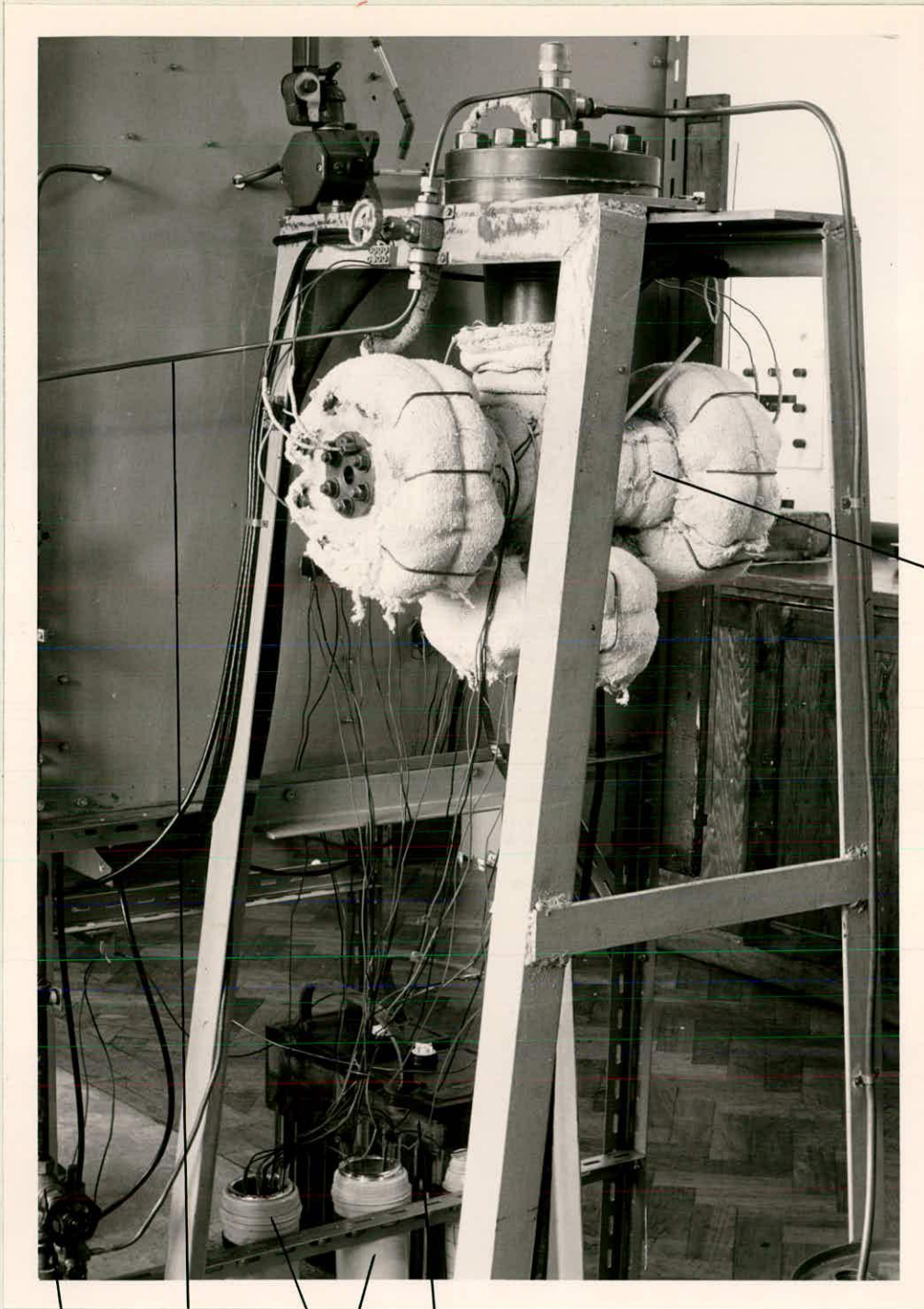


FIG. 2

PHOTOGRAPH OF BOILER AND OTHER PARTS OF THE APPARATUS






- 5
- 4
- 3
- 2

- 1. BOILER
- 2. 2 Volt CHLORIDE PLANTE ACCUMULATOR
- 3. COLD JUNCTIONS
- 4. NITROGEN SUPPLY TO BOILER
- 5. WATER SUPPLY TO JET PUMPS

FIG. 3

SECTIONAL VIEW OF BOILER WINDOW

SCALE :- FULL SIZE

-  STAINLESS STEEL
-  MILD STEEL
-  "WALKERITE" JOINTING

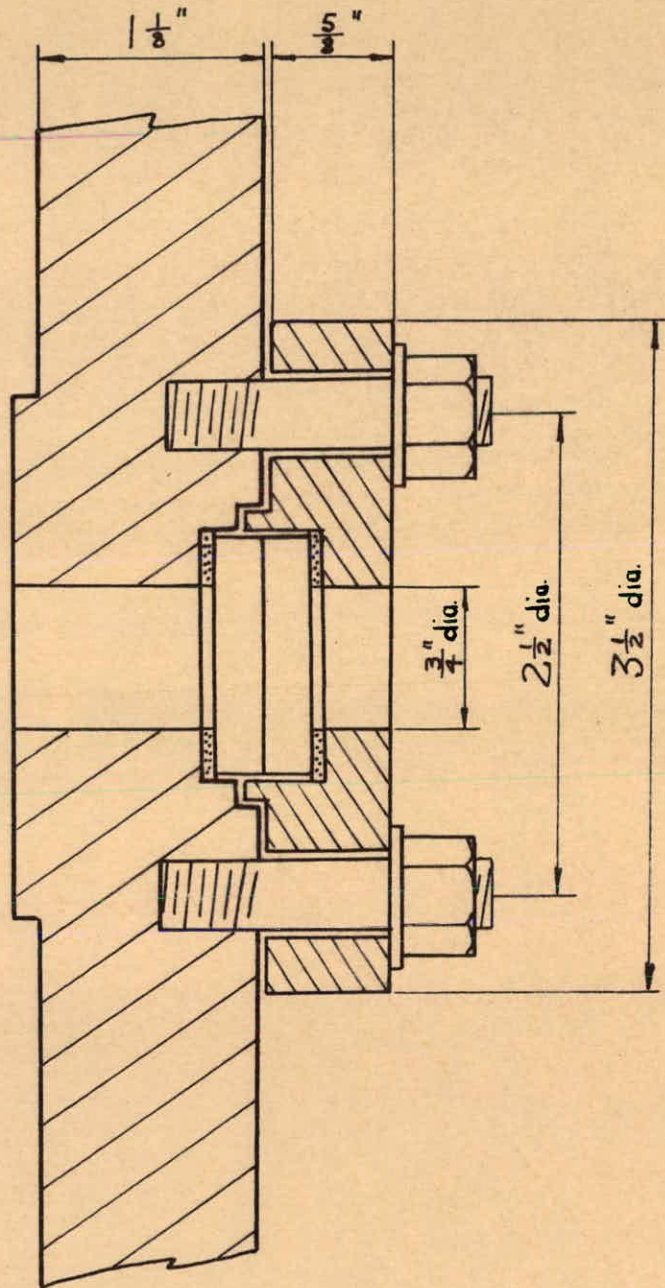


FIG. 4

HEATING STRIP ASSEMBLY

SCALE :- FULL SIZE

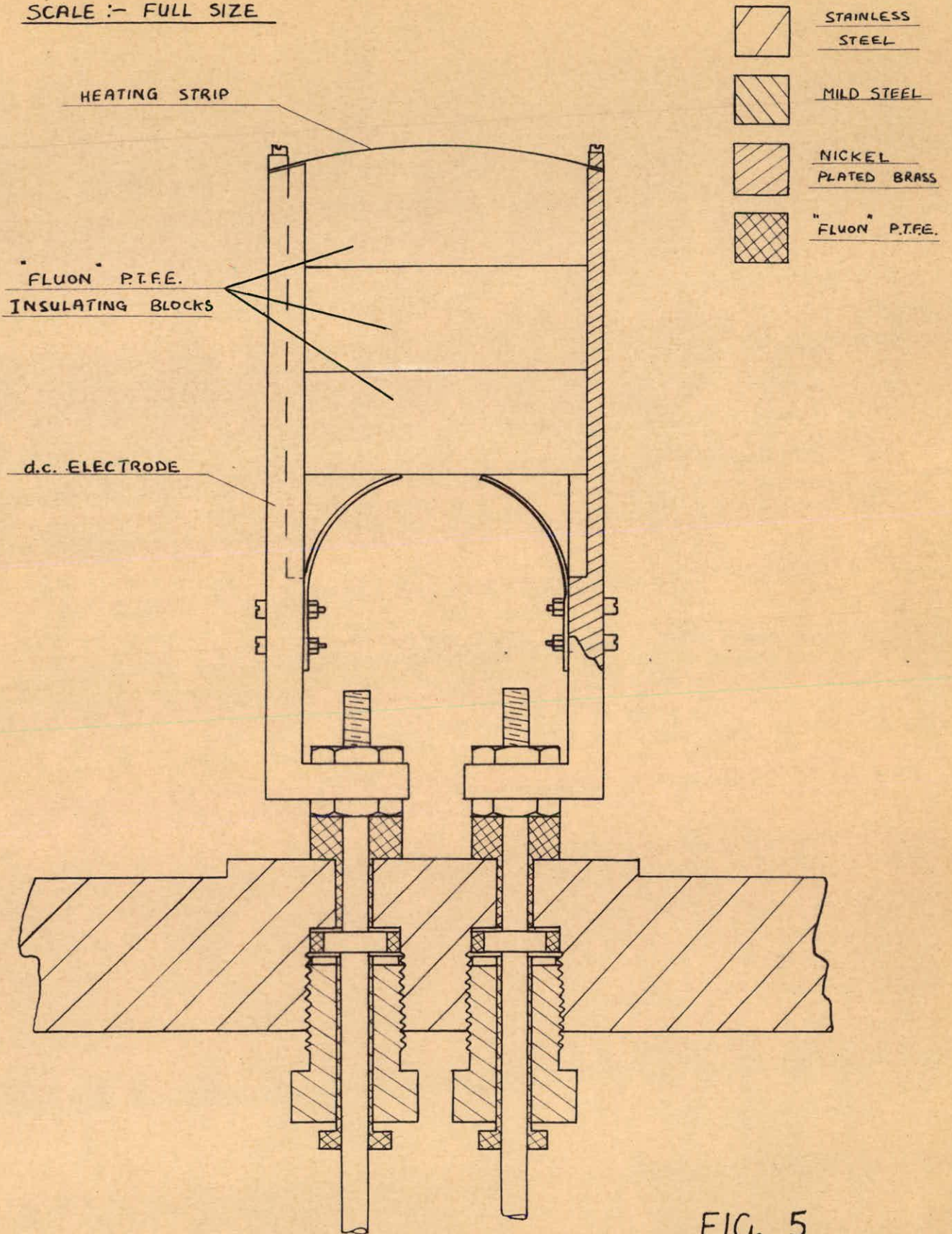


FIG. 5

CAVITY DISTRIBUTION

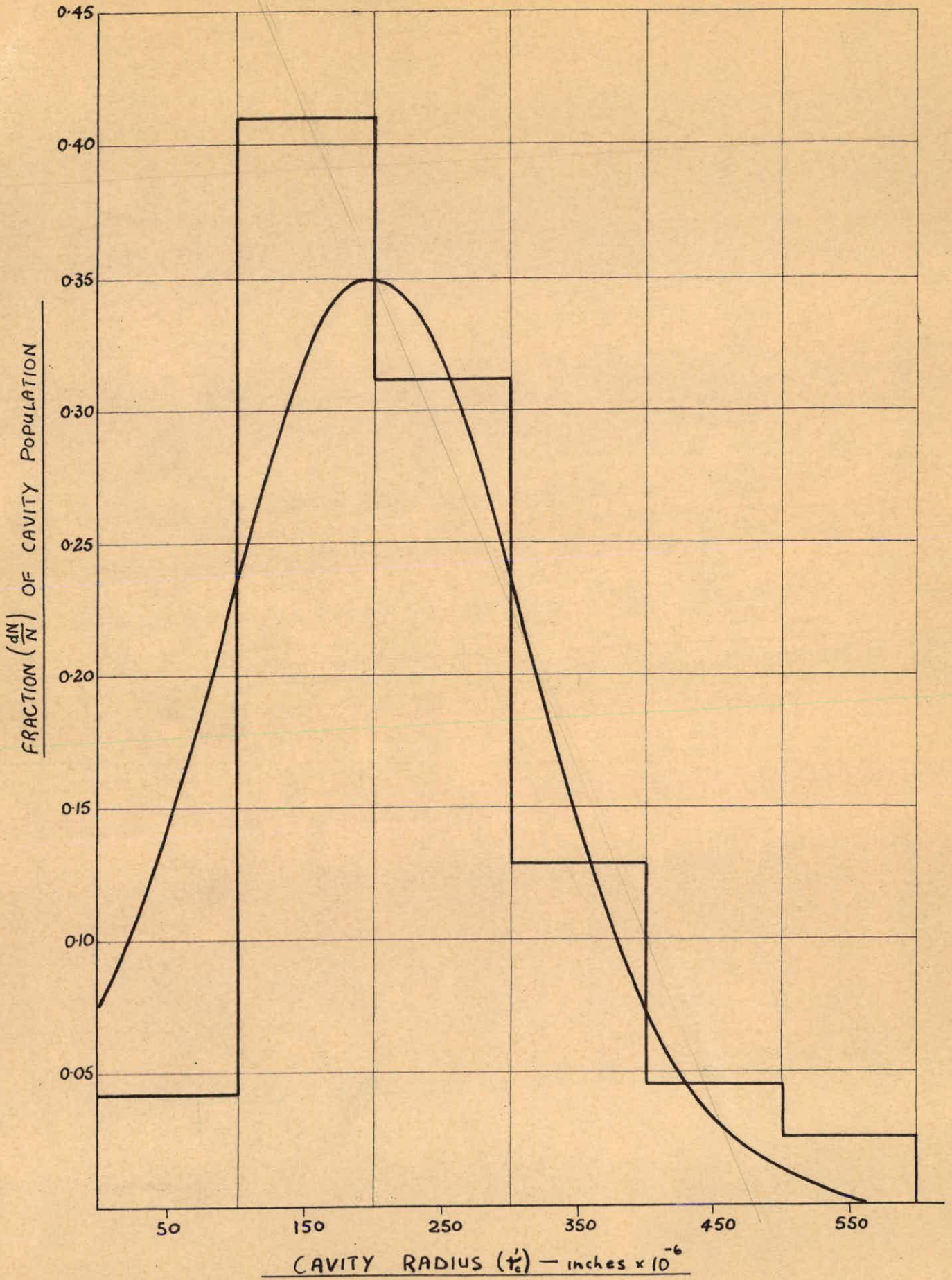


FIG. 6

PHOTOGRAPH OF TALYSURF RECORDS

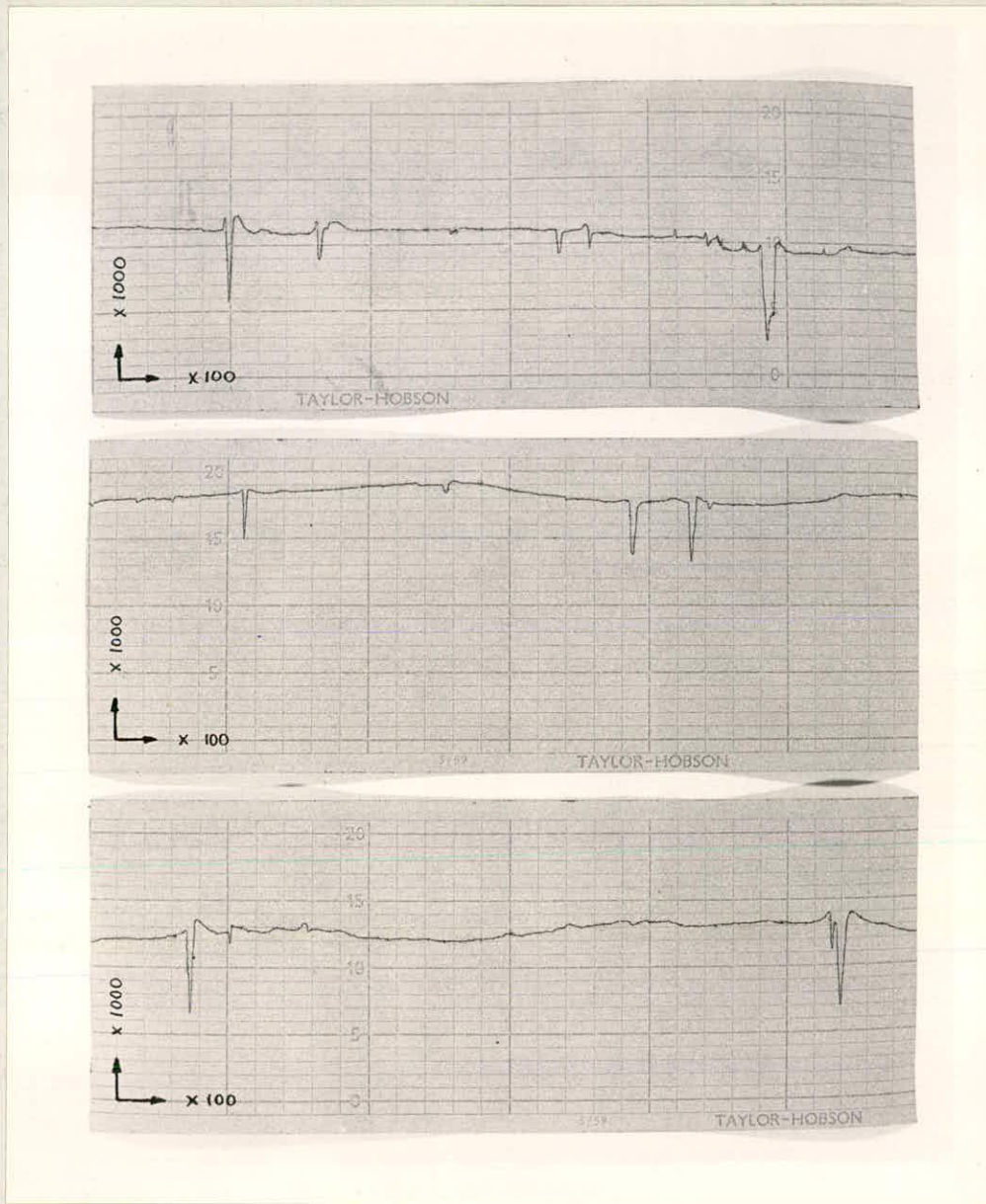


FIG. 7

WELDER FOR 0.002 inch dia. THERMOCOUPLE WIRES

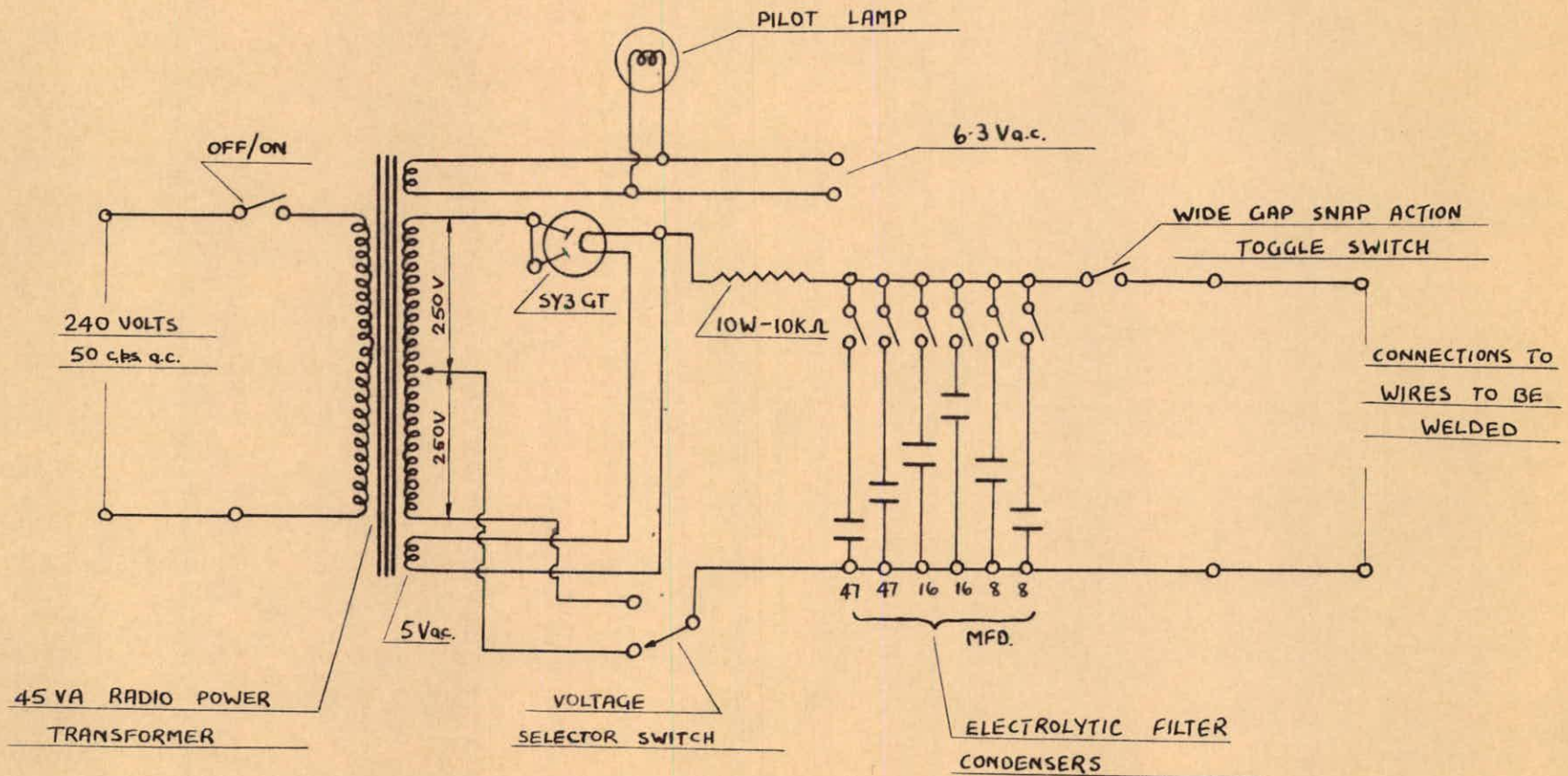
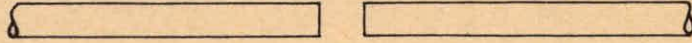


FIG. 10

STAGES IN THE MANUFACTURE OF THE HEATING STRIP THERMOCOUPLE

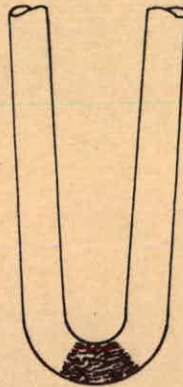
① 0.002 INCH DIAMETER WIRES PREPARED FOR WELDING



② WIRES DISCHARGE WELDED TO FORM THERMOCOUPLE JUNCTION



③ THERMOCOUPLE BENT AT JUNCTION



④ THERMOCOUPLE DISCHARGE WELDED TO HEATING STRIP
ALONG A CONSTANT VOLTAGE PLANE

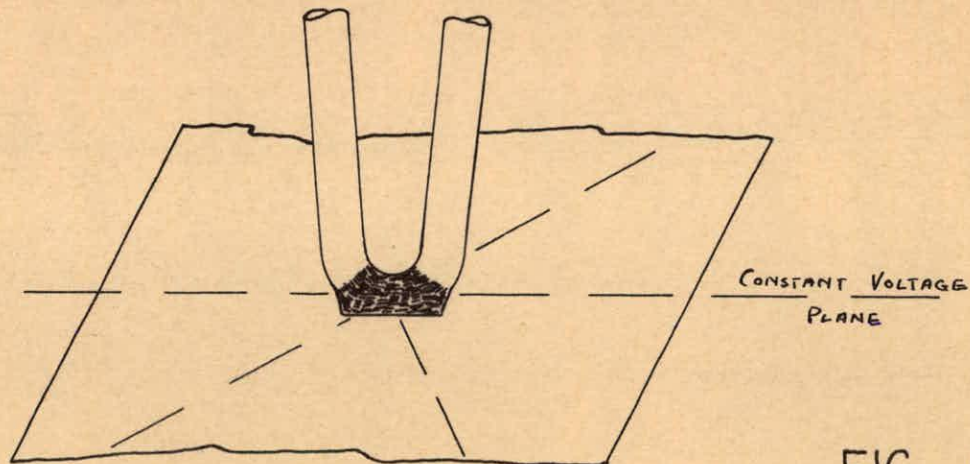


FIG. 11

SCHEMATIC ARRANGEMENT OF THERMOCOUPLE CIRCUITS

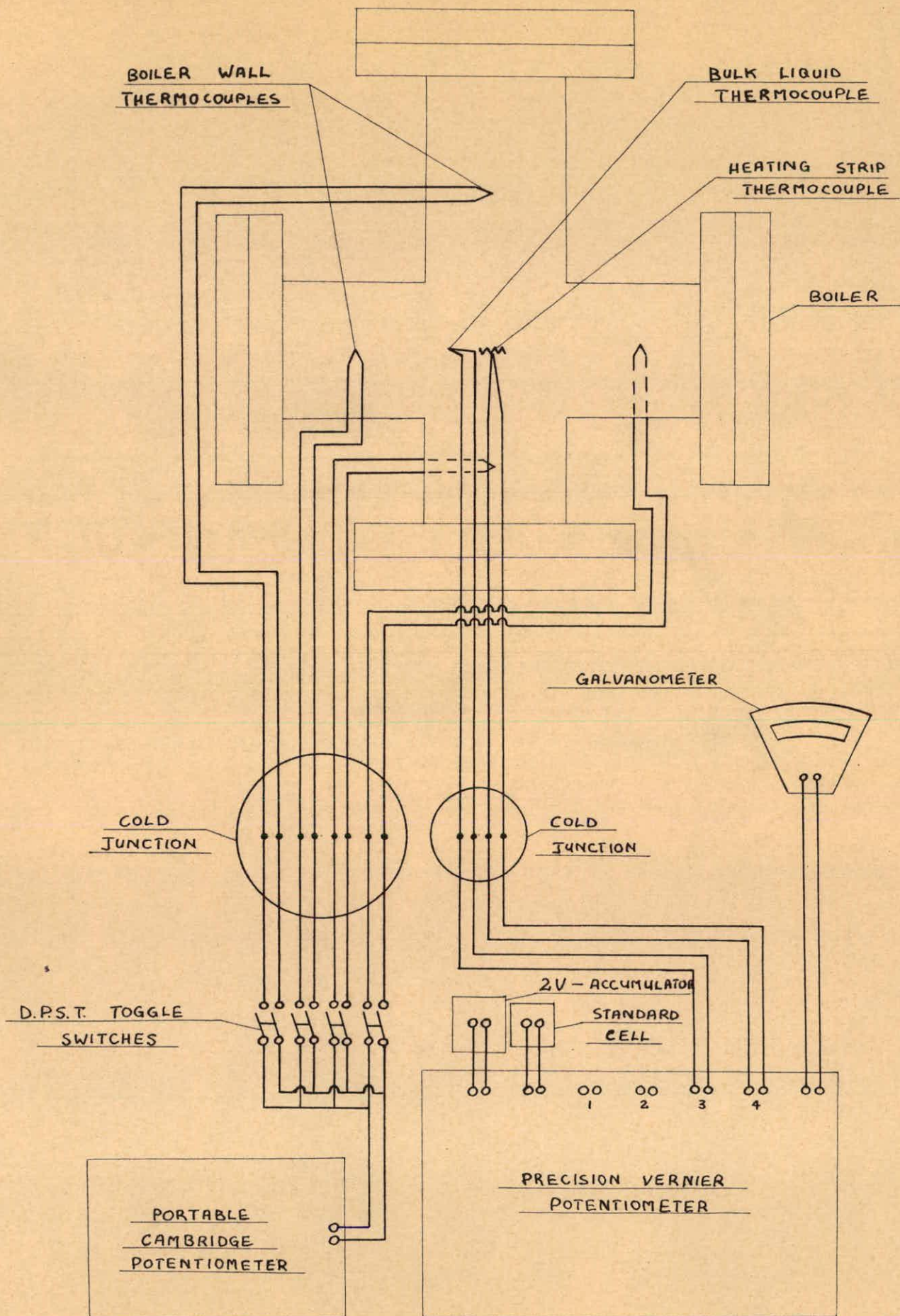
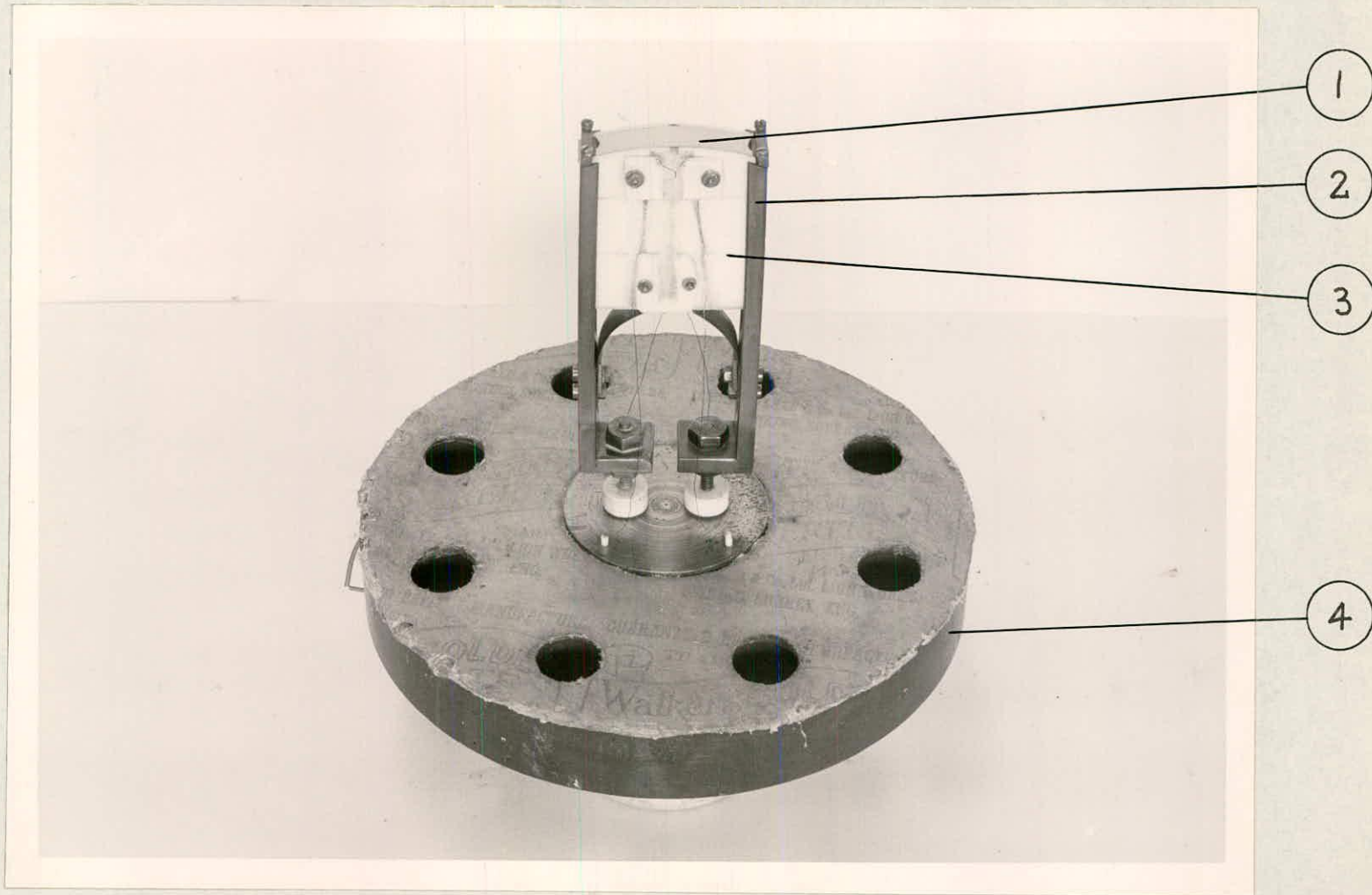


FIG. 12

PHOTOGRAPH OF HEATING STRIP ASSEMBLY



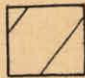


1. HEATING STRIP
2. d.c. ELECTRODE
3. p.t.f.e. INSULATION
4. BOILER BOTTOM FLANGE

FIG. 13

SECTIONAL VIEW OF THERMOCOUPLE

PRESSURE SEAL

SCALE:- FULL SIZE

-  STAINLESS STEEL
-  CAST IRON
-  "FLUON" P.T.F.E.

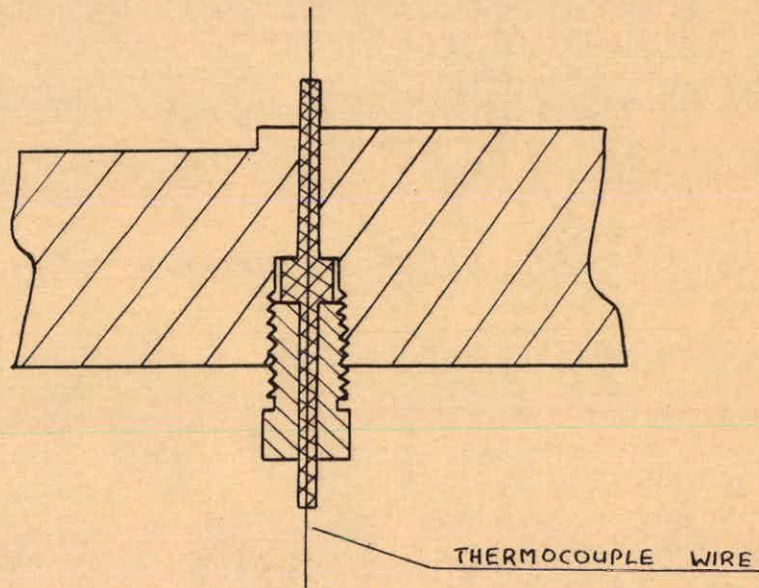


FIG. 14

SCHEMATIC ARRANGEMENT OF d.c. POWER SUPPLY AND MEASUREMENT CIRCUITS

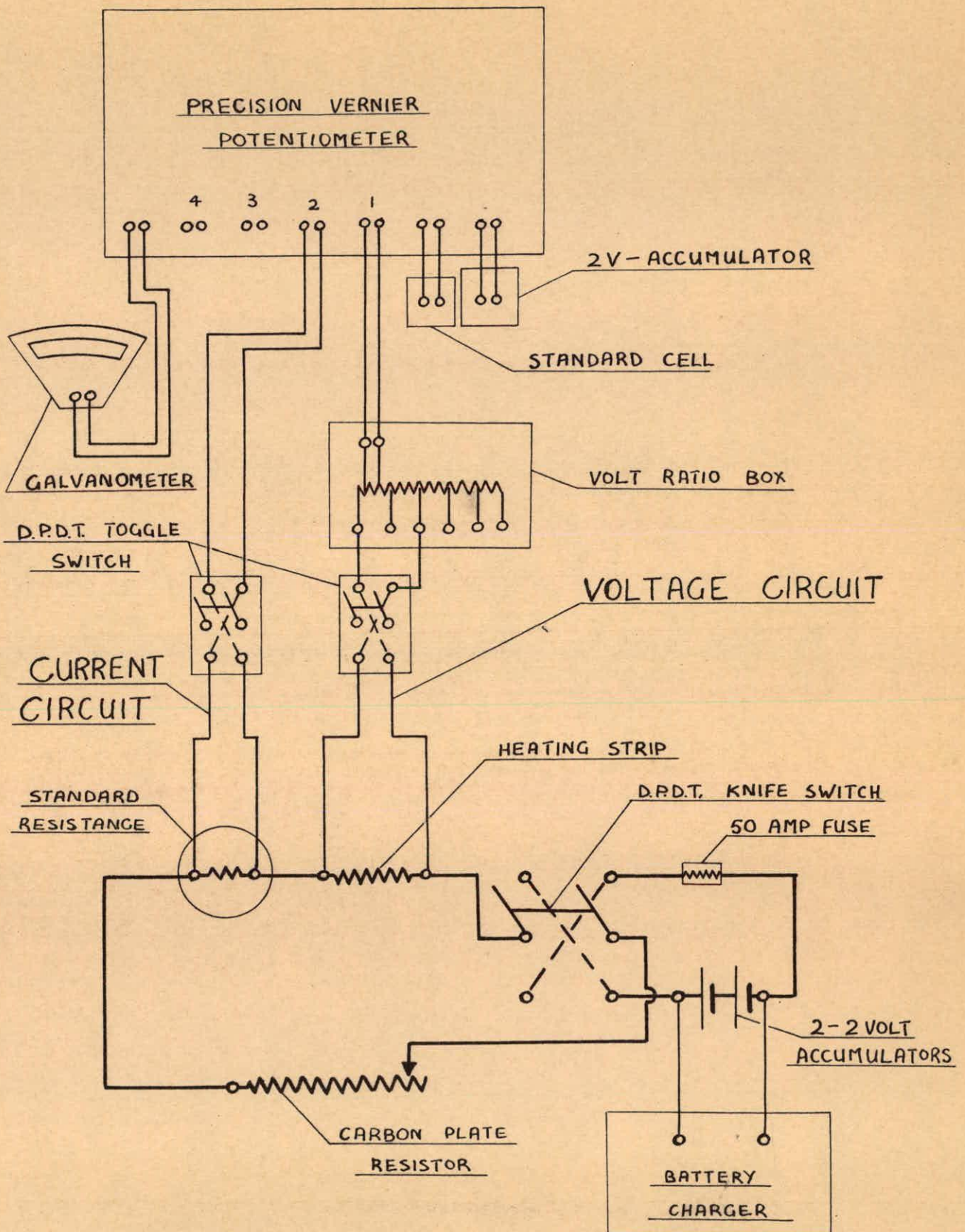
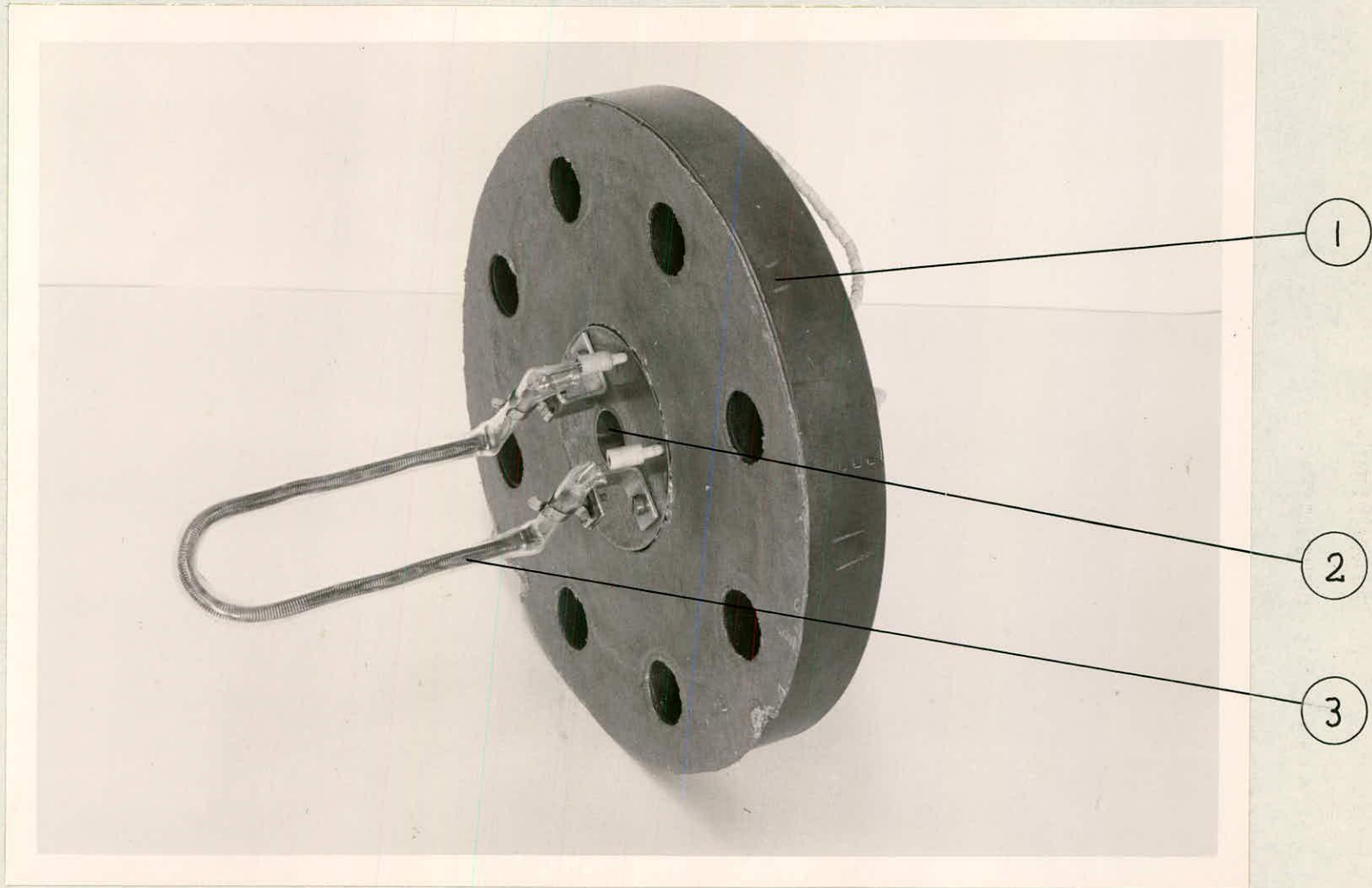


FIG. 15

PHOTOGRAPH OF BULK LIQUID HEATER

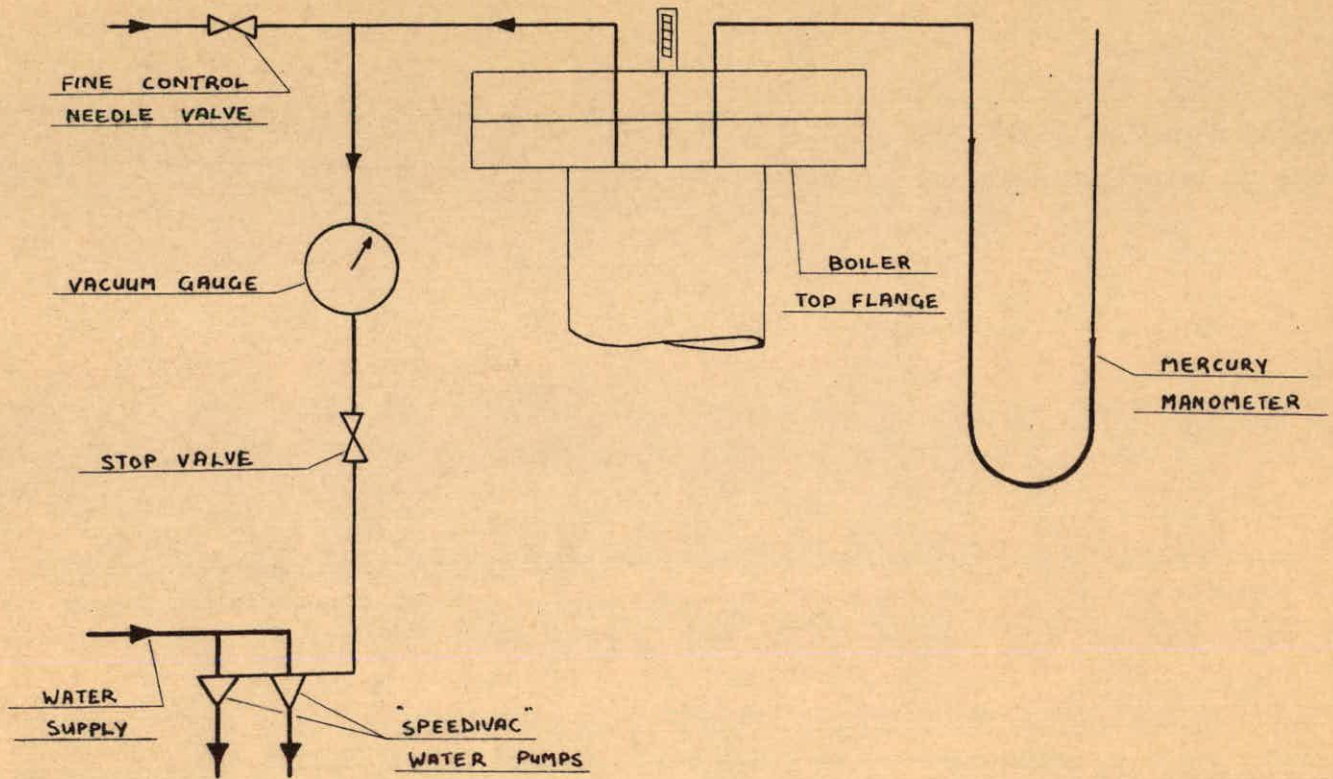


1. BOILER SIDE FLANGE
2. BOILER WINDOW
3. 500 watt HEATING ELEMENT IN "PYREX" GLASS TUBE

FIG. 16

BOILER PRESSURE SYSTEMS

(a) ATMOSPHERIC TO 116./inch² abs.



(b) ATMOSPHERIC TO 1000 lb./inch² abs.

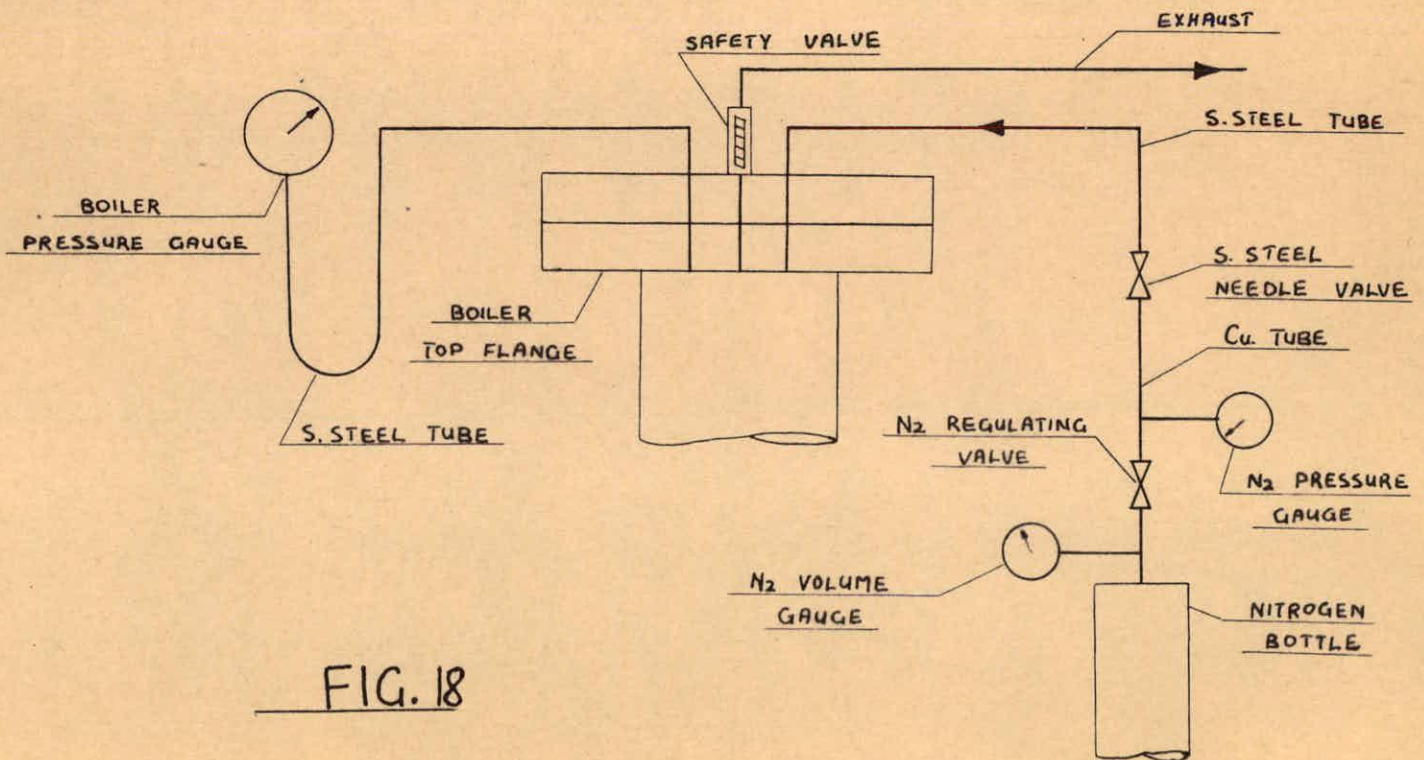


FIG. 18

SCHEMATIC ARRANGEMENT OF BULK LIQUID AND BOILER WALL a.c. HEATER CIRCUITS

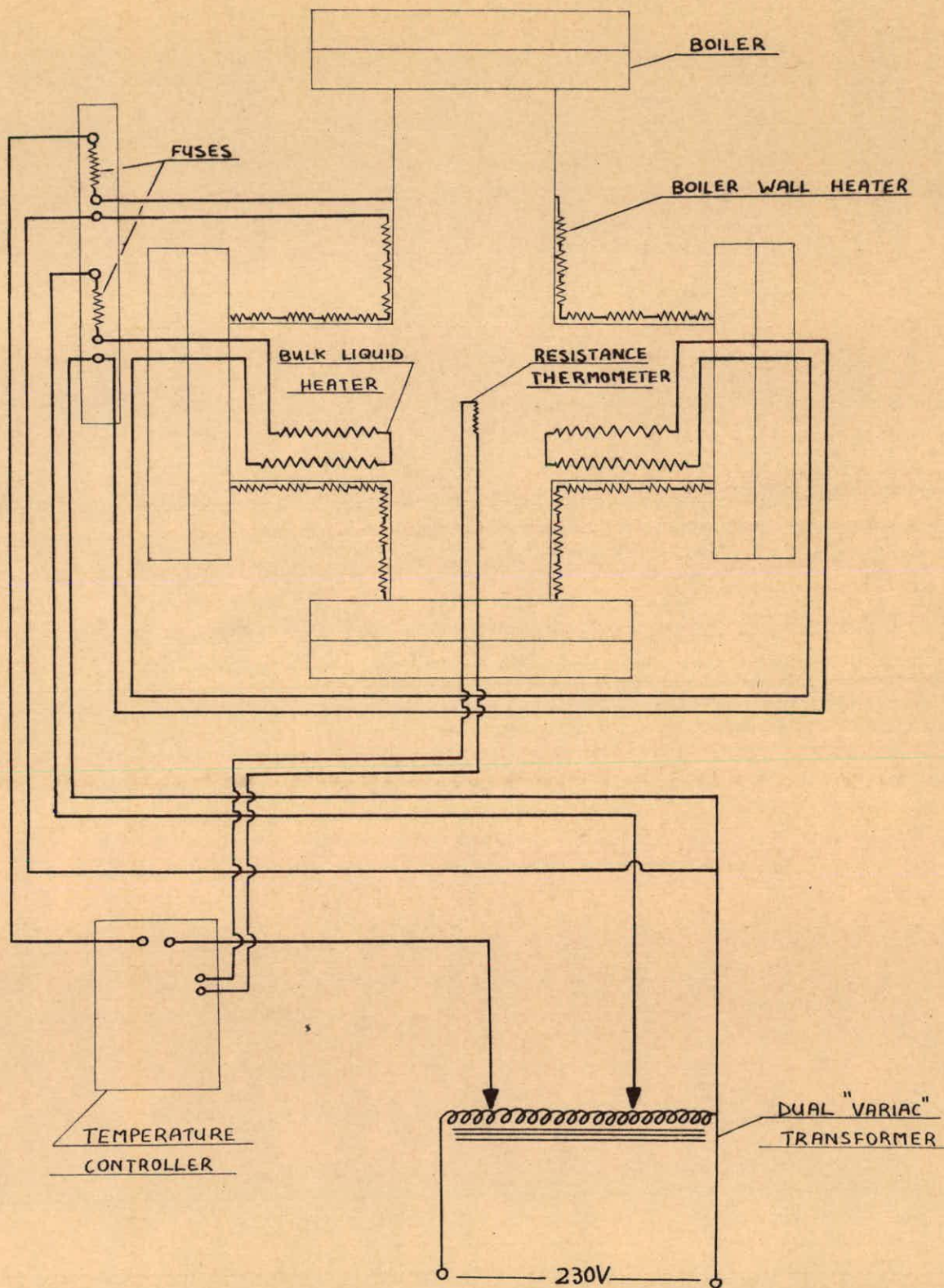
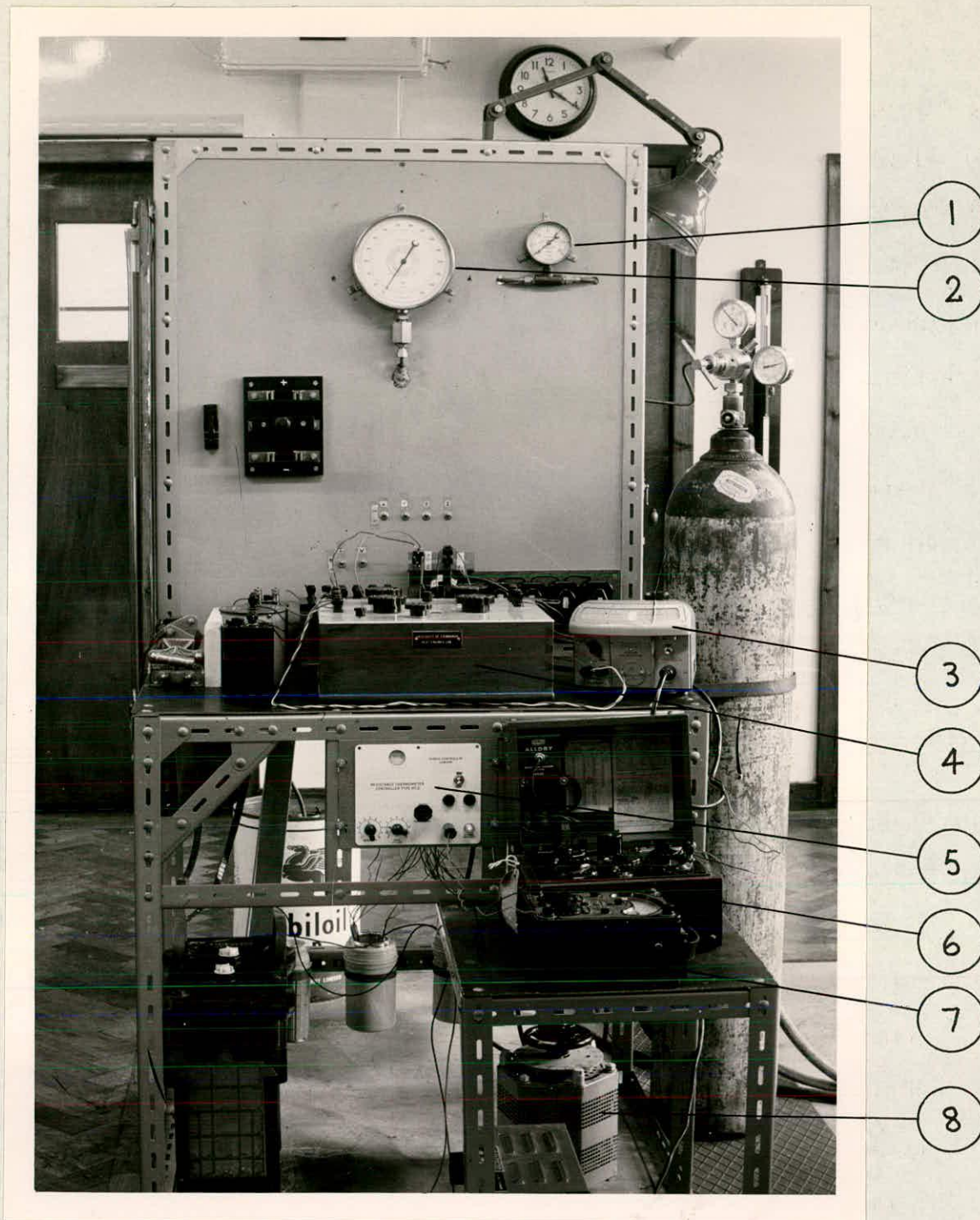


FIG. 17

PHOTOGRAPH OF RECORDING EQUIPMENT



1. VACUUM GAUGE
2. PRESSURE GAUGE
3. GALVANOMETER
4. PRECISION POTENTIOMETER
5. TEMPERATURE CONTROLLER
6. PORTABLE POTENTIOMETER
7. AVOMETER
8. DUAL "VARIAC" TRANSFORMER

FIG. 19

HEATING STRIP THERMOCOUPLE e.m.f. DIFFERENCE vs.
HEATING STRIP VOLTAGE

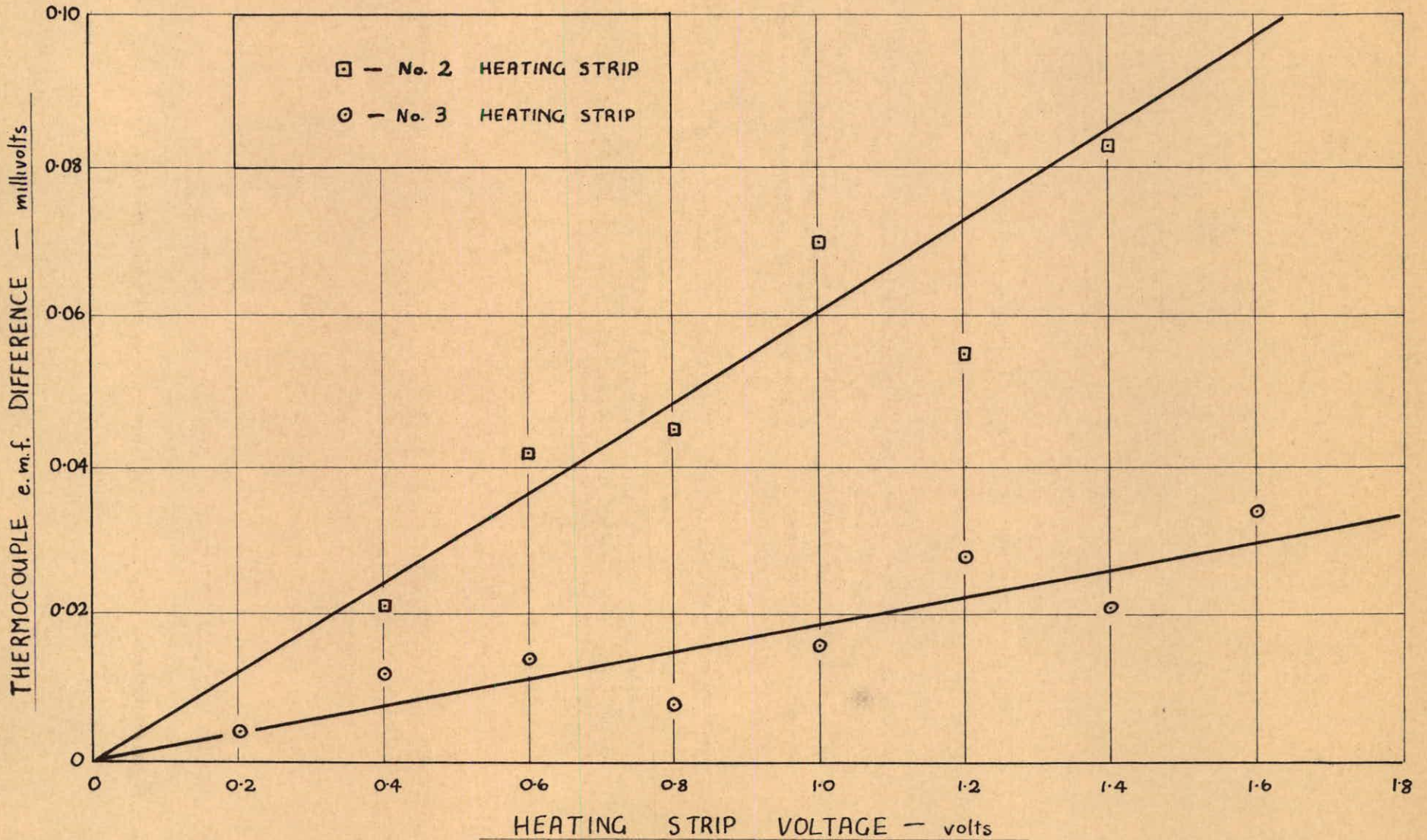


FIG. 20

INITIATION SUPERHEAT TEMPERATURE DIFFERENCE FOR
FIRST BUBBLE SITE vs. LIQUID PRESSURE

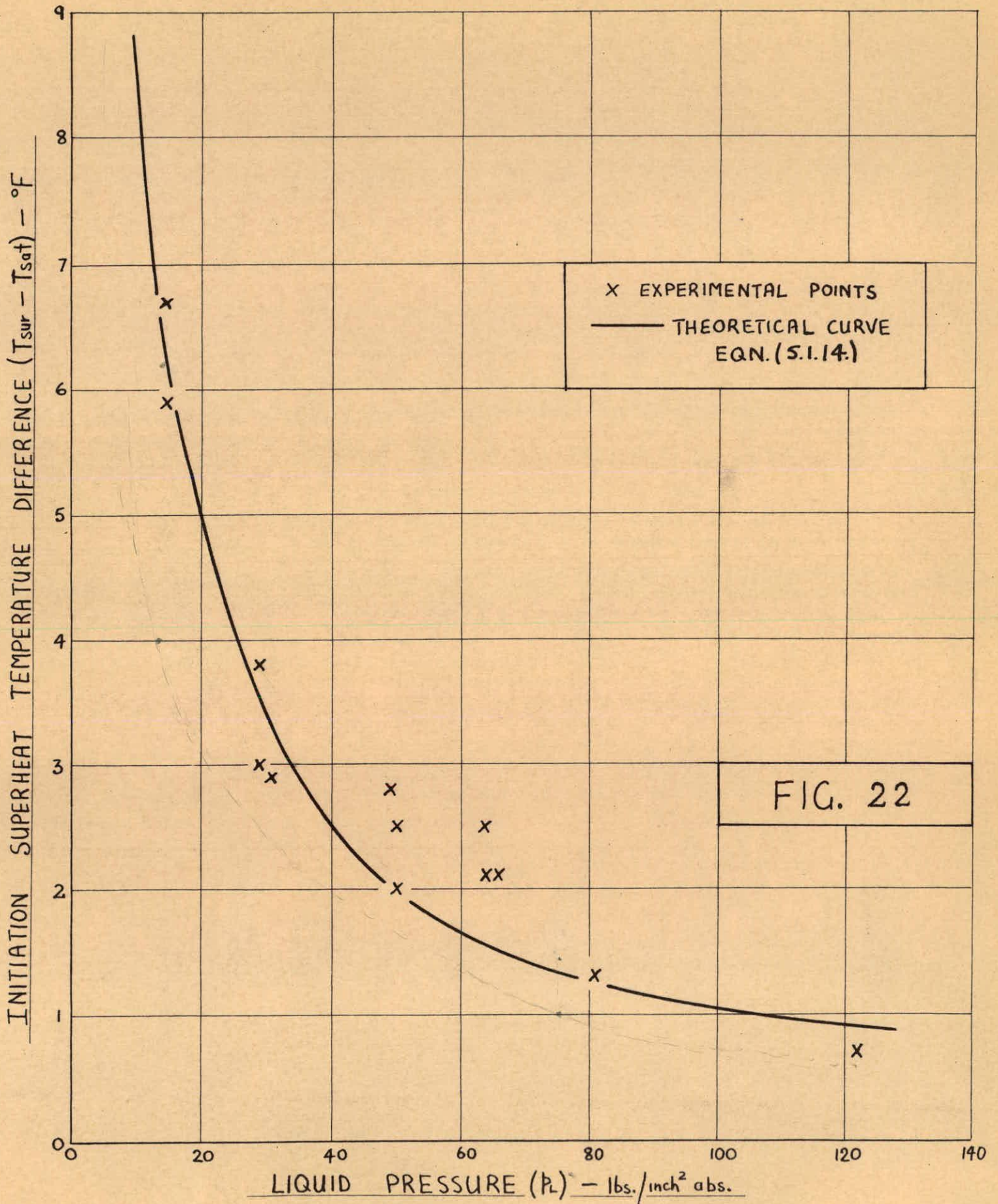


FIG. 22

NUMBER OF BUBBLE SITES vs.
SUPERHEAT TEMPERATURE DIFFERENCE

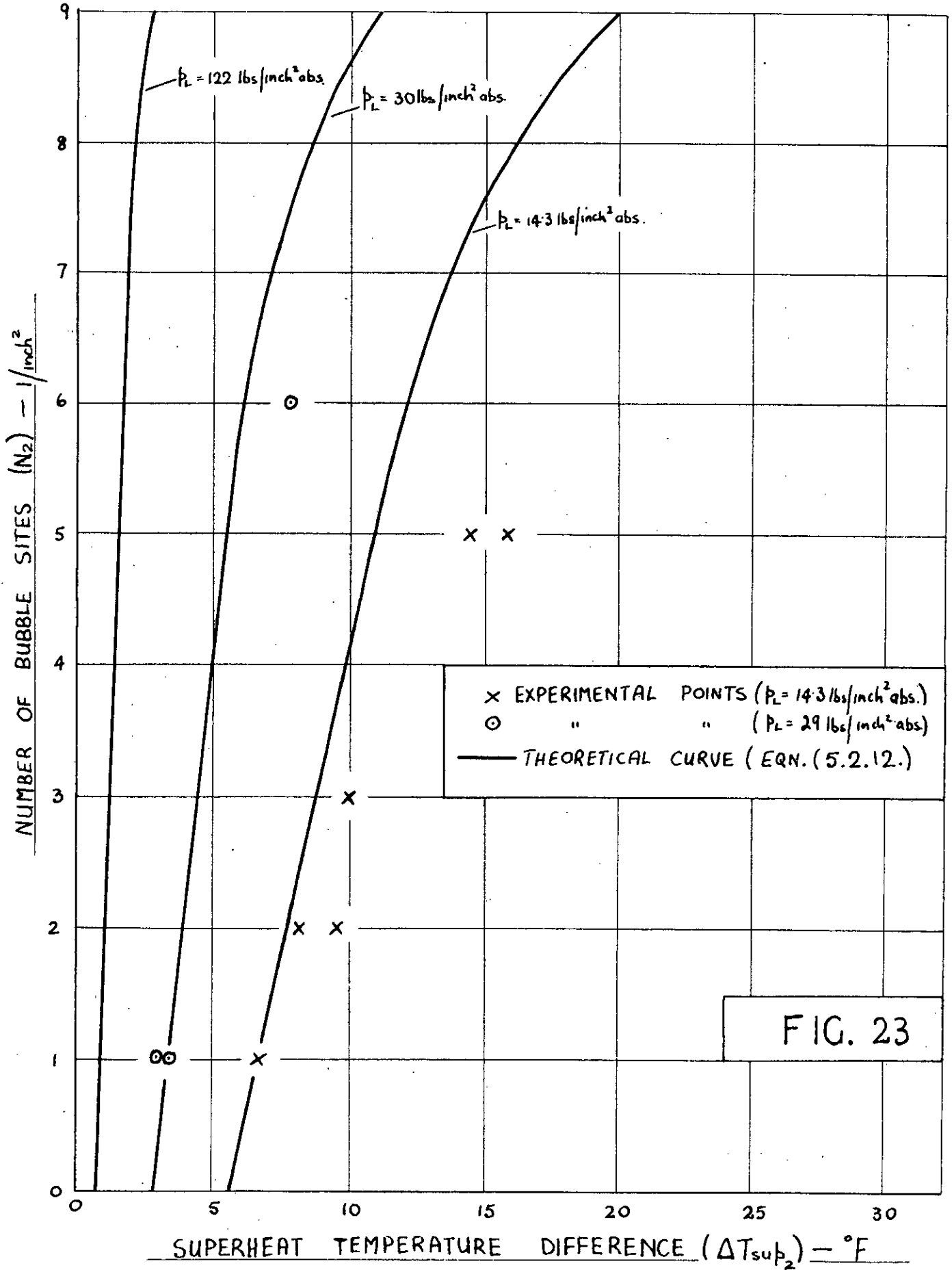


FIG. 23

BUBBLE FREQUENCY vs.

SUPERHEAT TEMPERATURE DIFFERENCE

(LIQUID PRESSURE = 14.3 lbs/inch² abs.)

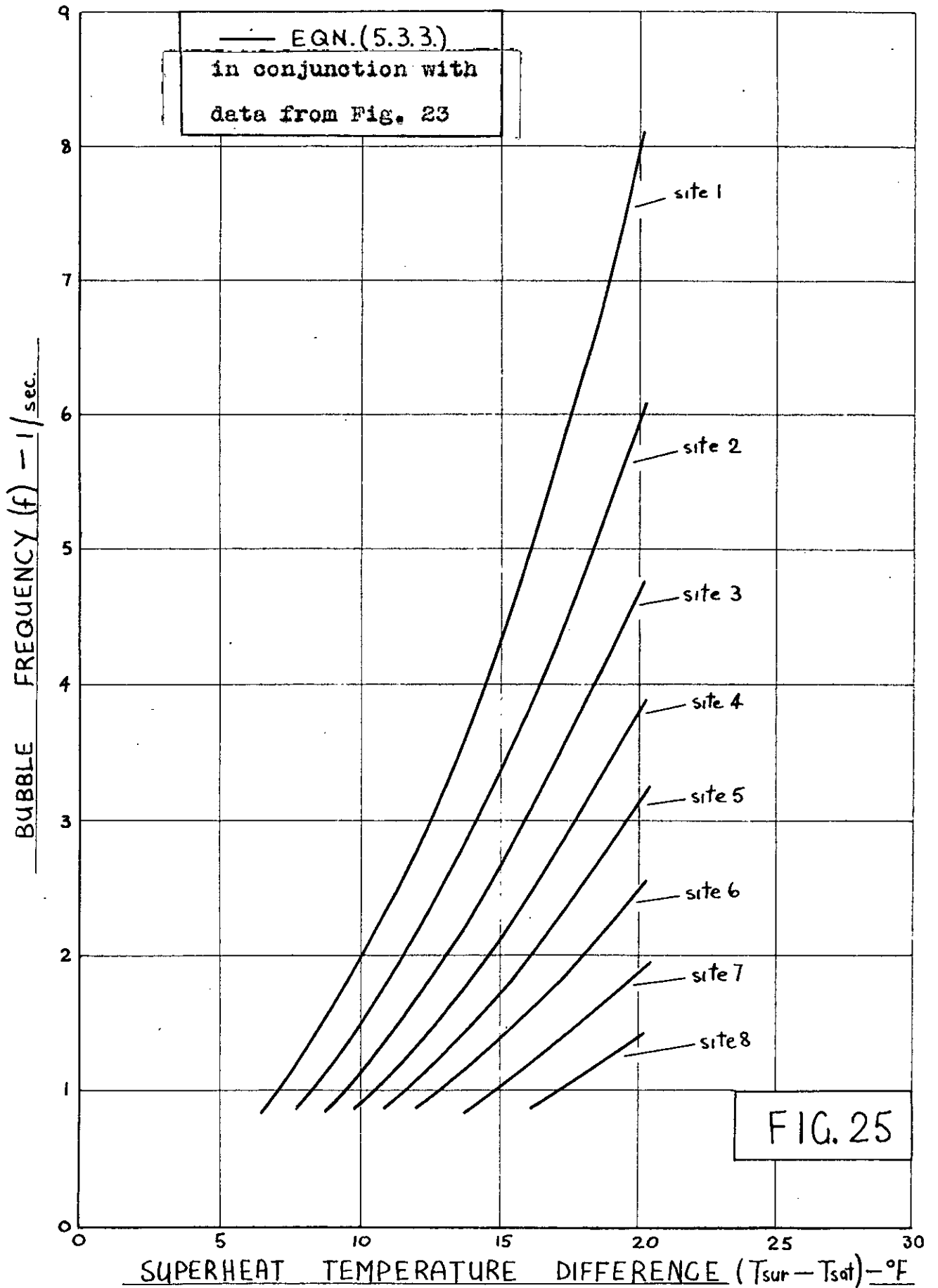


FIG. 25

BUBBLE FLUX vs.
SUPERHEAT TEMPERATURE DIFFERENCE

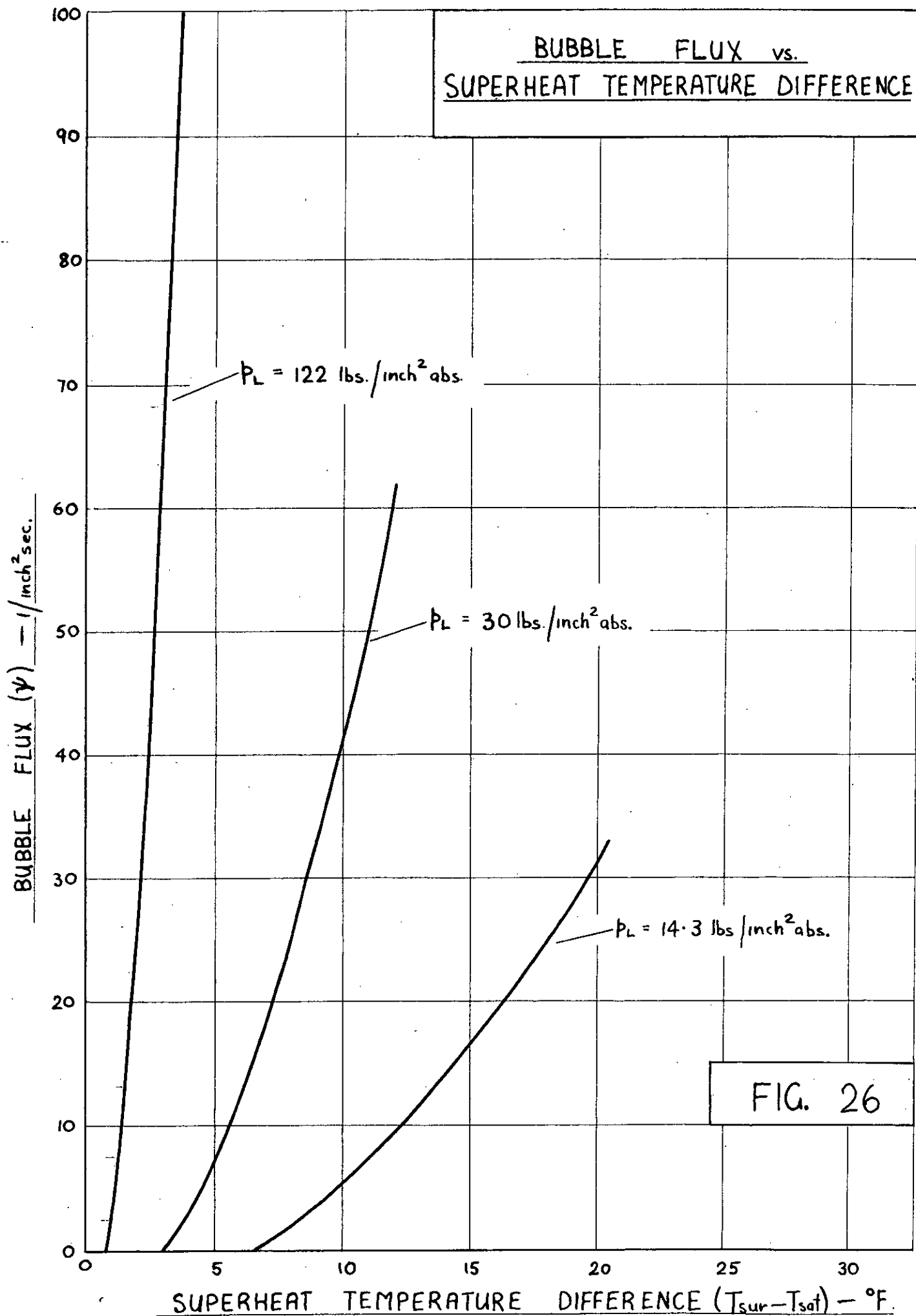


FIG. 26

CORRELATION OF WEAK BOILING REGION

(LIQUID PRESSURE $P_L = 14.3 \text{ lbs./inch}^2 \text{ abs.}$)

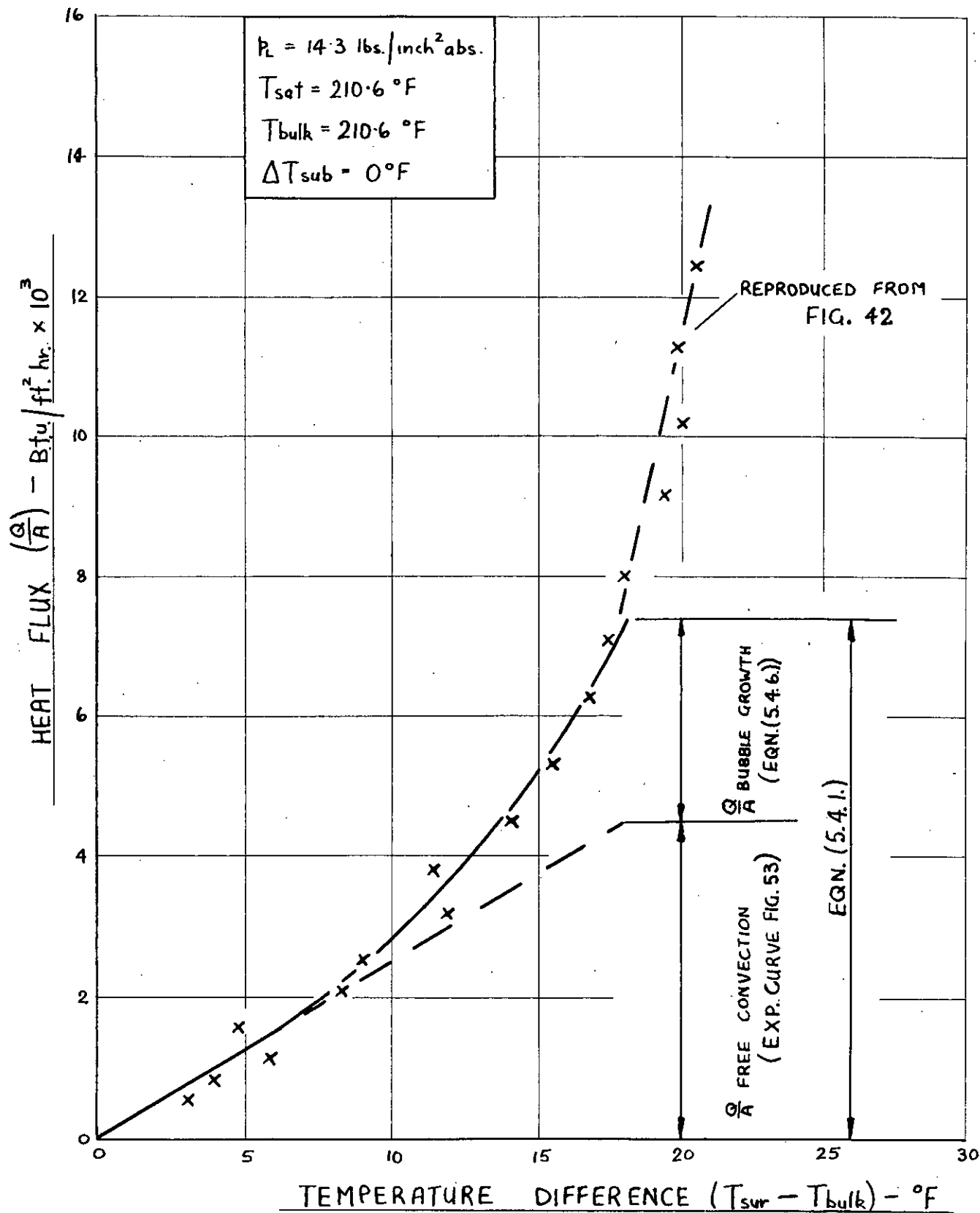


FIG. 27

CORRELATION OF WEAK BOILING REGION

(LIQUID PRESSURE $P_L = 30 \text{ lbs./inch}^2 \text{ abs.}$)

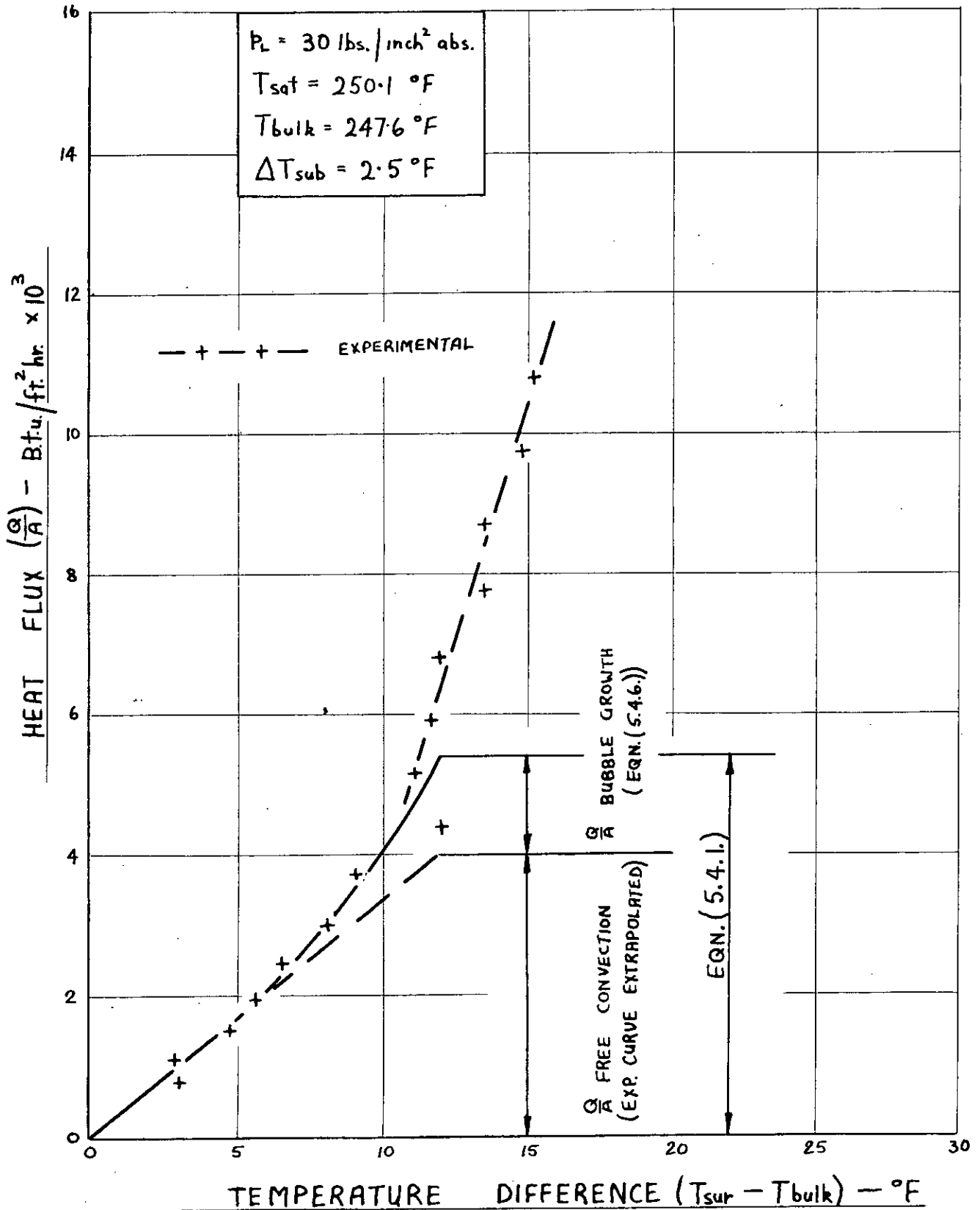


FIG. 28

MAXIMUM BUBBLE DIAMETER vs. HEAT FLUX

EXPERIMENTAL RESULTS OF STANISZEWSKI [21]

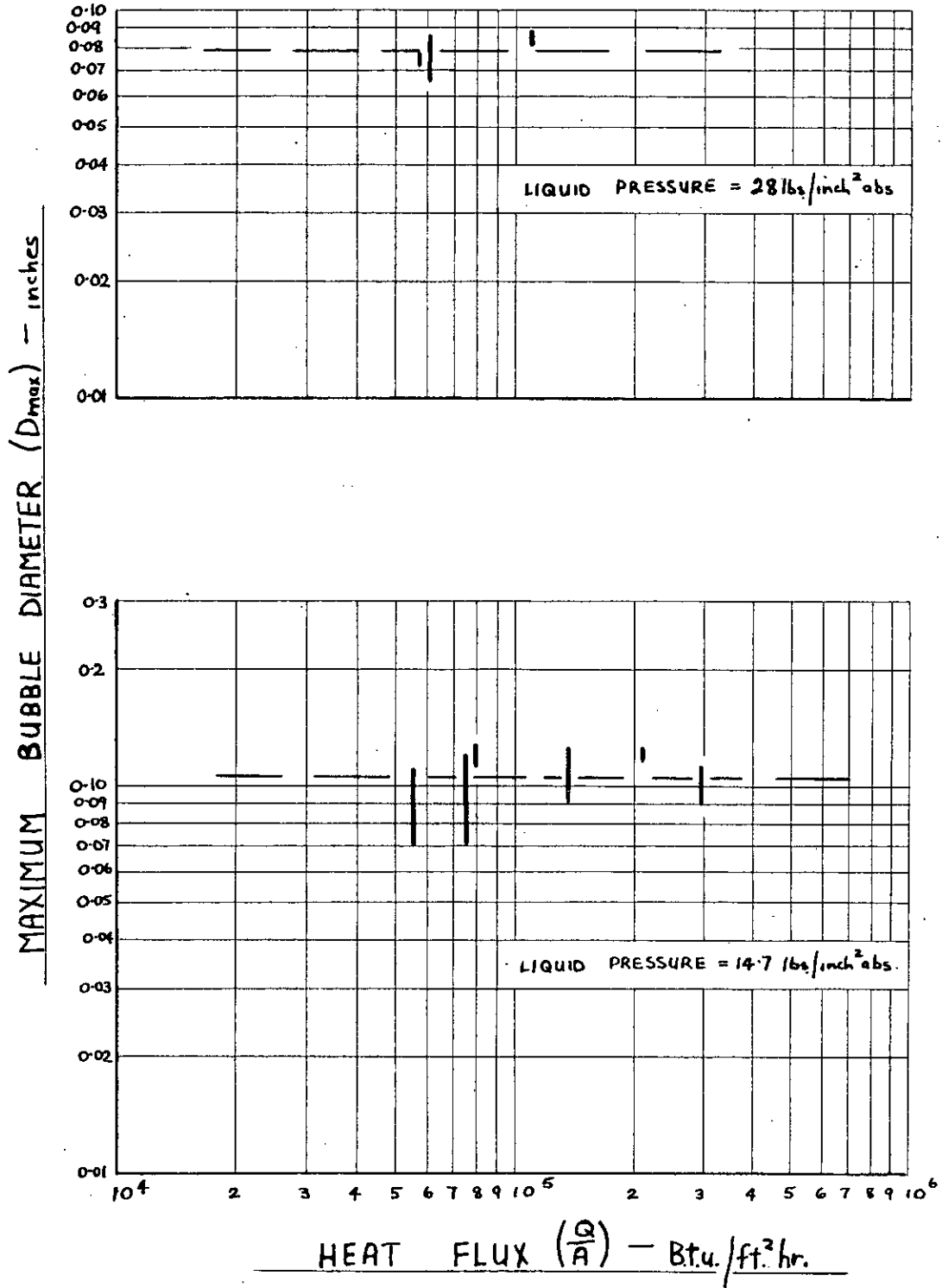


FIG. 29

SHADOWGRAPH OPTICAL BENCH

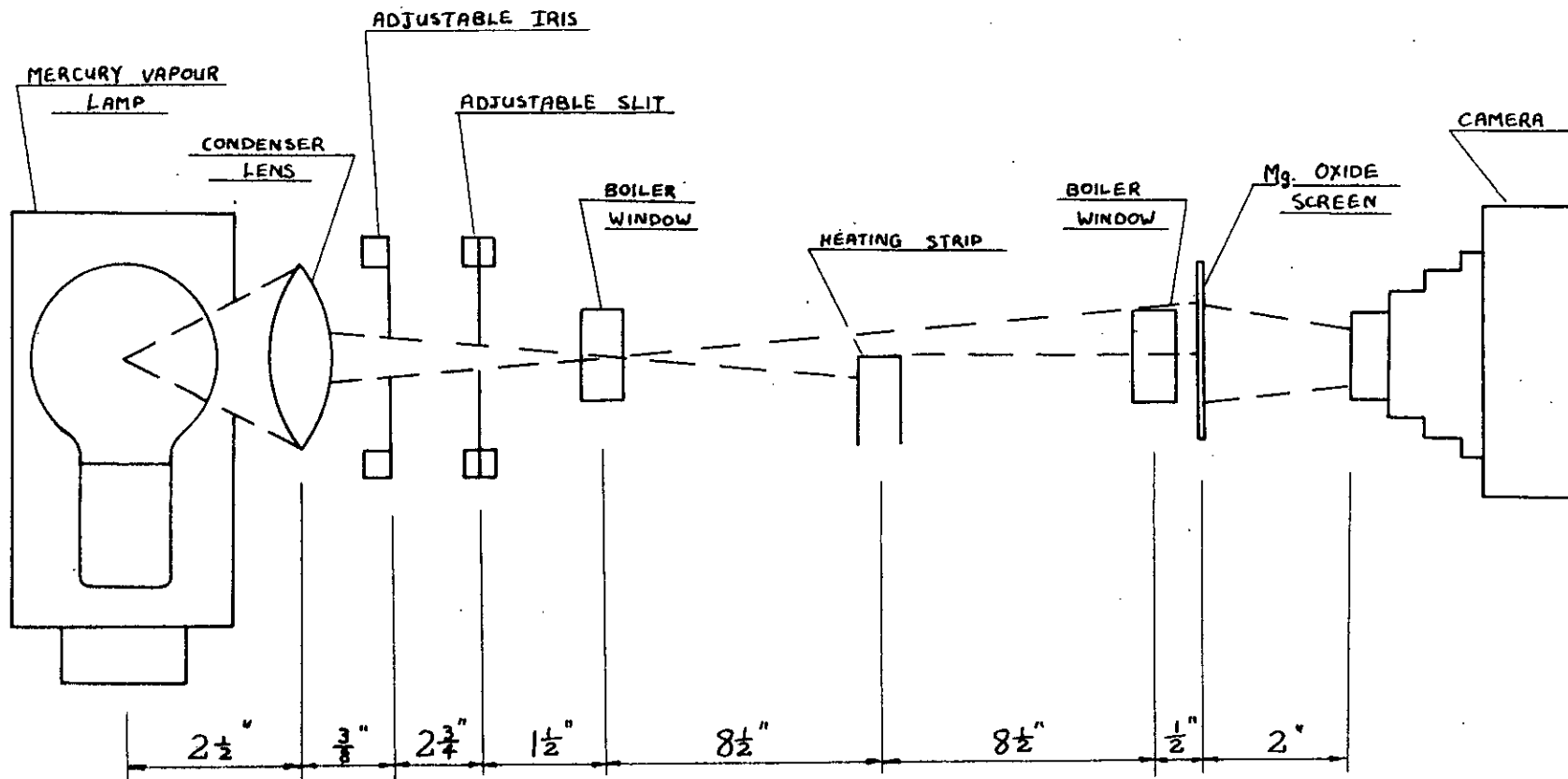


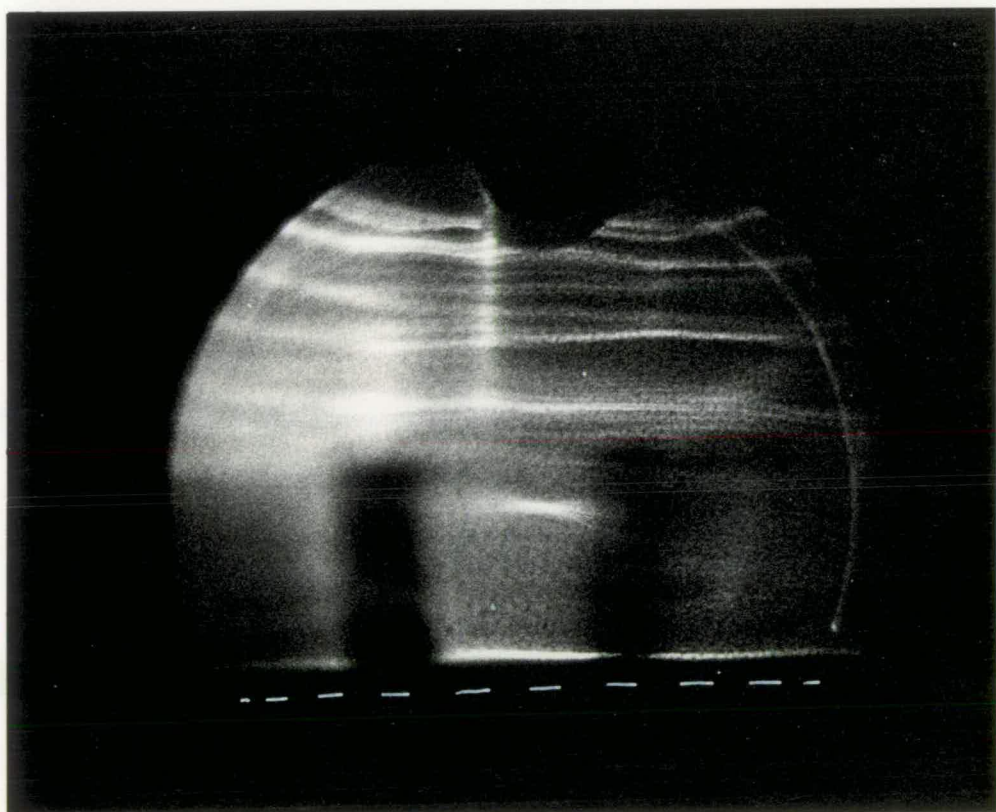
FIG. 31



(a)

$$Q/A = 0 \text{ B.t.u./ft.}^2 \text{ hr.}$$

$$T_{\text{bulk}} = 197.8^{\circ}\text{F}$$



(b)

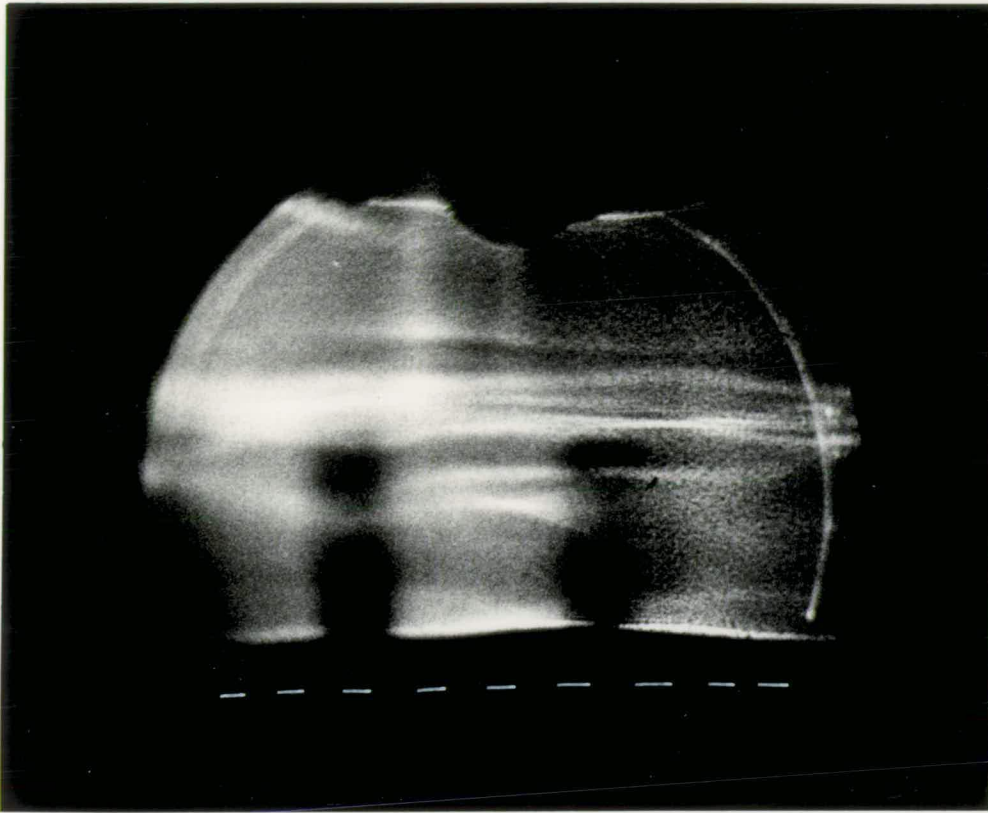
$$Q/A = 975 \text{ B.t.u./ft.}^2 \text{ hr.}$$

$$T_{\text{sur}} = 202.6^{\circ}\text{F}$$

$$T_{\text{bulk}} = 198.7^{\circ}\text{F}$$

$$\delta = 0.017 \text{ inches}$$

FIG. 32



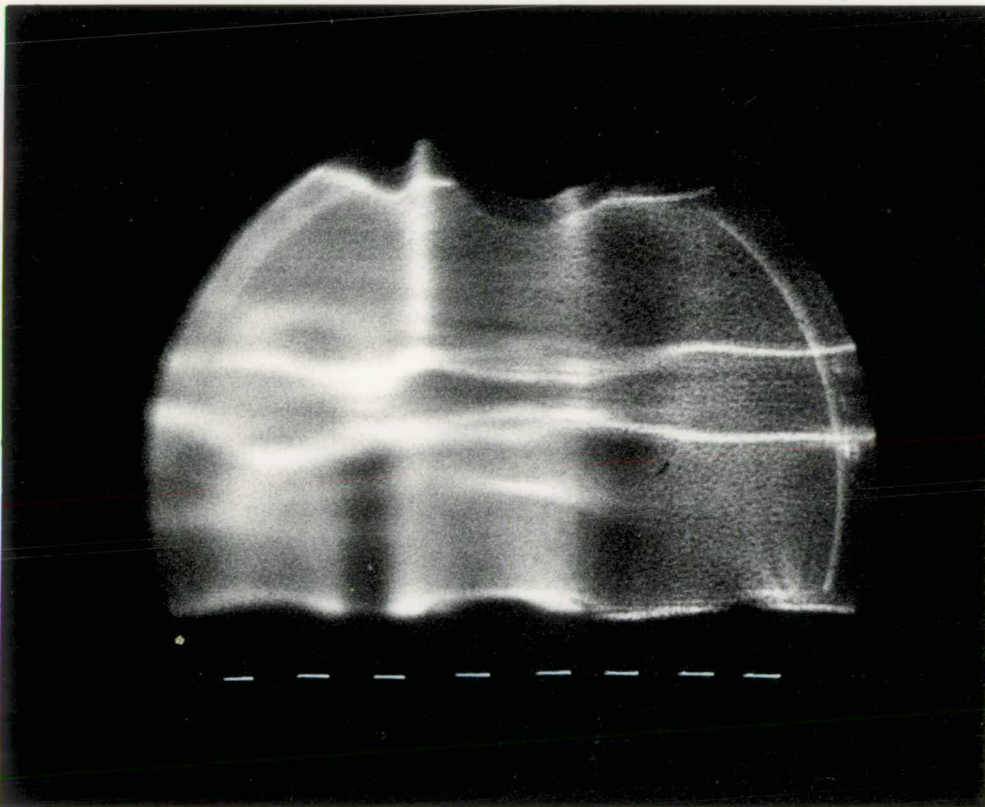
(c)

$$Q/A = 2020 \text{ B.t.u./ft.}^2 \text{ hr.}$$

$$T_{\text{sur}} = 207.1^\circ\text{F}$$

$$T_{\text{bulk}} = 198.4^\circ\text{F}$$

$$\delta = 0.027 \text{ inches}$$



(a)

$$Q/A = 3990 \text{ B.t.u./ft.}^2 \text{ hr.}$$

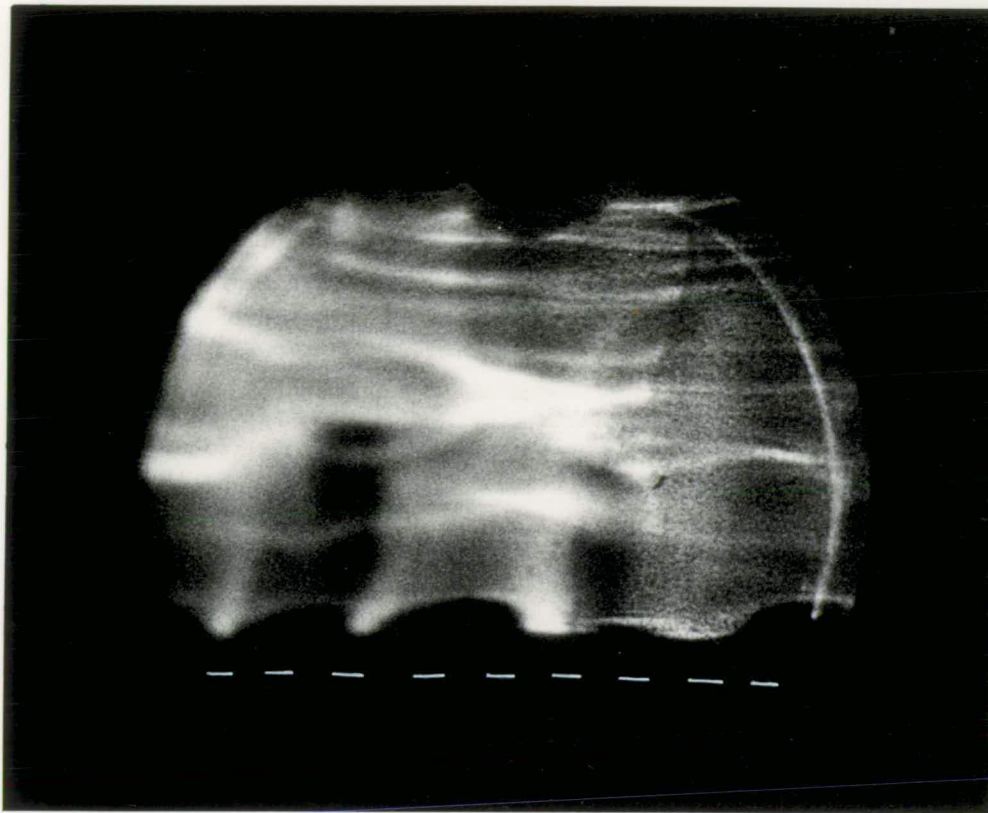
$$T_{\text{sur}} = 213.6^\circ\text{F}$$

$$T_{\text{bulk}} = 198.5^\circ\text{F}$$

$$(T_{\text{sur}} - T_{\text{sat}}) = 3.6^\circ\text{F}$$

$$\delta = 0.030 \text{ inches}$$

FIG. 32



(e)

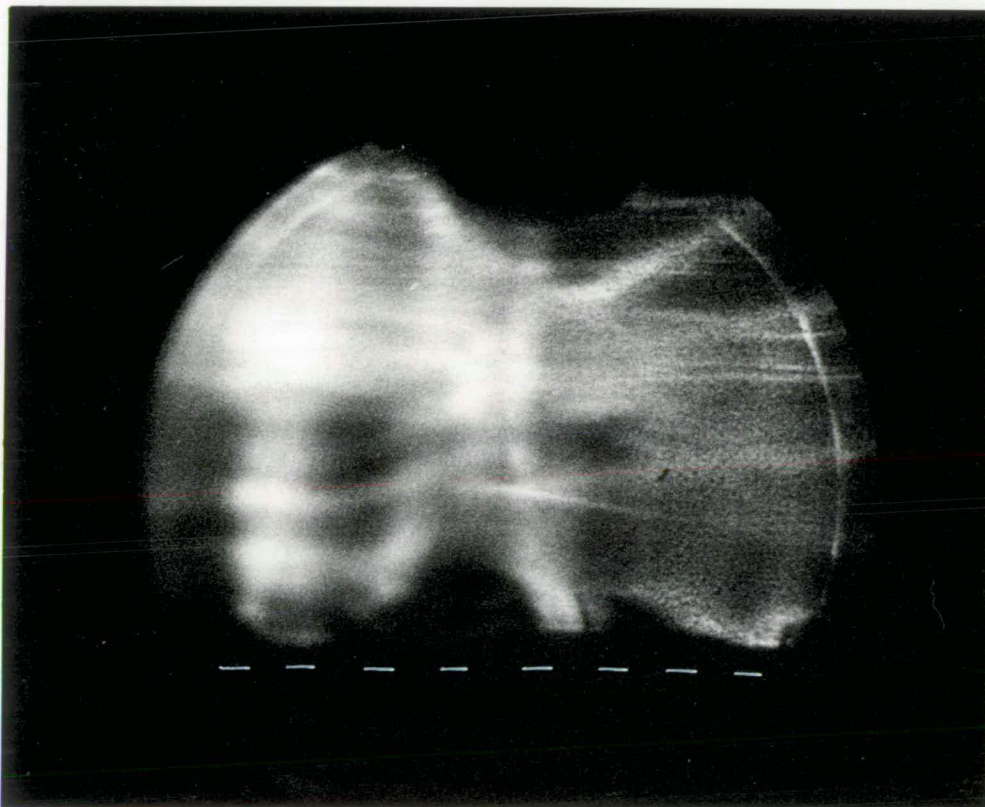
$$Q/A = 5380 \text{ B.t.u./ft.}^2 \text{ hr.}$$

$$T_{\text{sur}} = 218.7^\circ\text{F}$$

$$T_{\text{bulk}} = 198.7^\circ\text{F}$$

$$(T_{\text{sur}} - T_{\text{sat}}) = 8.6^\circ\text{F}$$

$$\delta = 0.030 \text{ inches}$$



(f)

$$Q/A = 8150 \text{ B.t.u./ft.}^2 \text{ hr.}$$

$$T_{\text{sur}} = 227.2^\circ\text{F}$$

$$T_{\text{bulk}} = 198.4^\circ\text{F}$$

$$(T_{\text{sur}} - T_{\text{sat}}) = 17.1^\circ\text{F}$$

$$\delta = 0.025 \text{ inches}$$

FIG. 32

THERMAL LAYER THICKNESS vs.

HEATING SURFACE TEMPERATURE

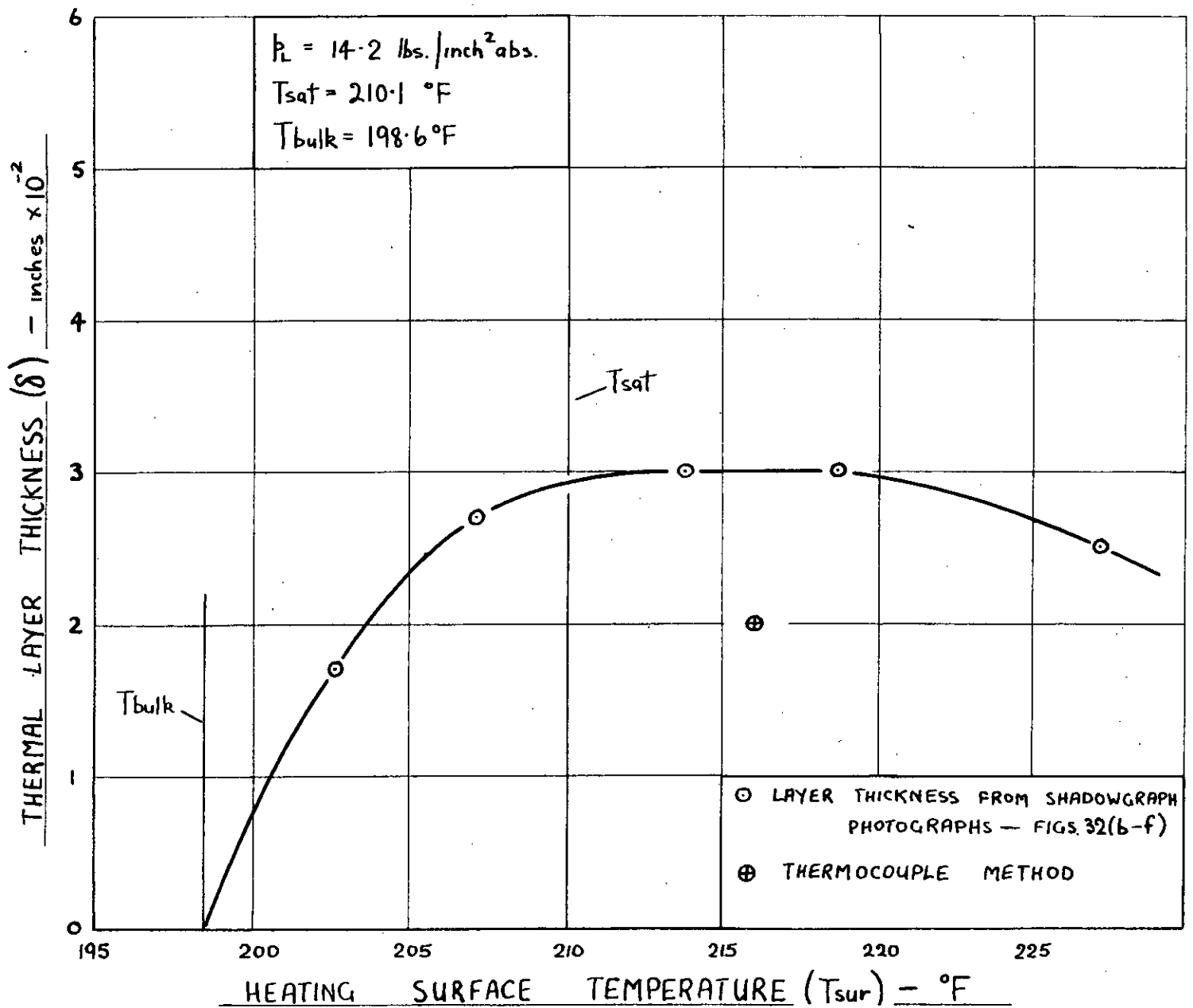


FIG. 33

THERMAL LAYER THICKNESS vs.
HEATING SURFACE TEMPERATURE

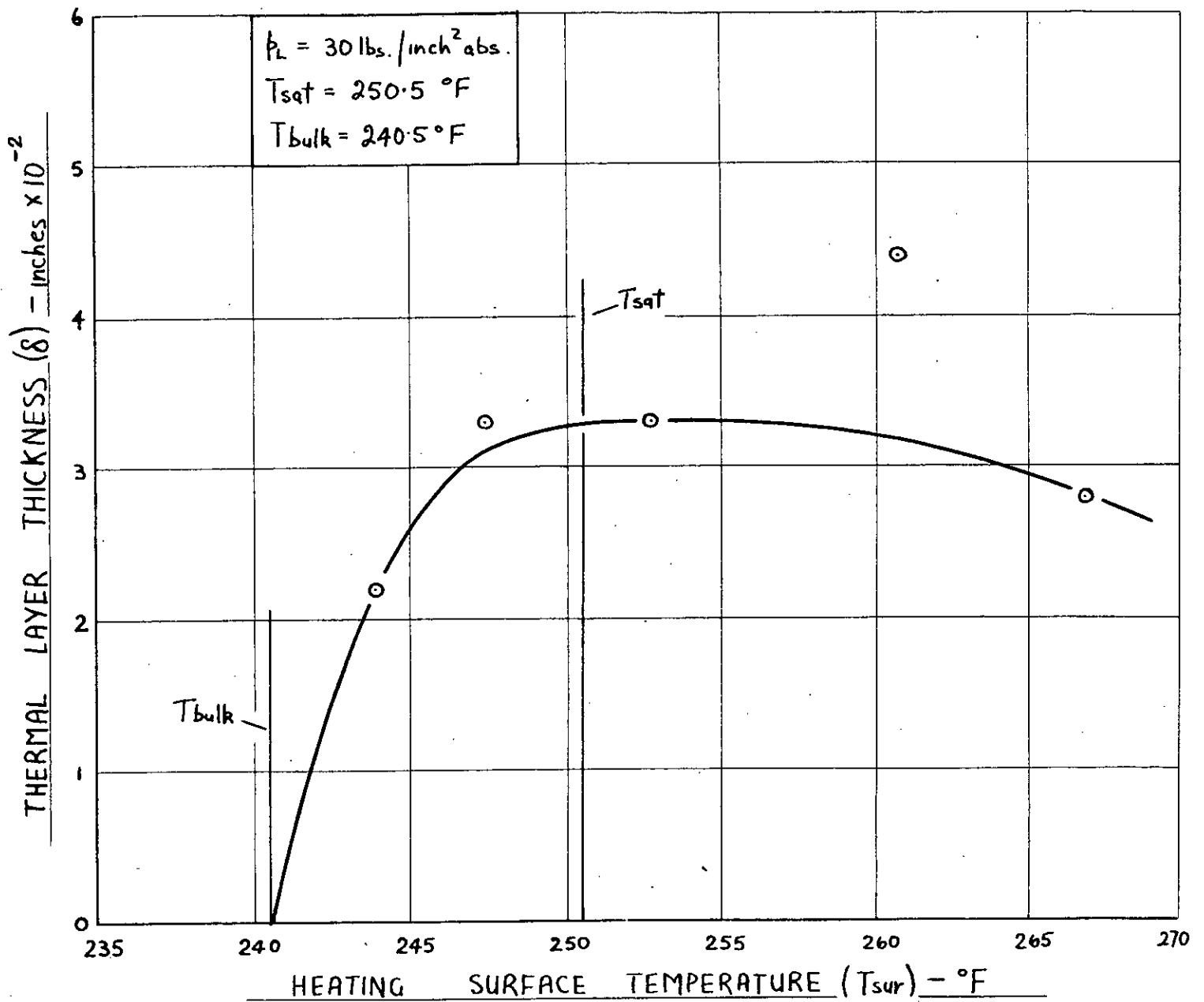


FIG. 34

SECTIONAL VIEW OF THERMOCOUPLE PROBE

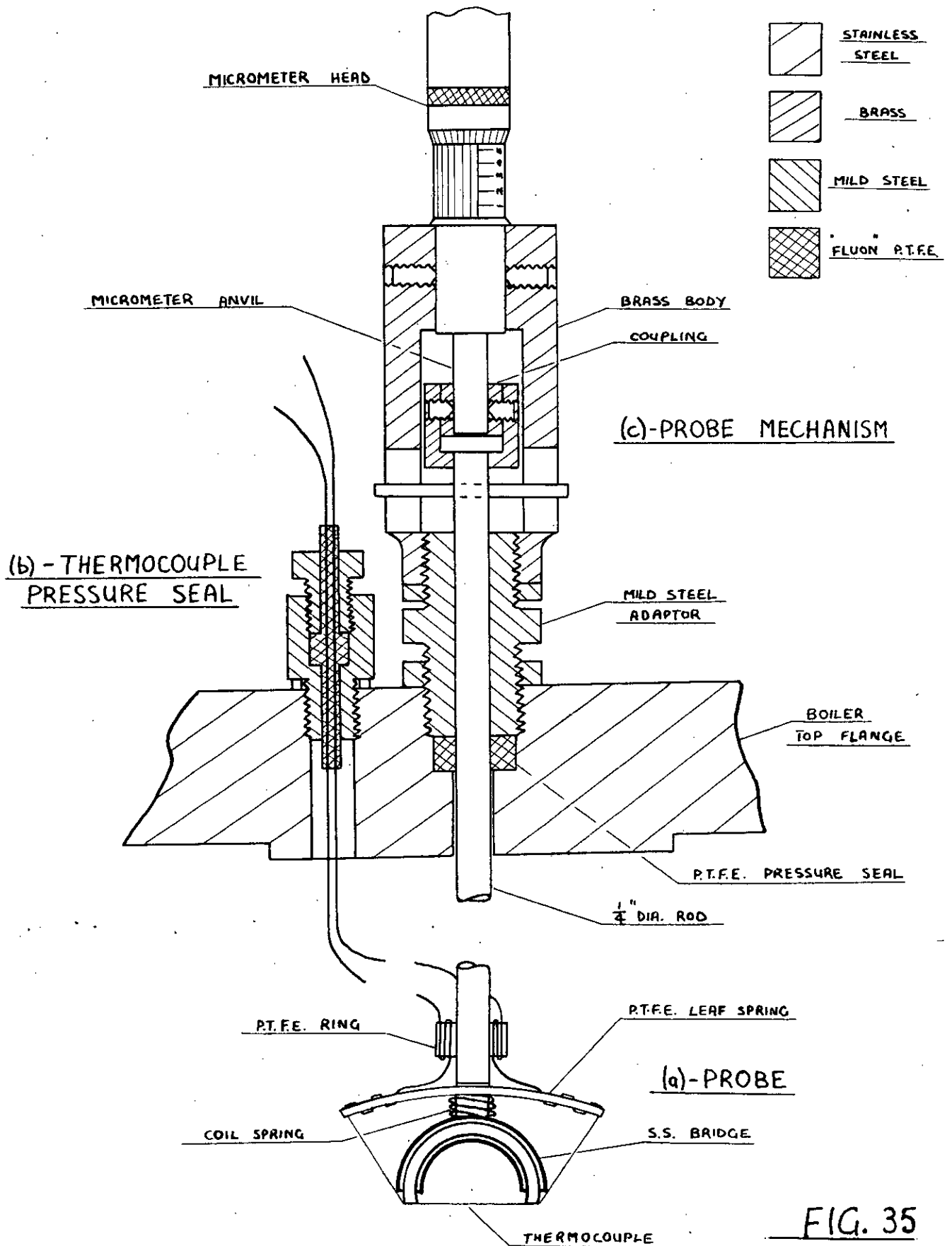


FIG. 35

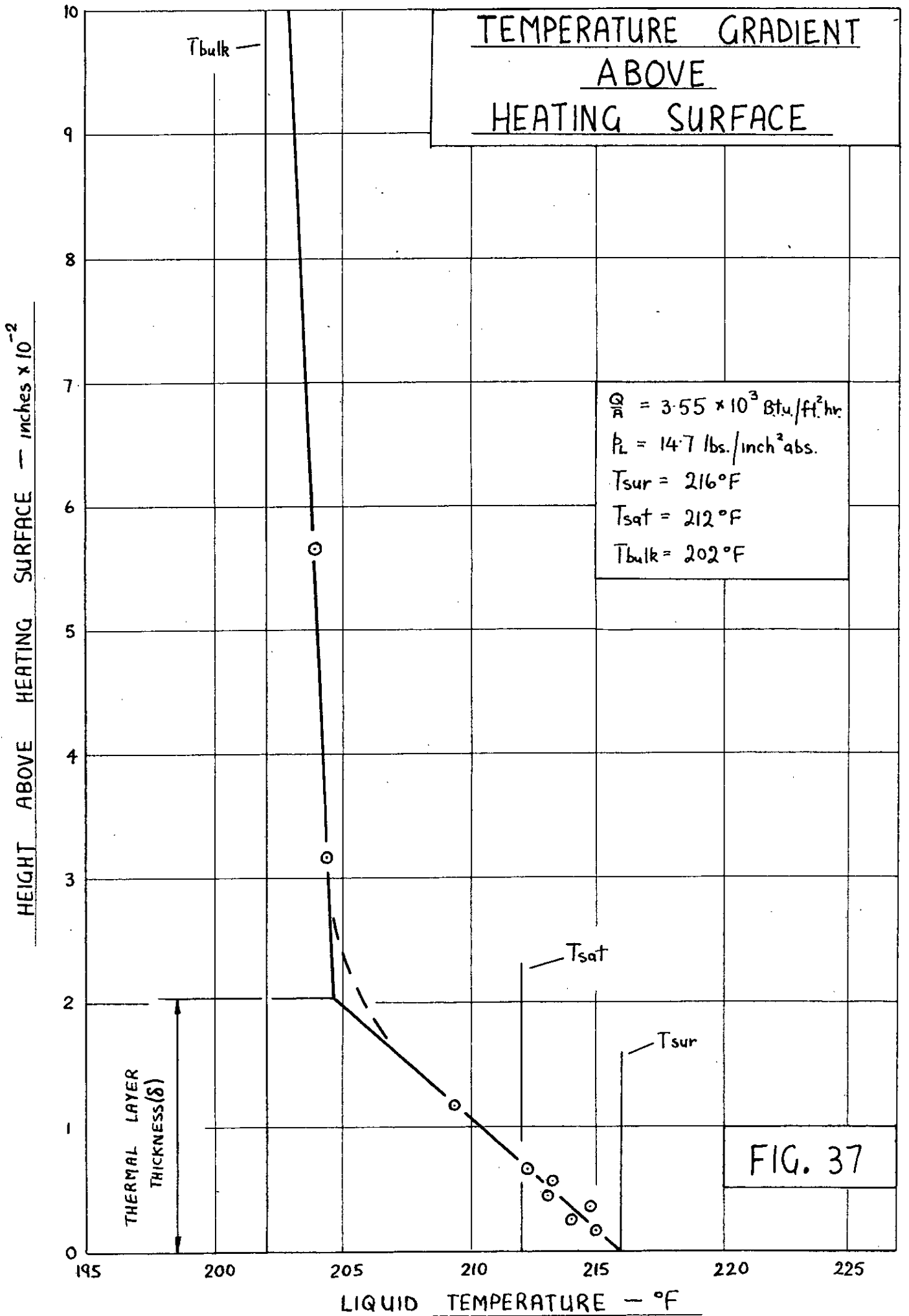
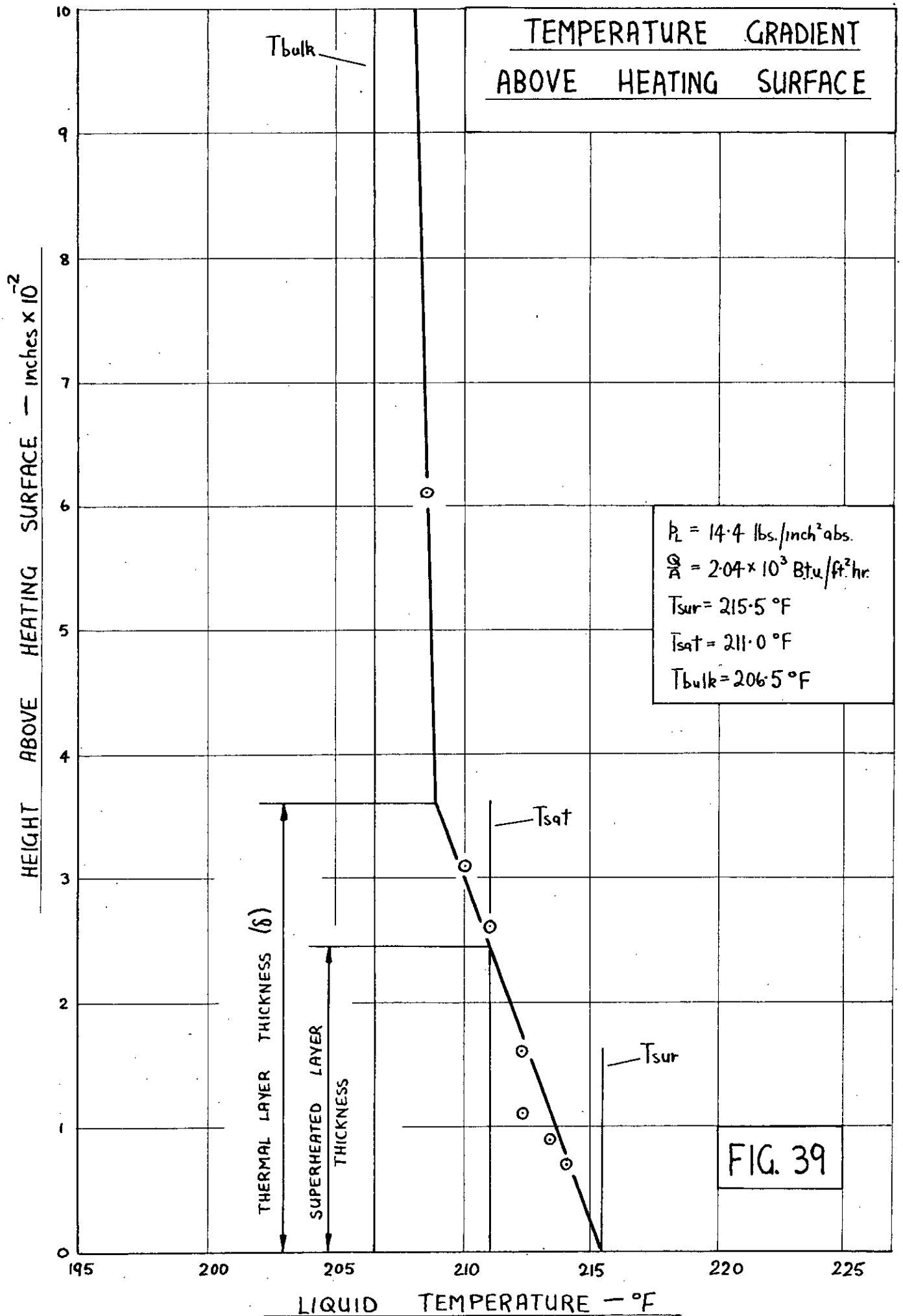


FIG. 37



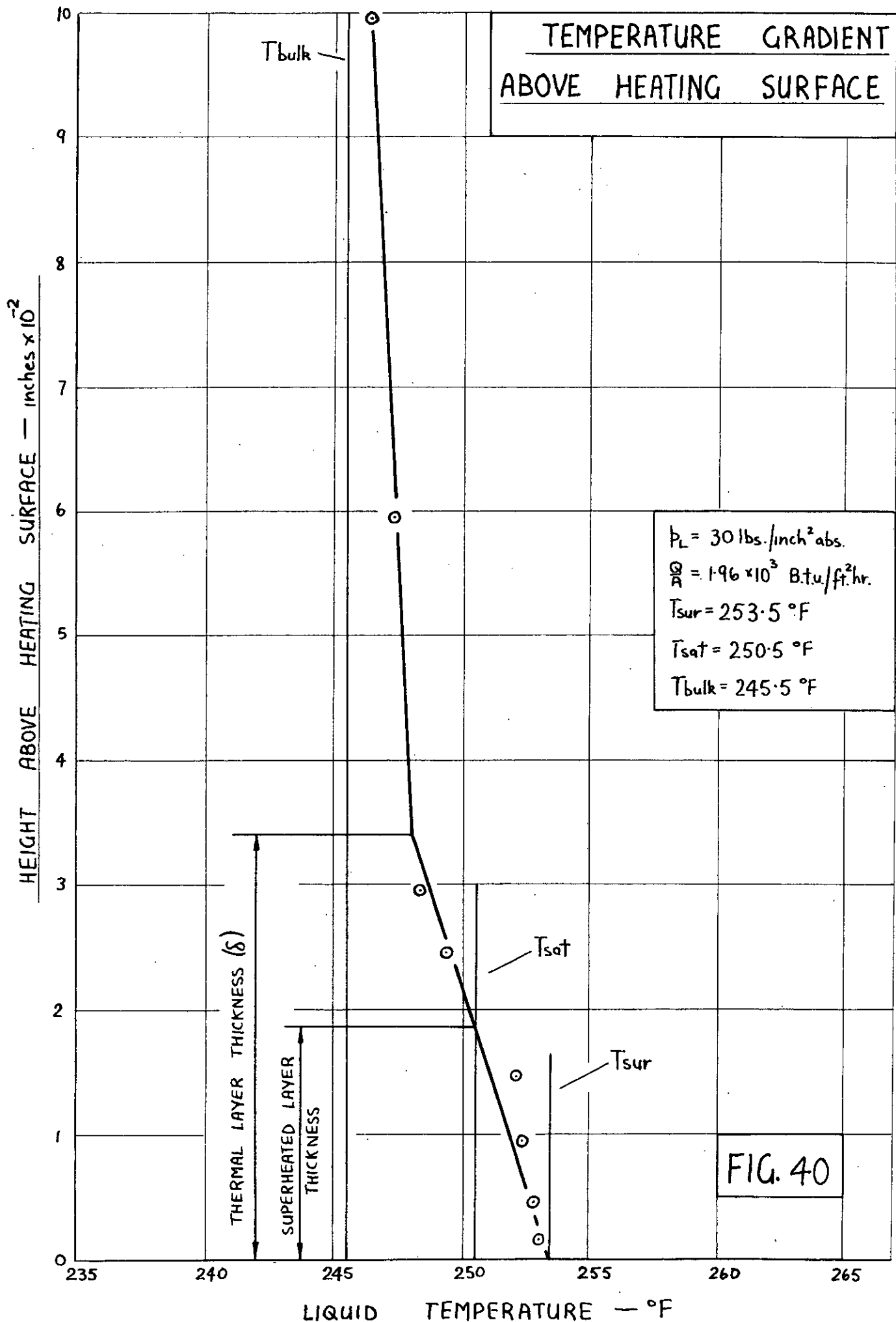


FIG. 40

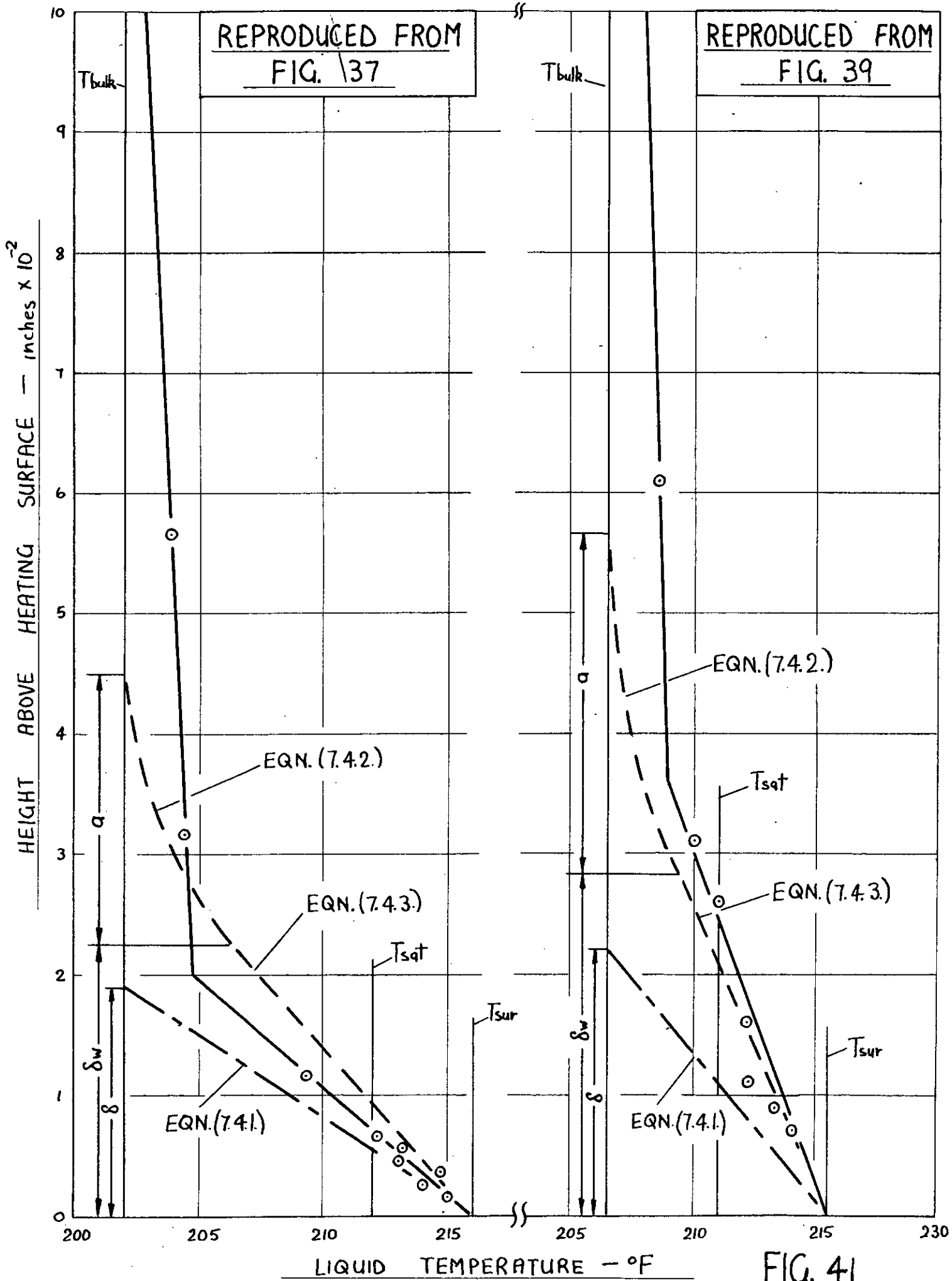
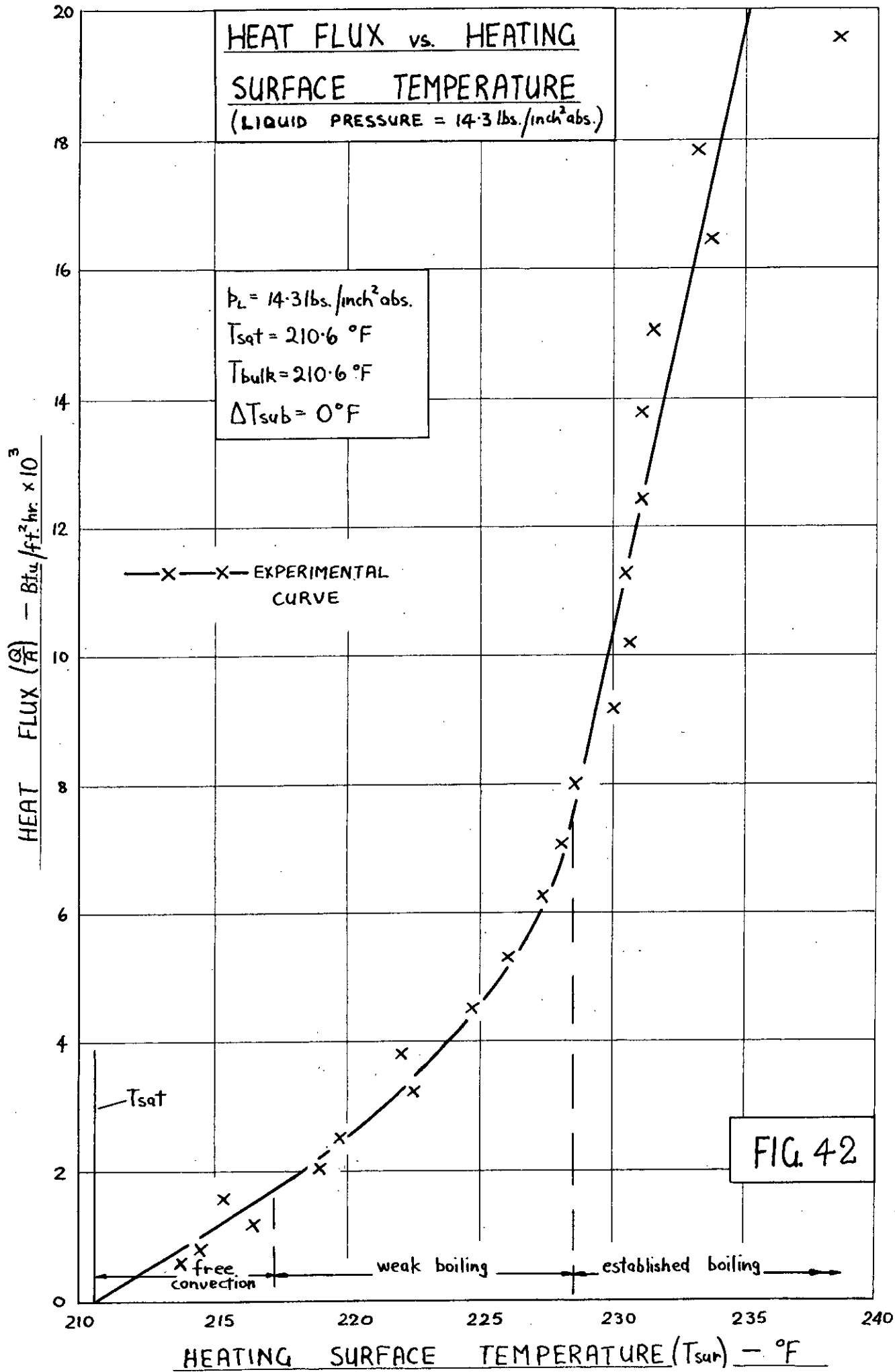
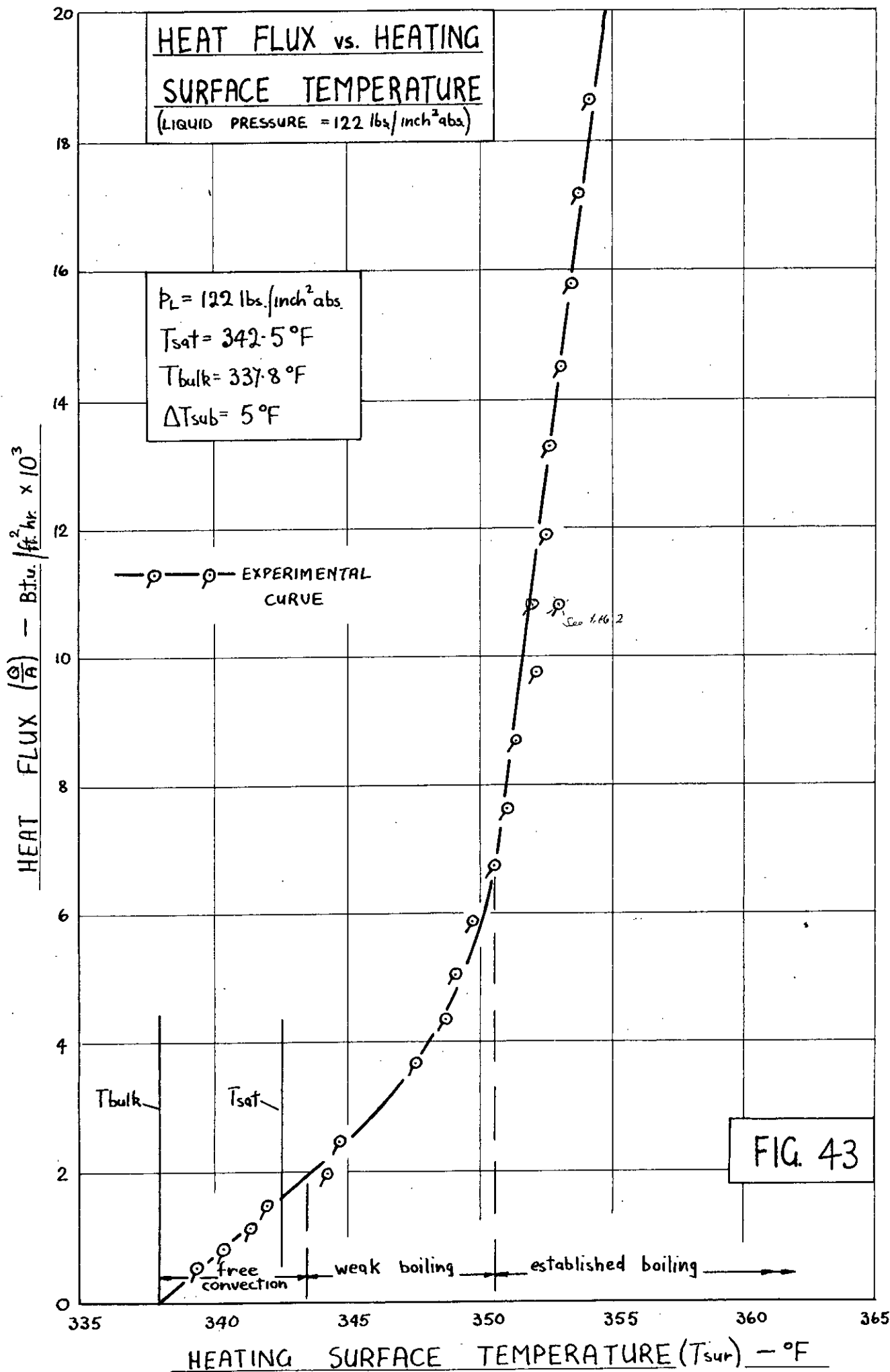


FIG. 41





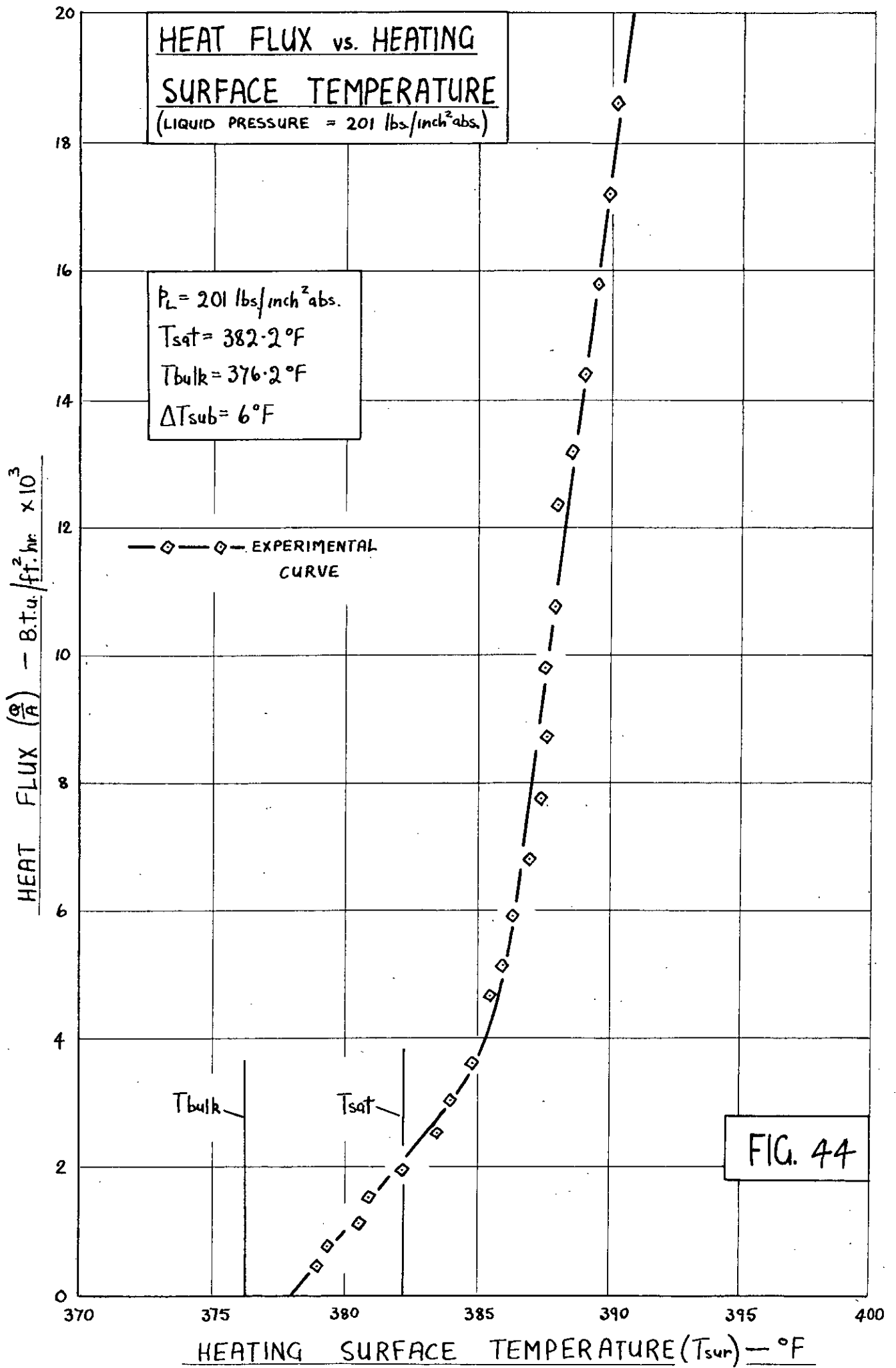
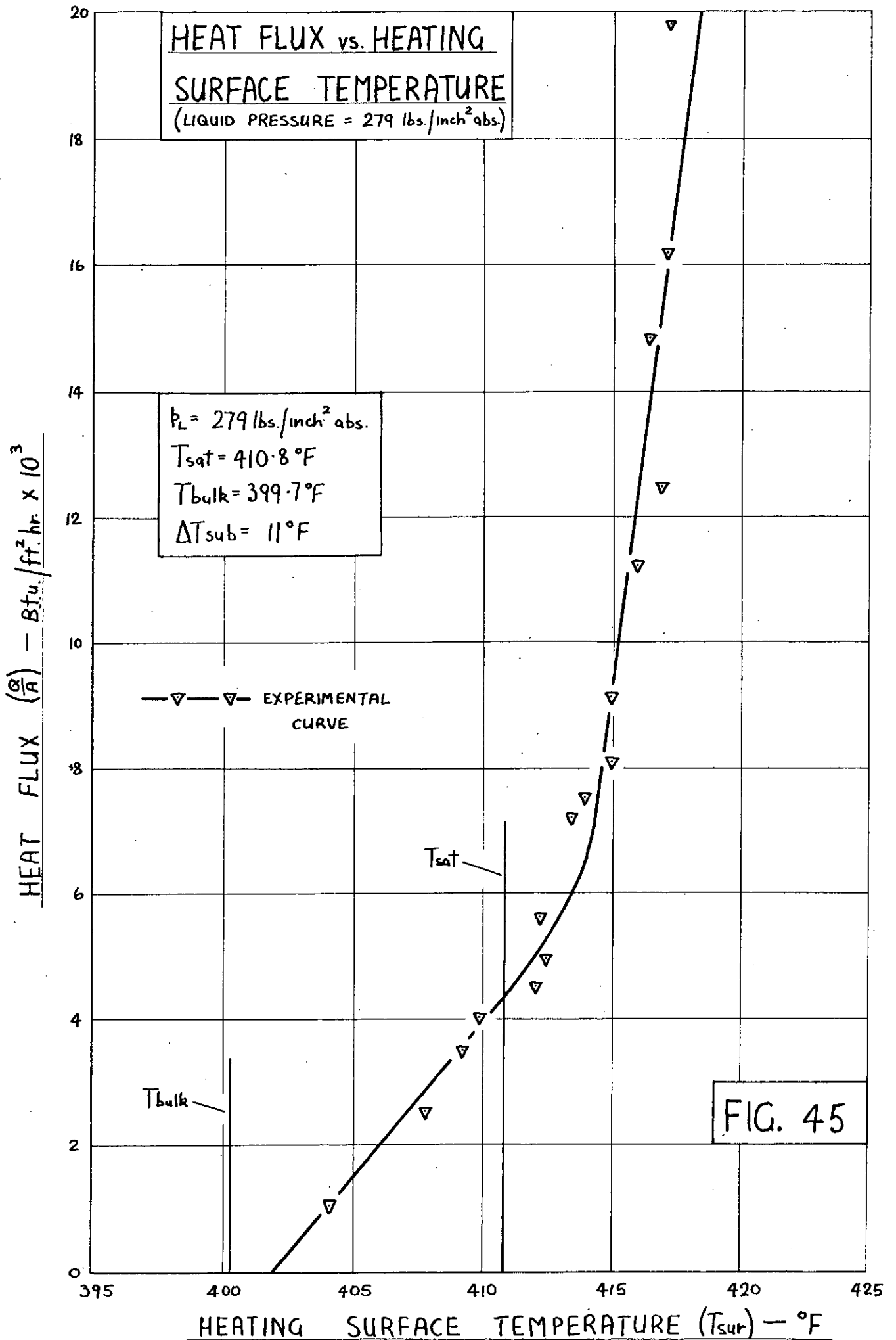


FIG. 44



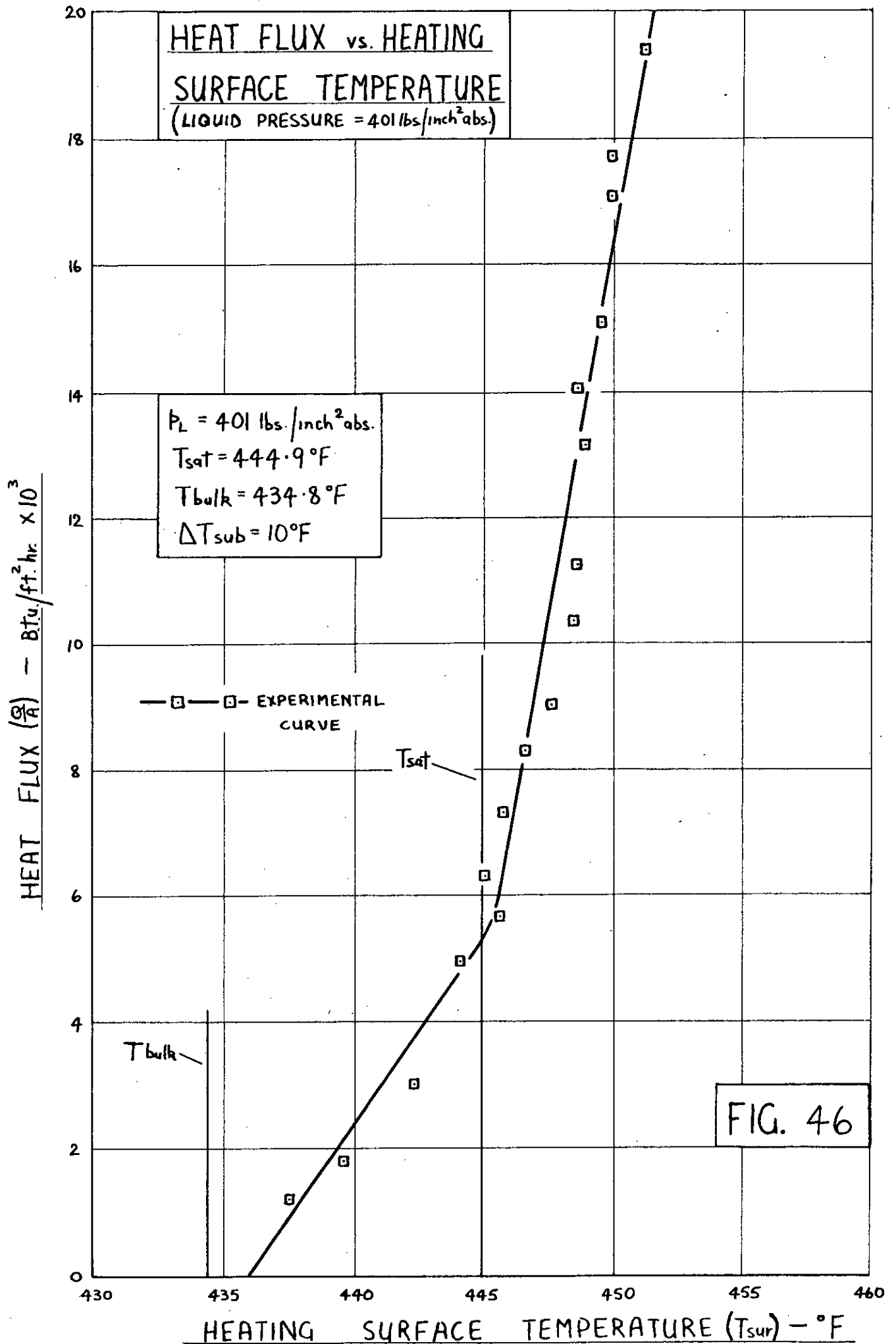
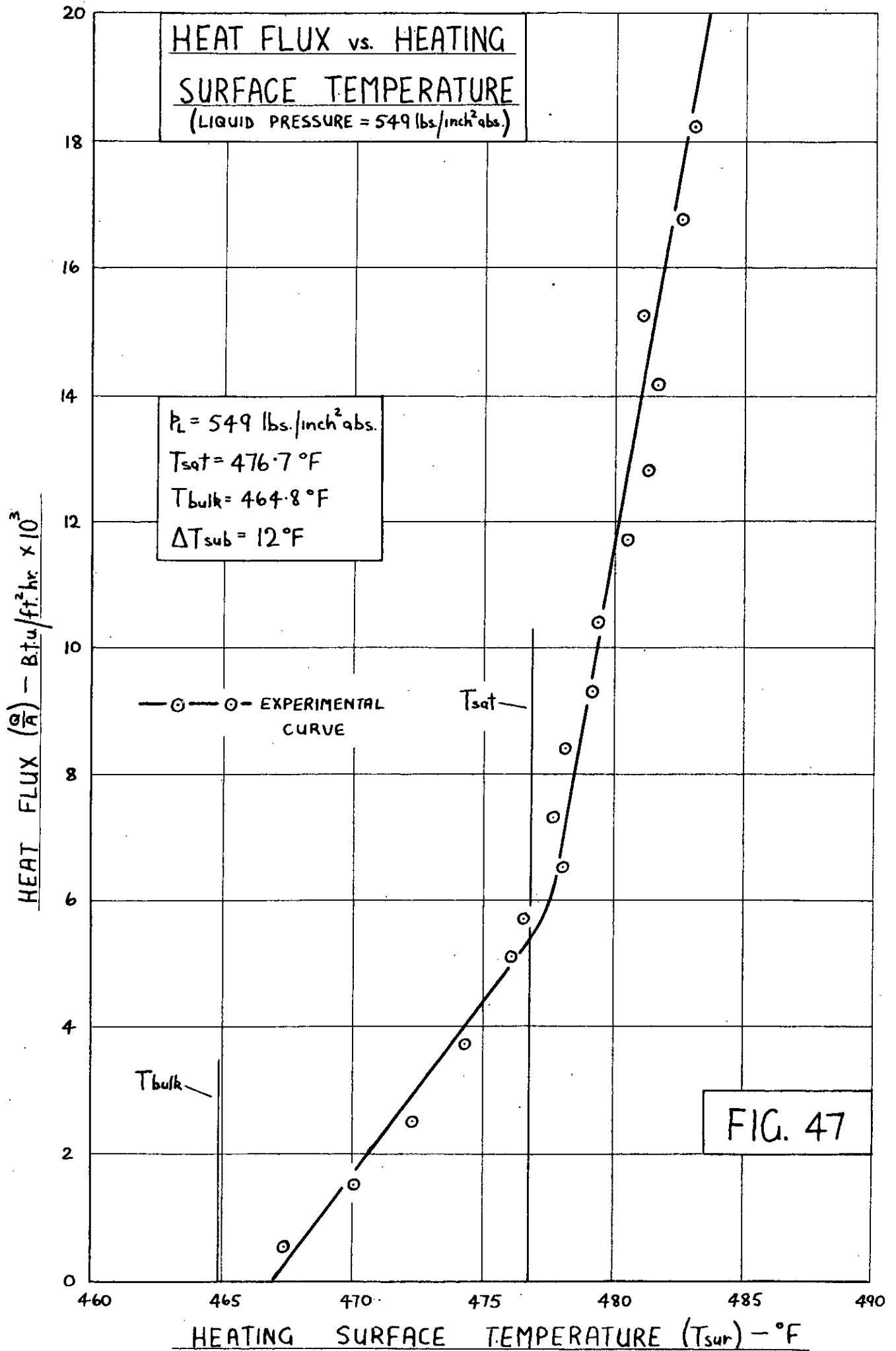
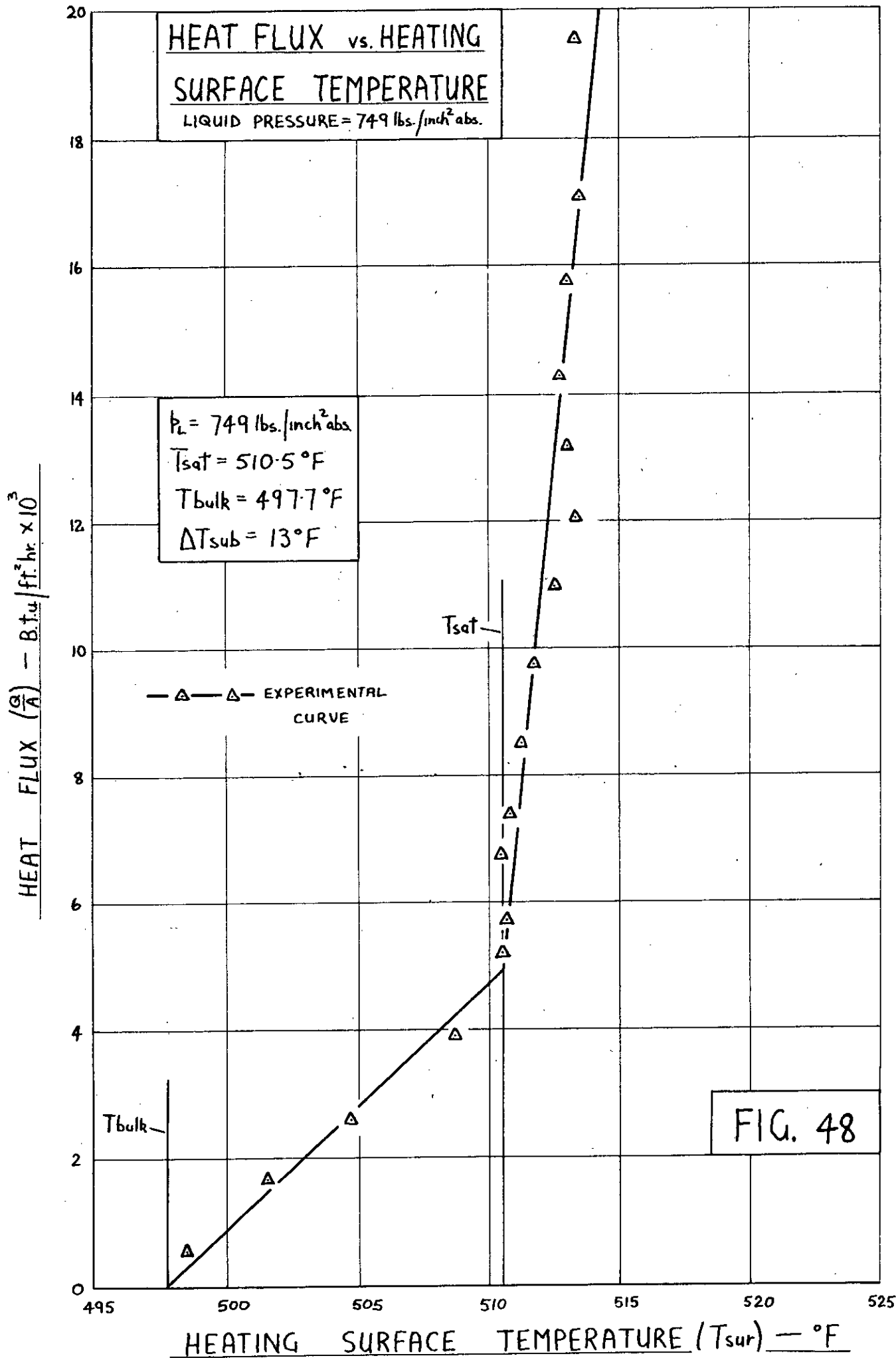
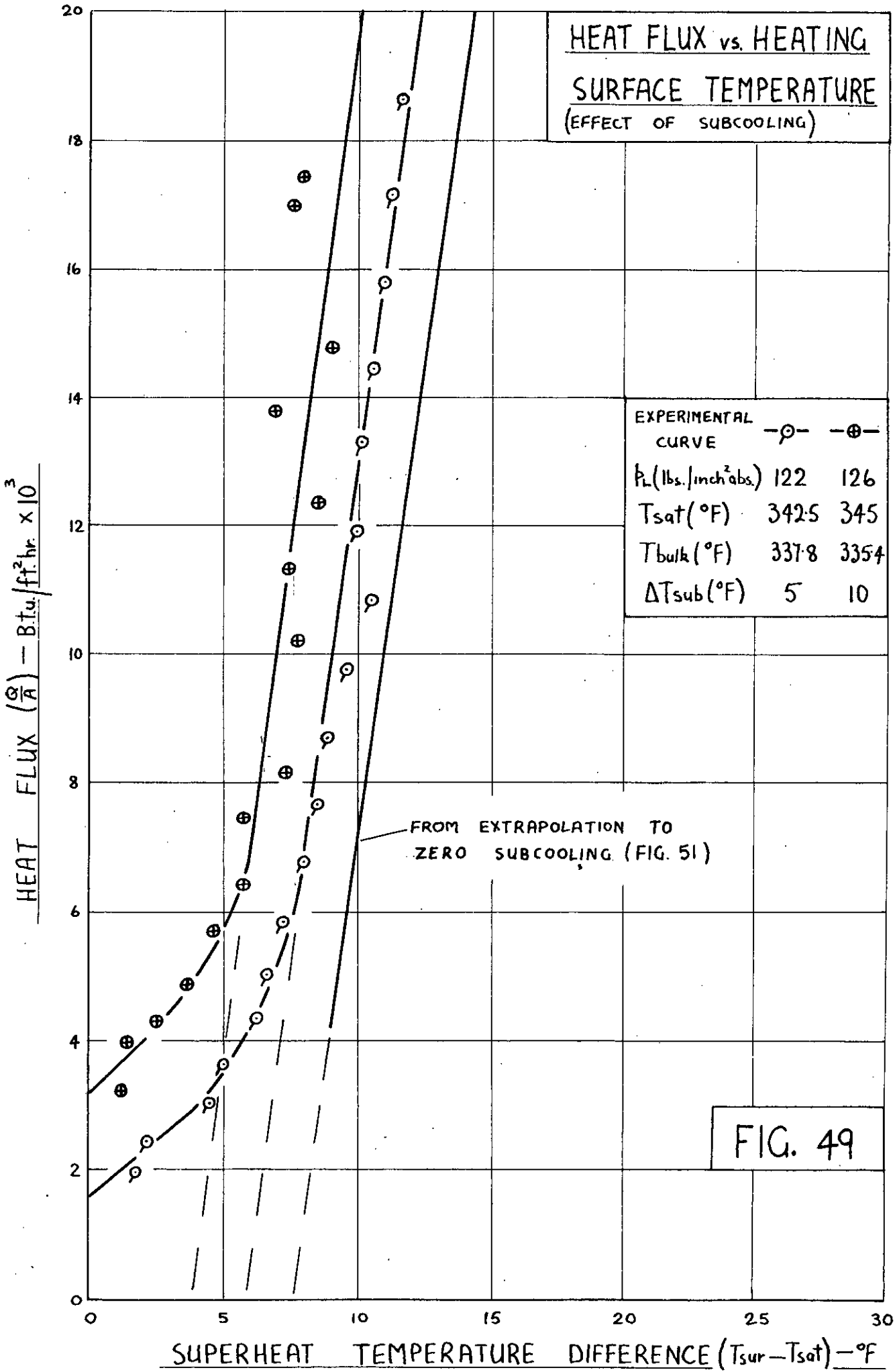


FIG. 46







HEAT FLUX vs. HEATING
SURFACE TEMPERATURE
 (EFFECT OF SUBCOOLING)

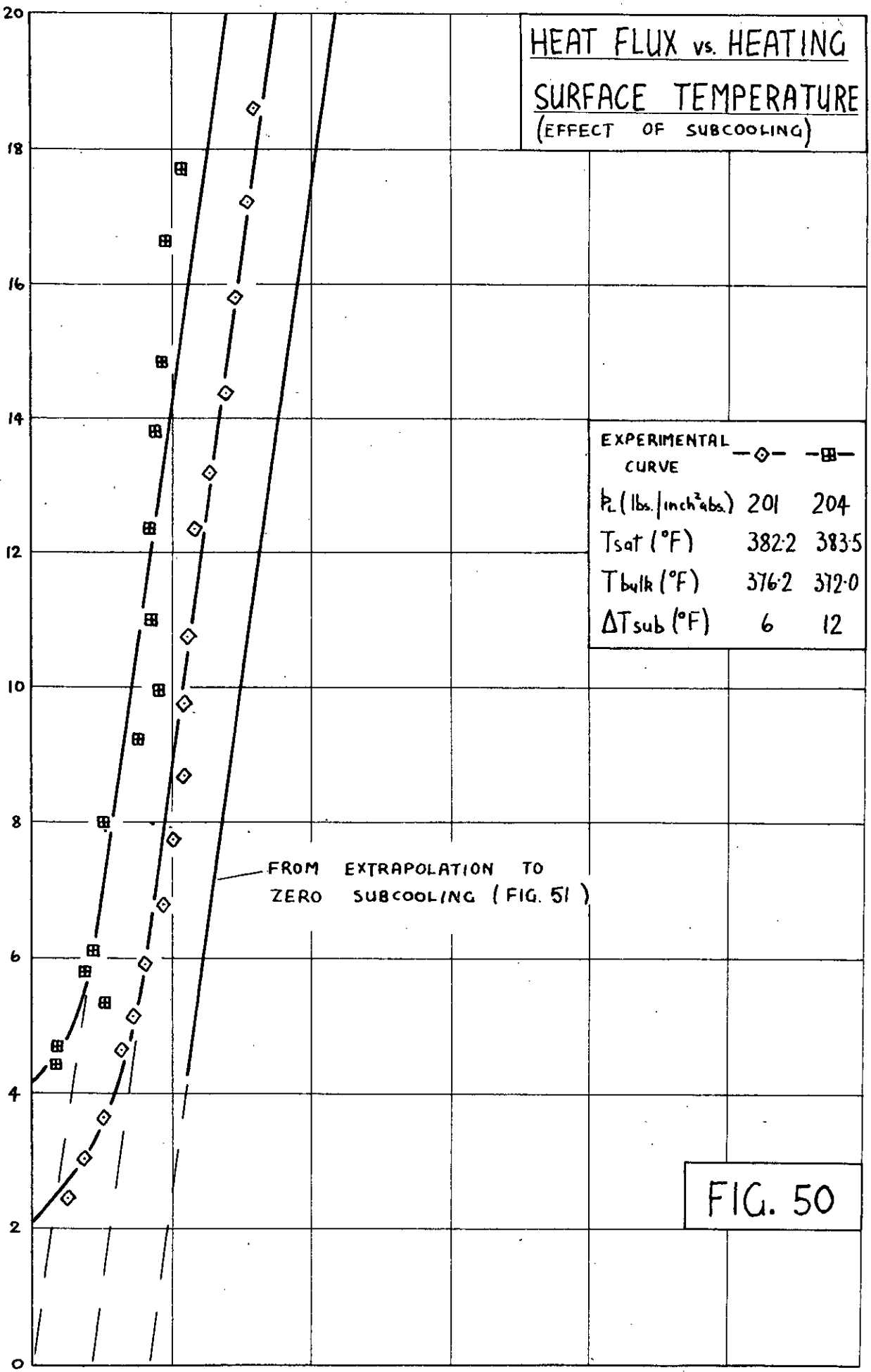
EXPERIMENTAL CURVE	-○-	-⊕-
P_L (lbs./inch ² abs.)	122	126
T_{sat} (°F)	342.5	345
T_{bulk} (°F)	337.8	335.4
ΔT_{sub} (°F)	5	10

FROM EXTRAPOLATION TO ZERO SUBCOOLING (FIG. 51)

FIG. 49

HEAT FLUX $\left(\frac{Q}{A}\right) - \text{B.t.u./ff.hr} \times 10^3$

HEAT FLUX vs. HEATING
SURFACE TEMPERATURE
(EFFECT OF SUBCOOLING)



EXPERIMENTAL CURVE	—◇—	—■—
P_L (lbs./inch ² abs.)	201	204
T_{sat} (°F)	382.2	383.5
T_{bulk} (°F)	376.2	372.0
ΔT_{sub} (°F)	6	12

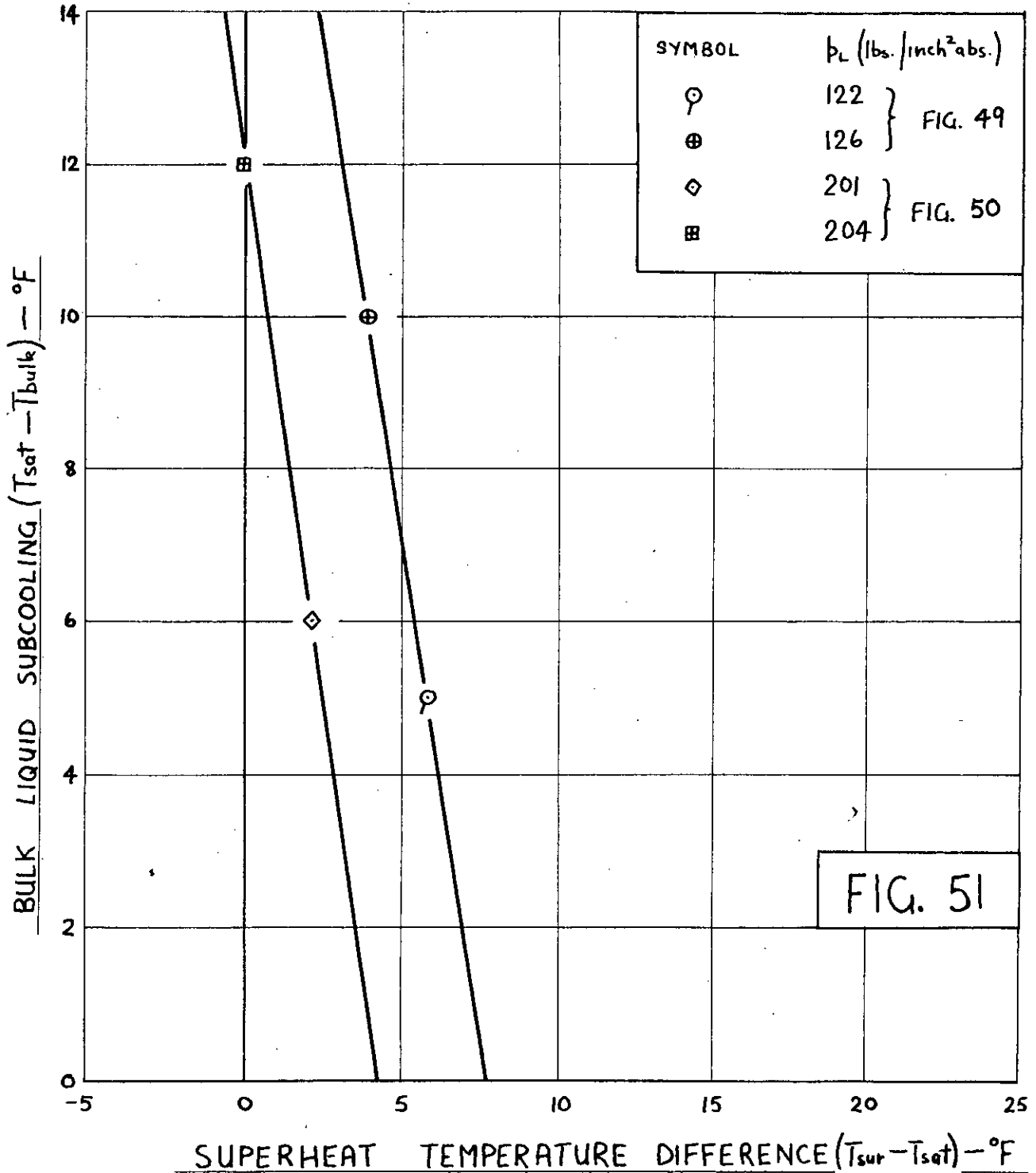
FROM EXTRAPOLATION TO ZERO SUBCOOLING (FIG. 51)

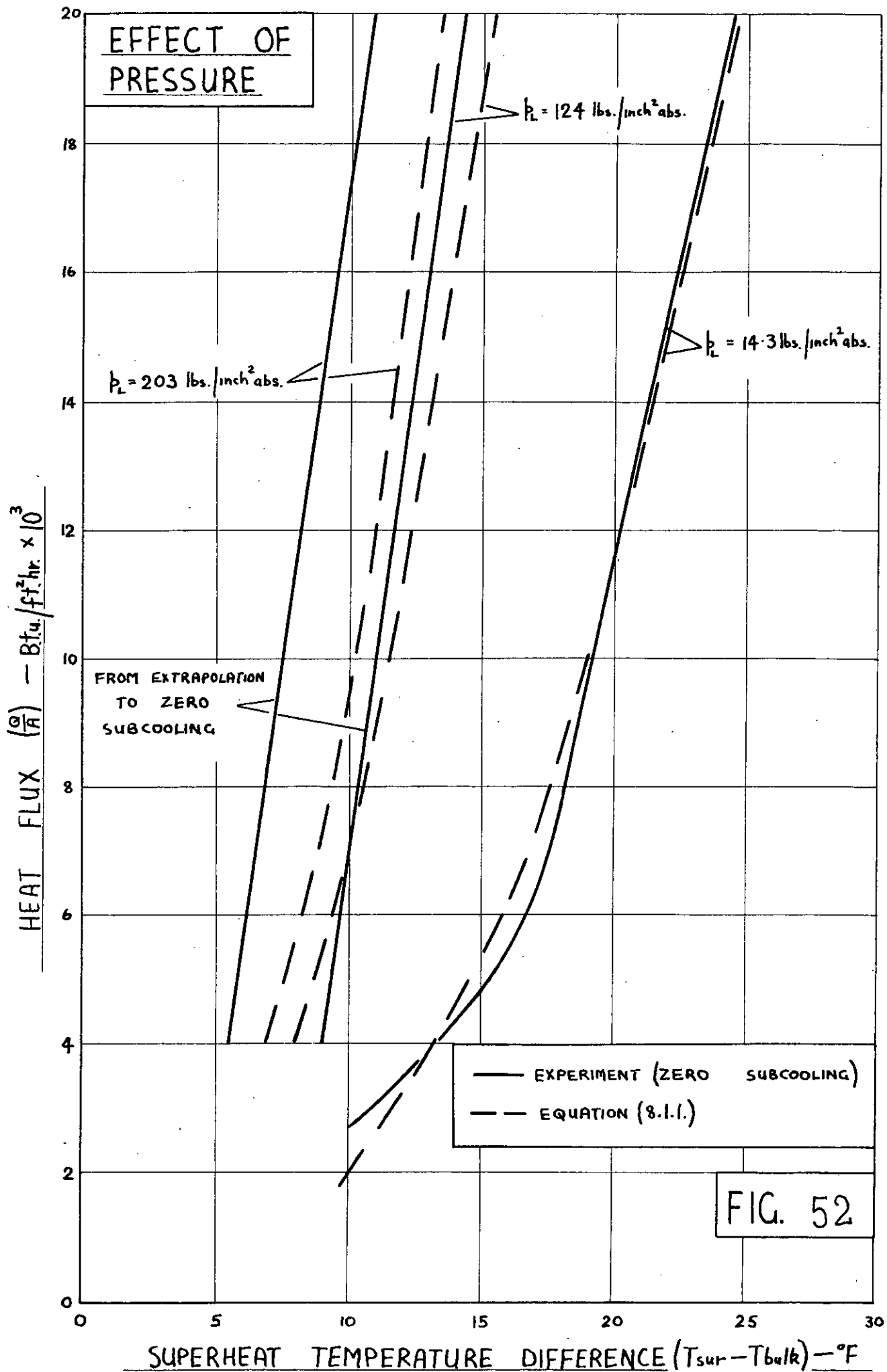
FIG. 50

SUPERHEAT TEMPERATURE DIFFERENCE ($T_{sur} - T_{sat}$) - °F

BULK LIQUID SUBCOOLING vs. SUPERHEAT

TEMPERATURE DIFFERENCE
(EXTRAPOLATION TO ZERO SUBCOOLING)





FREE CONVECTION HEAT TRANSFER

(LIQUID PRESSURE $p_L = 14.3 \text{ lbs./inch}^2 \text{ abs.}$)

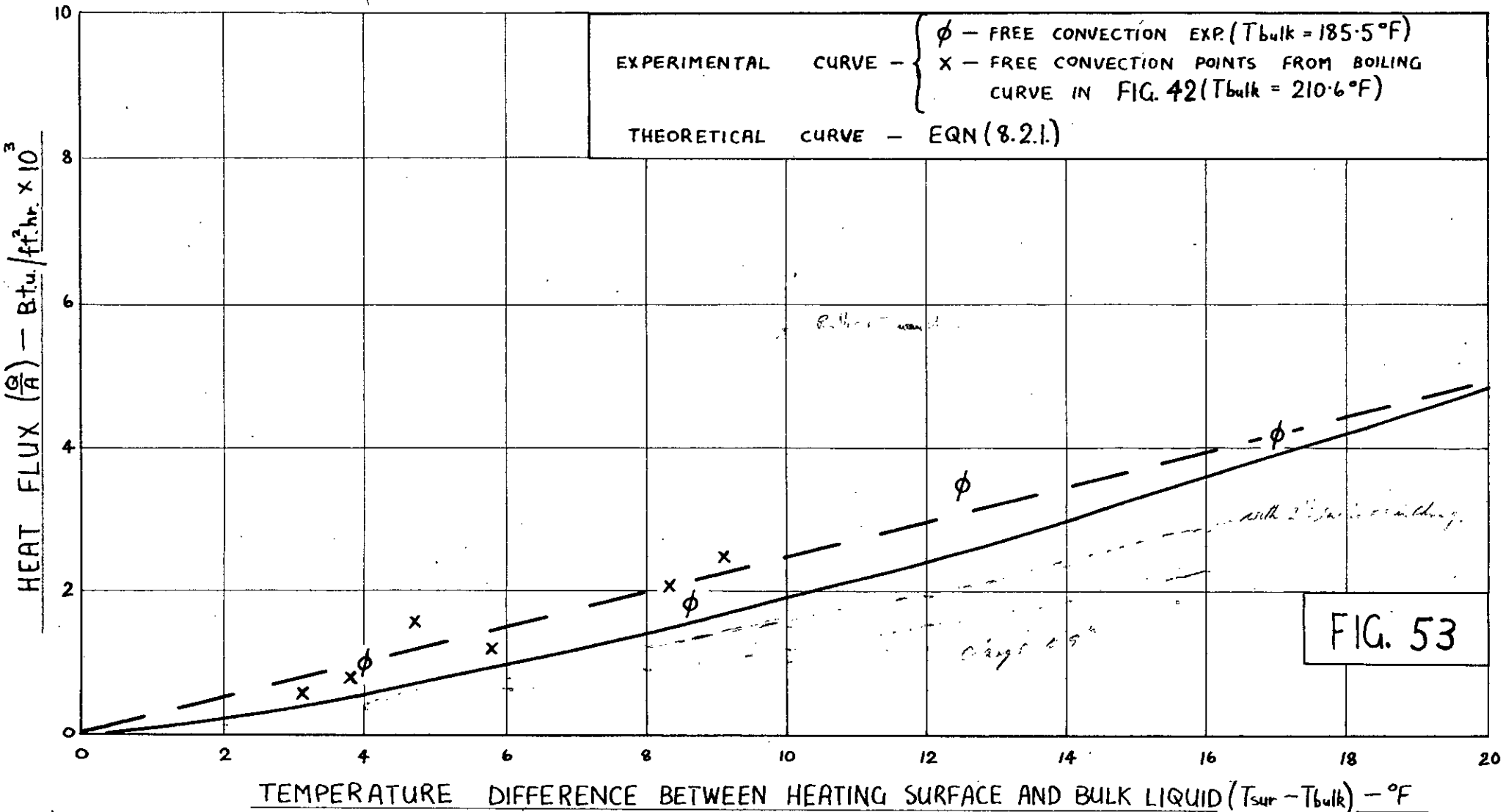
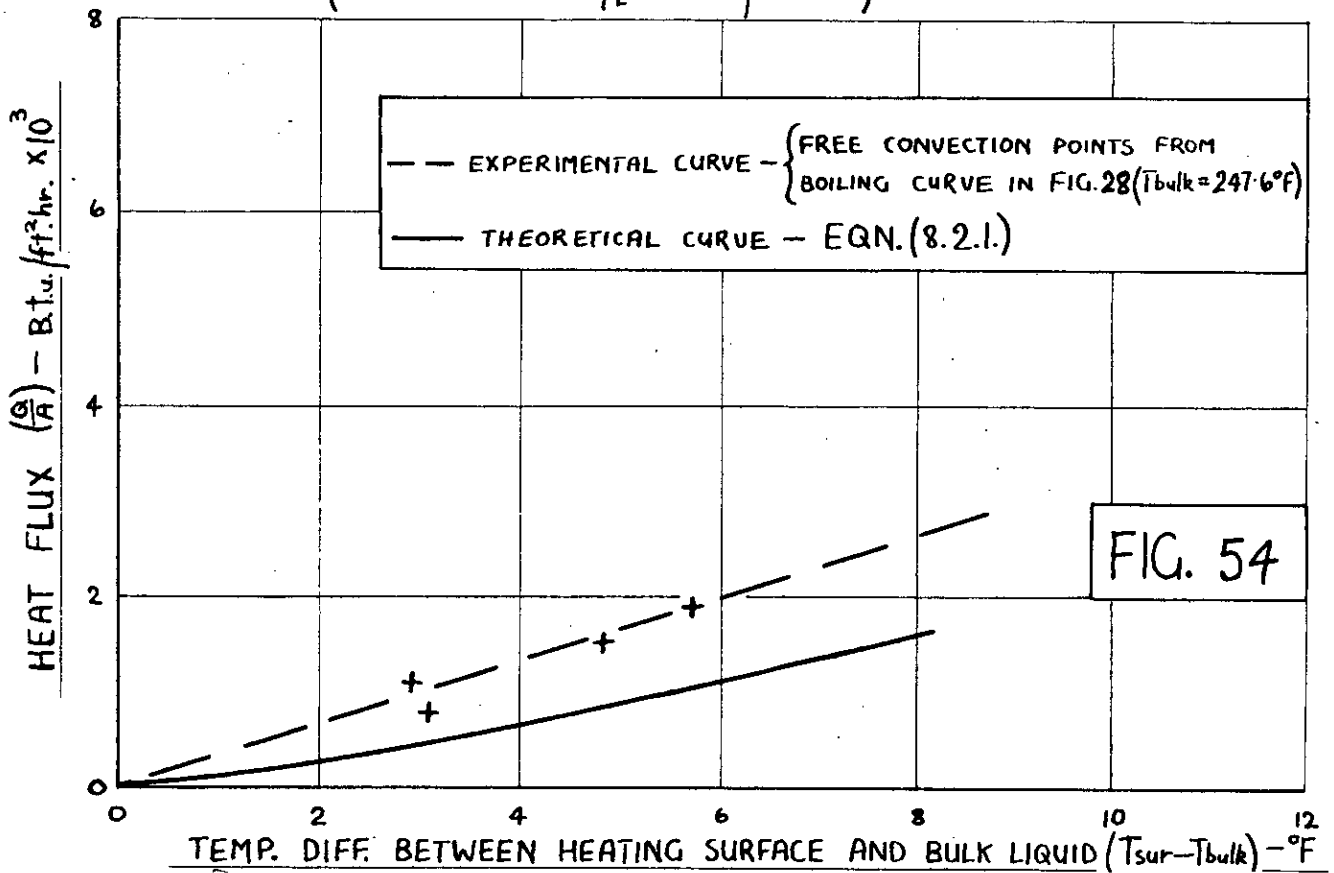


FIG. 53

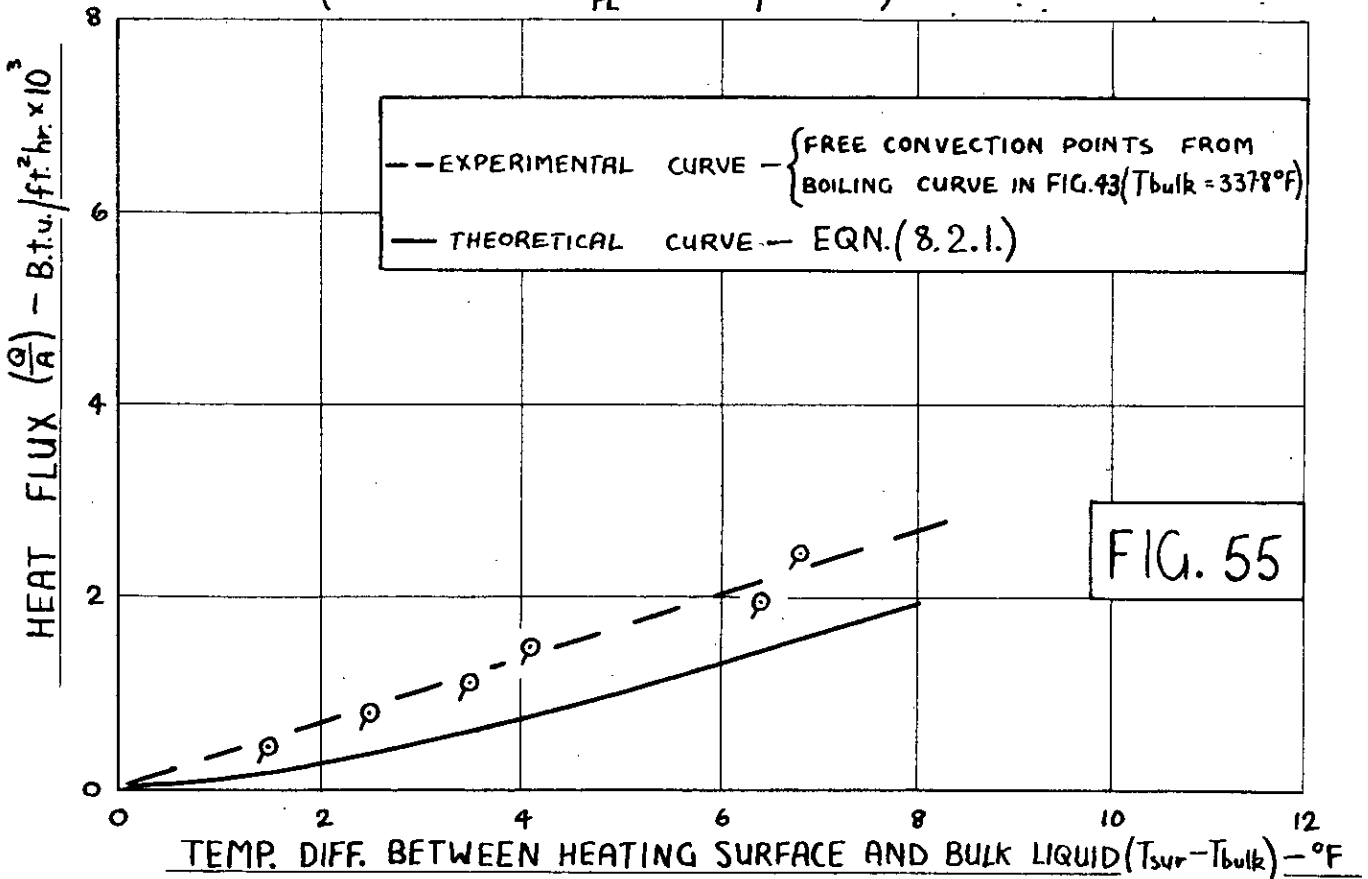
FREE CONVECTION HEAT TRANSFER

(LIQUID PRESSURE $p_L = 30 \text{ lbs./inch}^2 \text{ abs.}$)



FREE CONVECTION HEAT TRANSFER

(LIQUID PRESSURE $p_L = 122 \text{ lbs./inch}^2 \text{ abs.}$)



CAVITY RADIUS vs. INITIATION SUPERHEAT

TEMPERATURE DIFFERENCE

(LIQUID PRESSURE $p_L = 14.7 \text{ lbs./inch}^2 \text{ abs.}$)

